HIGH FIELD MAGNETOSTRICTION OF $TbFe_2$ AND $DyFe_2$

by

Karim M. Al-Rawi

DEPARTMENT OF PHYSICS
SOUTHAMPTON UNIVERSITY

September, 1976

CONTENTS

CONTENTS (continued)

ABSTRACT

Faculty of Science

Physics

Master of Philosophy

HIGH FIELD MAGNETOSTRICTION OF $TbFe_2$ AND $DyFe_2$ COMPOUNDS.

By KARIM M. AL-RAWI

Magnetostriction measurements have been carried out in the cubic laves phase compounds $TbFe_2$ and $DyFe_2$ from 16K – 300K. Pulsed magnetic fields up to 18 Tesla were applied. The observed magnetostrictions are very large ($\sim 10^{-3}$). These fields were not high enough to saturate the magnetostriction. In the case of $TbFe_2$ the magnetostriction curves were near saturation at all temperatures which allows an extrapolation to infinite field to be made. The infinite field extrapolation for $TbFe_2$ gives $\lambda_{total} = 5080 \times 10^{-6}$ at 0K and $\lambda_{total} = 2950$ at 300 K. For $DyFe_2$ the magnetostriction curves were far from saturation except at room temperature which made all extrapolation procedures impossible. At 300 K the infinite field extrapolated value of λ_{total} for $DyFe_2$ is estimated to be 1270×10^{-6}. The measurements confirm the extremely high anisotropy of these compounds. At the highest fields the polycrystalline samples are still undergoing rotational magnetization processes.

The magnetization of $DyFe_2$ was also measured between 4.2K – 300 K and at fields up to 18 Tesla. The measurements showed that there was a preferred alignment in the cooling direction of the sample. The applied fields were not high enough to achieve saturation.

From the shape of the magnetostriction curves of $DyFe_2$ and the initial jump of the magnetization curves, it is suggested that $DyFe_2$ contains only 180° domains. The results of the calculations for the total energy of the two possible configurations showed that due to the large magnetostrictive contribution the presence of 90° walls might be energetically unfavourable in $DyFe_2$ compound.

ACKNOWLEDGEMENTS

I would like to thank my supervisor Dr. D. Melville for introducing me to magnetism and high magnetic fields and for his continuous advice and encouragement. Also I would like to thank Professor E.W. Lee for his helpful advice and useful discussions.

A number of colleagues in the magnetism group have been friendly and helpful, but I am especially grateful to Dr. P. Lanchester, P. Hendy, A. Prezeslak, W.I. Khan and J. Burd for their invaluable discussions.

Mr. C.D. Strange for his technical help and for tracing the diagrams of this thesis.

Professor Barnes for providing laboratory facilities.

Mr. P. Cleverley for supplying liquid helium.

Mrs. W. Rogers for typing this thesis.

Also my thanks to my brother Ismaeil M. Al-Rawi for his encouragement.

Finally, many thanks to the government of the Republic of Iraq for providing financial assistance.

CHAPTER I

INTRODUCTION: The aim of this thesis has been to investigate the magnetostrictive distortions in some ferrimagnetically ordered, RFe_2, (R = rare earth) cubic laves phase compounds.

High pulsed magnetic field up to 18 Tesla, (~ 180 KOe) were applied. Resistive strain gauges were used to detect the strain in conjunction with an A – C bridge employing synchronous phase sensitive detection. The apparatus was sensitive to strains of the order of one microstrain and could be used over a wide range of temperatures.

Magnetostriction which is defined as the lattice distortion of a magnetic crystal when it is magnetized, is closely related to magnetic anisotropy and plays an important role in the understanding of ferromagnetic and antiferromagnetic phenomena like magnetization processes, permeability and magnetoelastic interactions.

In the case of magnetisation, magnetostriction data can be used to distinguish between the different processes involved. This is because (for polycrystalline sample of metals such as iron) – the regions associated with these mechanisms e.g. domain wall displacement and the rotation of magnetisation against anisotropy are more clearly defined than in the corresponding magnetisation curves.

Studies of magnetostriction also have technological utility in the production of electromechanical transducers, magnetostrictive oscillators and filters, and in reducing transformer noises which are produced by magnetostrictive vibration of the core.

The deformation $\delta\ell/\ell$ due to magnetostriction is as small as 10^{-5} in ferromagnetic materials such as iron, nickel and cobalt. In some of the magnetic rare earth cubic laves phase compounds, owing to the large anisotropy energies, the observed magnetostriction is larger by almost a factor of 100. Measurements have been previously reported in the

isostructural compounds, RFe_2, by Clark and Callen[1], Koon, Schindler and Carter[2] and Clark and Belson[3]. Huge magnetically induced strains were observed in the cubic $TbFe_2$ at room temperature. This discovery has stimulated interest in the possibility that these or related materials may be useful for practical magnetostrictive devices. One of the problems associated with the use of these materials is that they also possess a large magnetocrystalline anisotropy so that large applied magnetic fields are needed to fully realize the large strain.

The origin of the large magnetostriction in the $TbFe_2$ and $DyFe_2$ compounds is the large strain dependent anisotropy of the rare earth ions, the contribution from the Fe, ions being negligible. The magnetostriction of YFe_2, have been measured, it is only $\sim 2 \times 10^{-6}$[3], which indicates the negligible contribution of the iron ions. The magnetostriction of RFe_2 compounds remain large, even at room temperature because of the large rare earth iron exchange interaction which, via the spin orbit interaction couples the angular momentum responsible for the anisotropy energy.

Anisotropy and Magnetostriction will be discussed in more detail in Chapter Two.

Chapter Three will be about the techniques used in measuring magnetostriction and the difficulties experienced, while Chapter Four includes the results and discussion.

CHAPTER II – Magnetostriction

2.1 Introduction:

So far we have broadly defined the phenomena of magnetostriction as a process that alters the dimensions of a body when its magnetization is changed. In this chapter the basic process will be subdivided in a way which will become clear when we attempt a theoretical description at an atomic level. However, before this we know that the measurement technique allows us to divide the effects into linear and volume magnetostriction.

Linear, or joule magnetostriction after its discoverer is the change in the linear dimensions of a magnetic sample at constant external stress that occurs when there is a rearrangement of the magnetic domains. In this process the absolute value of the domain magnetization remains constant. For example, a single crystal sphere in a demagnetized state will become a spheroid in an applied field.

Volume magnetostriction is a general title for the isotropic effects that may occur. The most dominant, usually, is the change in volume when a magnetic material passes through its ordering temperature. In fact this contributes to the thermal expansion and gives an anomolous break expected from the usual Grueisen curve. This arises due to the strain dependence of the exchange field, also, as we shall see in this chapter, there is a volume effect when the domain magnetizations are rotated away from the easy direction and this is due to higher order magnetic interactions between the atomic moments. Finally we shall consider the effects of applied field and sample shape.

2.2 The Anisotropy and Magnetostriction

The Free energy of a magnetically ordered crystal is expressed by Taylor expansion as follows:

$$F = F_0 + F_1 + F_2 + \ldots\ldots \qquad (2\text{–}1)$$

where F_0, F_1, F_2 are terms of Anisotropy, magnetostrictive and elastic energies respectively.

The energy required or in turn stored in the crystal to turn the magnetization vector away from the preferred or easy axis to non-easy axis is called magnetocrystalline anisotropy energy and generally it possesses the symmetry of the crystal.

The term F_0 is independent of strain and it is a function of the direction of magnetization. It is expressed in a power series of the direction cosines α_i of the magnetization vector M_S with respect to the principal axis of the crystal.

The energy expression up to sixth order terms for several crystal symmetries has been calculated by Mason[1].

For cubic crystals the anisotropy energy is:

$$E = K_0 + K_1(\alpha_1^2\alpha_2^2 + \alpha_2^2\alpha_3^2 + \alpha_3^2\alpha_1^2) + K_2(\alpha_1^2\alpha_2^2\alpha_3^2) + \qquad (2\text{–}2)$$

where K_0, K_1, K_2, are the anisotropy constants.

The easy direction of magnetization is determined by both the sign and magnitudes of K_1 and K_2.

The anisotropy energy of a hexagonal crystal may be expressed in polar co-ordinates as:

$$E = K_1 \sin^2\theta + K_2 \sin^4\theta + K_3 \sin^6\theta + K_4 \sin^6 \cos 6\Phi \qquad (2\text{–}3)$$

where Φ is the angle between the projection of the magnetization on the basal plane and the $<1\bar{2}10>$ direction and θ is the angle between the C-axis and the magnetization.

The magnetic anisotropy could result from a combination of spin-orbit coupling and crystal field splitting[2].

In crystals the orbital angular momentum is coupled with both the spin and the lattice. When the spins are rotated by an applied field the orbital moment will rotate with the rotation of the spin magnetic moment due to spin orbit coupling. This will

cause a change in the overlap of the orbitals leading to a change in the coulomb interaction.

In the case of rare-earths the spin orbit coupling is relatively strong compared to the crystal field and J is a good quantum number so we need a large field to rotate the moments from the preferred direction.

The strong coupling of the angular momentum ℓ of the unfilled 4f spin to the low symmetry crystaline electric field gives rise to a large anisotropy of coulomb origin (single ion) [3].

The second term in equation (2–1) is the magnetoelastic part of the free energy

$$E_{magel} = \Sigma\Sigma A_{ij} e_{ij}$$

where e_{ij} are the strain components, and A's are function of the magnetization.

The last term is the elastic energy term, which is for a cubic crystal is given by:

$$E_{el} = \tfrac{1}{2} C_{11} (e^2_{xx} + e^2_{yy} + e^2_{zz}) + \tfrac{1}{2} C_{44} (e^2_{xy} + e^2_{yz} + e^2_{zx}) + C_{12} (e_{yy}e_{zz} + e_{yy}e_{xx} + e_{zz}e_{xx}) \qquad (2–4)$$

where C_{ij} are the elastic moduli constants.

It is aquadratic function of the strain of the crystal. It increases rapidly with increasing strain, so that the equilibrium is attained at some finite strain.

2.3 Mechanism of Magnetostriction

Consider a regular lattice of atomic magnetic moments, and suppose that there are nearest neighbour interactions only. In this case we can formulate the theory according to the pair model of Neel.

According to Neel's theory, when the distance between the atomic magnetic moments is variable, the interaction energy is expressed as:

$$w(r, \cos\Phi) = g(r) + \ell(r)\left(\cos^2\Phi - \frac{1}{3}\right) + q(r)\left(\cos^4\Phi - \frac{6}{7}\cos^2\Phi + \frac{3}{35}\right) + \qquad (2–5)$$

The interaction energy above is expressed by a convenient way using legendre

polynomials. An exactly analogous procedure is often used in electrostatics for an arbitrary charge distribution so that we can separate the effects physically into dipole, quadrupole or multipole interactions. We see that the functional dependence on r may allow a spontaneous lattice distortion if it produces a strain dependence other than the quadratic variation of the elastic energy. In other words we are seeking a value of strain that will minimise the total energy.

The first term g(r) does not depend on the direction of magnetization so it does not contribute to the usual magnetostriction which depends on the direction of magnetization. The term g(r) plays an important role in the production of volume magnetostriction.

The second term is the main origin of the usual magnetostriction. It represents the dipole-dipole interaction, which depends on the direction of magnetization. The other terms also contribute to the usual magnetostriction, but they produce much smaller effects and may be ignored in the first approximations.

If we take the second term only, we can express the pair energy as:

$$w(r, \Phi) = \ell(r)\,(\cos^2\Phi - \frac{1}{3}) \qquad (2\text{–}6)$$

If $(\alpha_1, \alpha_2, \alpha_3)$ denotes the direction cosines of domain magnetization, and $(\gamma_1, \gamma_2, \gamma_3)$ those of the bond direction, we can write (2–6) as

$$w = \ell(r)\ [\ (\alpha_1\gamma_1 + \alpha_2\gamma_2 + \alpha_3\gamma_3)^2 - \frac{1}{3}] \qquad (2\text{–}7)$$

If we consider a deformed simple cubic lattice whose strain tensor components are given by the nine component matrix e_{ij}, i, j = x, y, z. Under this strain each pair changes its bond direction as well as its bond length. For a spin pair with its bond direction parallel to the x-axis has an energy in the unstrained state given by (2–7) with $\gamma_1 = 1, \gamma_2 = \gamma_3 = 0$; that is,

$$wx = \ell(r_0)\,(\alpha_1^{\,2} - \frac{1}{3}) \qquad (2\text{–}8)$$

If the crystal strains, its bond length r_0 will be changed as well as the direction cosines of the bond directions, so the pair energy will be changed.

Adding the changes of the pair energy in the x, y, z directions for all nearest neighbour pairs in a unit volume of a simple cubic lattice, we have

$$E_{magel} = B_1 \left[e_{xx}(\alpha_1^2 - \frac{1}{3}) + e_{yy}(\alpha_2^2 - \frac{1}{3}) + e_{zz}(\alpha_3^2 - \frac{1}{3}) \right] + B_2 (e_{xy}\alpha_1\alpha_2 + e_{yz}\alpha_2\alpha_3 + e_{zz}\alpha_3\alpha_1) \qquad (2-9)$$

$$B_1 = N \left(\frac{\partial \ell}{\partial r}\right) r_0 \ , \ B_2 = 2N\ell$$

Equation (2–9) tells us that the magnetoelastic energy is a linear function with respect to e_{xx}, e_{yy}, ... e_{zz}, and the crystal will deform without limit unless it is counter balanced by the elastic energy which for a cubic crystal is given by:

$$E_{el} = \tfrac{1}{2} C_{11} (e^2_{xx} + e^2_{yy} + e^2_{zz}) + \tfrac{1}{2} C_{44} (e^2_{xy} + e^2_{yz} + e^2_{zx}) + C_{12} (e_{yy} e_{zz} + e_{yy} e_{xx} + e_{xx}) \qquad (2-10)$$

where C_{11}, C_{44}, C_{12} are the elastic moduli.

By looking at equation (2–10) we can see that the elastic energy is a quadratic function of the strain of the crystal and consequently will increase rapidly for positive or negative strains.

So we got the total energy $E = E_{magel} + E_{el}$

To find the strains e_{ij} we have to minimise the total energy by differentiating with respect to the strain and setting it equal to zero, then by solving it we obtain:

$$e_{xx} = -\frac{B_1}{C_{11} - C_{12}} (\alpha_1^2 - \frac{1}{3})$$

$$e_{yy} = -\frac{B_1}{C_{11} - C_{12}} (\alpha_2^2 - \frac{1}{3})$$

$$e_{zz} = -\frac{B_1}{C_{11} - C_{12}} (\alpha_3^2 - \frac{1}{3}) \qquad (2-11)$$

$$e_{xy} = -\frac{B_2}{C_{44}}\alpha_1\alpha_2$$

$$e_{yz} = -\frac{B_2}{C_{44}}\alpha_2\alpha_3$$

$$e_{zx} = -\frac{B_2}{C_{44}}\alpha_3\alpha_1$$

The elongation along a direction with directions cosines $(\beta_1, \beta_2, \beta_3)$ is given by:

$$\frac{\delta\ell}{\ell} = e_{xx}\beta_1^2 + e_{yy}\beta_2^2 + e_{zz}\beta_3^2 + e_{xy}\beta_1\beta_2 + e_{yz}\beta_2\beta_3 + e_{zx}\beta_3\beta_1 \qquad (2-12)$$

Substituting (2–11) into (2–12) we get:

$$\frac{\delta\ell}{\ell} = -\frac{B_1}{C_{11}-C_{12}}(\alpha_1^2\beta_1^2 + \alpha_2^2\beta_2^2 + \alpha_3^2\beta_3^2 - \frac{1}{3}) - \frac{B_2}{C_{44}}(\alpha_1\alpha_2\beta_1\beta_2 + \alpha_2\alpha_3\beta_2\beta_3 + \alpha_3\alpha_1\beta_3\beta_1) \qquad (2-13)$$

If the domain magnetization is along [100] then the elongation along (100) is given by

$$\lambda 100 = -\frac{2}{3}\frac{B_1}{C_{11}-C_{12}} \qquad (2-13)$$

Similarly for [111], by putting $\alpha_i = \beta_i = \frac{1}{\sqrt{3}}$ $(i = 1, 2, 3)$ we get:

$$\lambda 111 = -\frac{1}{3}\frac{B_2}{C_{44}} \qquad (2-14)$$

So equation (2–13) becomes if we utilize expressions (2–13) and (2–14),

$$\frac{\delta\ell}{\ell} = \frac{3}{2}\lambda 100\left[(\alpha_1^2\beta_1^2 + \alpha_2^2\beta_2^2 + \alpha_3^2\beta_3^2) - \frac{1}{3}\right] + 3\lambda 111\,(\alpha_1\alpha_2\beta_1\beta_2 + \alpha_2\alpha_3\beta_2\beta_3 + \alpha_3\alpha_1\beta_3\beta_1) \qquad (2-15)$$

For isotropic magnetostriction $\lambda 100 = \lambda 111 = \lambda$

$$\frac{\delta\ell}{\ell} = \frac{3}{2}\lambda\left[(\alpha_1\beta_1 + \alpha_2\beta_2 + \alpha_3\beta_3)^2 - \frac{1}{3}\right] = \frac{3}{2}\lambda\left(\cos^2\theta - \frac{1}{3}\right) \qquad (2-16)$$

where θ is the angle between the measuring and magnetization directions and describes

the distortion of a single crystal sphere discussed in the introduction

For a polycrystalline sample the longitudinal magnetostriction is calculated by averaging eq. (2–15) for different crystalline orientations by assuming:

$$\alpha_i = \beta_i \quad (i = 1, 2 \text{ and } 3)$$

$$\text{Thus } \bar{\lambda} = \frac{2}{5}\lambda 100 + \frac{3}{5}\lambda 111 \tag{2–17}$$

In the previous calculations we considered only the dipole-dipole interaction term. Now if we consider the third term of equation (2–5) we get a much more precise expression for the magnetostriction as given below:

$$\begin{aligned}\frac{\delta \ell}{\ell} = {} & h_1\left((\alpha_1^2\beta_1^2 + \alpha_2^2\beta_2^2 + \alpha_3^2\beta_3^2) - \frac{1}{3}\right) + h_2(2\alpha_1\alpha_2\beta_1\beta_2 + 2\alpha_2\alpha_3\beta_2\beta_3 + \\ & 2\alpha_3\alpha_1\beta_3\beta_1) + h_4(\alpha_1^4\beta_1^2 + \alpha_3^4\beta_3^2 + \frac{2}{3}S - \frac{1}{3}) + h_5(2\alpha_1\alpha_2\alpha_3^2\beta_1\beta_2 + \\ & 2\alpha_2\alpha_3\beta_2\beta_3 + 2\alpha_3\alpha_1\alpha_2^2\beta_3\beta_1) + h_3(S - \frac{1}{3}) \quad \text{for } k_1 > 0 \\ & + h_3(S) \qquad \text{for } k_1 < 0\end{aligned} \tag{2–18}$$

$$s = \alpha_1^2\alpha_2^2 + \alpha_2^2\alpha_3^2 + \alpha_3^2\alpha_1^2 \;,\; h_1 = \frac{3}{2}\lambda 100 \;,\; h_2 = \frac{3\lambda 111}{2}$$

2.4 Volume Magnetostriction

To find the change in the volume of a specimen when it is magnetized, we have to consider the strains e_{xx}, e_{yy}, e_{zz} only, where the fractional change of the volume is expressed in terms of strain tensor components as:

$$\frac{\delta V}{V} = (e_{xx} + e_{yy} + e_{zz}) \tag{2–19}$$

By substituting the values found from minimising the total energy which involves the dipole interaction only, we find that $\frac{\partial V}{V} = 0$, consequently the first approximation, a rotation of the magnetization does not give rise to any volume magnetostriction.

Now if we include the next higher order term of equation (2–5), which is the

quadrupole interaction term, $q(r)\,(\cos^4\Phi - \frac{6}{7}\cos^2\Phi - \frac{3}{35})$, we find that

$$\frac{\Delta V}{V} = e_{xx} + e_{yy} + e_{zz} = \frac{2N(\frac{\partial q}{\partial r})_{r_0}}{C_{11} + 2C_{12}} (\alpha_1^2\alpha_2^2 + \alpha_2^2\alpha_3^2 + \alpha_3^2\alpha_1^2 - \frac{1}{5}) \quad (2-20)$$

This volume magnetostriction is attributed to the rotation of the magnetization against the crystal anisotropy and is called the crystal effect. So, as we rotate the magnetic moment by external field, the volume will change by small amounts.

2.5 Exchange Magnetostriction:

This is different effect to the previous volume magnetostriction. It refers to the change in volume when the materials becomes magnetically ordered because of the first term of equation (2–5), which is the exchange interaction term g(r). This term g(r) is isotropic and independent of magnetization direction.

The atomic moments begin to align below the ordering temperature and the interaction energy at the atomic site may be expressed in terms of a molecular field within the material, and this is represented by the isotropic term g(r). Hence, the energy independent of magnetization direction is:

$$w = g(r_0) \quad (2-21)$$

Now if the bond length changes due to crystal strains e_{ij}, we can write the new energy, say for a bond pair, along the [100] direction of a simple cubic lattice as:

$$w + \Delta w = g(r_0 + r_0 e_{xx}) = g(r_0) + r_0 e_{xx} (\frac{\partial g}{\partial r})_{r_0} \quad (2-22)$$

$\Delta w = r_0 e_{xx} (\frac{\partial g}{\partial r})$, or for all bond pairs in the [100], [010] and [001] directions:

$$\Delta w_{total} = r_0 (\frac{\partial g}{\partial r}) (e_{xx} + e_{yy} + e_{zz}) \quad (2-23)$$

And hence for N pairs per unit volume of the material gives the magnetoelastic interaction energy as:-

$$Nr_0 \left(\frac{\partial g}{\partial r}\right)\left(e_{xx} + e_{yy} + e_{zz}\right) = E_{magel} \qquad (2-24)$$

Now we have energy change proportional to the strain we find the total energy change due to crystal strains:

$$\text{Total energy} = E_{magel} + E_{elastic}$$

As before $E_{elastic} = \frac{1}{2} C_{11}(e_{xx^2} + e_{yy^2} + e_{zz^2}) + C_{12}(e_{yy}e_{zz} + e_{yy}e_{xx} + e_{zz}e_{xx})$

And that is for axial strain only.

$$E_T = Nr_0 \left(\frac{\partial g}{\partial r}\right)\left(e_{xx} + e_{yy} + e_{zz}\right) + \tfrac{1}{2} C_{11}(e^2_{xx} + e^2_{yy} + e^2_{zz}) +$$

$$C_{12}(e_{yy}e_{zz} + e_{yy}e_{xx} + e_{zz}e_{xx}).$$

Again we minimise the expression with respect to the individual strain components:

$$\frac{\partial E_T}{\partial e_{xx}} = N r_0 \left(\frac{\partial g}{\partial r}\right) + C_{11}\, e_{xx} + C_{12}\,(e_{yy} + e_{zz}) = 0$$

$$\frac{\partial E_T}{\partial e_{yy}} = N r_0 \left(\frac{\partial g}{\partial r}\right) + C_{11}\, e_{yy} + C_{12}\,(e_{xx} + e_{zz}) = 0 \qquad (2-25)$$

$$\frac{\partial E_T}{\partial e_{zz}} = N r_0 \left(\frac{\partial g}{\partial r}\right) + C_{11}\, e_{zz} + C_{12}\,(e_{xx} + e_{yy}) = 0$$

Solving for $\frac{\Delta V}{V} = (e_{xx} + e_{yy} + e_{zz})$ we have:-

$$\frac{\Delta V}{V} = \frac{3 N r_0 \left(\frac{\partial g}{\partial r}\right)}{C_{11} + 2C_{12}} \qquad (2-26)$$

Equation (2–26) tells us that the volume change is independent of magnetization directions but it depends on $\left(\frac{\partial g}{\partial r}\right)$, the strain dependence of the molecular field. So we need a strain dependent molecular field, that is if $\left(\frac{\partial g}{\partial r}\right) \neq 0$ then there is an extra energy term proportional to the strain which will produce a spontaneous volume distortion.

2.6 Forced Magnetostriction and Form Effect

In a magnetically ordered material the magnetic moment will usually vibrate about a mean position, and the average value of the moment will depend on the temperature and the applied field. When the material subjected to an increasing applied field, a field strength will be reached where all the domains are aligned parallel to the field. This is sometimes called "Technical Saturation".

A further increase in the magnetic field will align the individual atomic moments against their thermal motion. This result is an additional "paramagnetic" increase of the magnetic moment until at infinite field strength the ultimate saturation is obtained. Then the magnetization is equal to the Technical Saturation magnetization at absolute zero. These paramagnetic magnetization processes are accompanied by a volume effect called "forced magnetostriction".

The isotropic term g(r) in the energy expression depends on the value of the molecular field and hence it will be affected by an applied field, more strictly we are concerned with the strain dependence of the molecular field and if this changes with applied field we shall observe a change in the volume strain.

We can go in further insight into the origin of this effect from the quantum mechanical viewpoint. The degenerate angular momentum states of the free rare-earth ion are split by both the molecular and crystal fields in the solid, the amount can be calculated from perturbation theory. In fact one can use strain dependent perturbation Hamiltonian in direct anology to Neel's theory to find the lattice distortions in terms of the crystal field parameters. The application of an external field will cause not only a change in the energy separation of the crystal field levels but also it will affect the mixing of the original ionic wavefunctions. In other words the strain dependence of the individual energy levels are

affected and consequently the thermally averaged energy at the rare-earth site will minimise to a slightly different strain value. This is termed forced magnetostriction and results from a purification of the energy levels.

Finally, there is also another effect called "the form effect" which can also influence the volume magnetostriction. When a magnetically ordered material is magnetized in an external field Hc its magnetic poles will interact with each other and with external field resulting in a change in volume and shape. This effect depends on the shape of the body. So this time there is a minimisation of the energy of a finite sample with respect to changes in its demagnetizing factors.

For an ellipsoidal sample it produces a volume strain quadratic in the magnetization.

2.7 The dependence of magnetostriction on temperature

One way of treating the temperature dependence of the anisotropy coefficients is to study the effect of the crystal field Hamiltonian of a finite temperature. This Hamiltonian can be treated as perturbation on the ground state of the magnetic ion, and represents the effects of the surrounding electrostatic charges on its 4F electrons. The potential energy of this interaction may conveniently be expanded in terms of either spherical or tesseral harmonics to represent the monopole, dipole, quadrupole etc., energy terms. This can be then expressed directly as a Hamiltonian by replacing all co-ordinates by their corresponding operators ie. $x \rightarrow \hat{x}$, $y \rightarrow \hat{y}$, $z \rightarrow \hat{z}$. However, the evaluation of the matrix elements using the Hamiltonian in this form is extremely complicated as it involves finding first the appropriate ionic wave function and then performing an all space integral. To avoid this Stevens has recognised [4] that the Wigner-Eckhart theorem allows the co-ordinate operators to be replaced by angular momentum operators and a proportionality constant, this is a property of irreducible tensor operators. This indeed

reduces the labour of finding the matrix elements since the basis set of wave functions are labelled by the quantum numbers J and J_z. In fact Stevens calculates numerical values for the possible matrix elements of different operators so even the problem of finding the ionic wave function in terms of the single electron determinental wave function is removed. At zero degrees Kelvin the matrix elements are derived in terms of the total angular momentum operator $\hat{J}^2$ and the quantized angular momentum operator $\hat{J}_z$. For example the crystal field Hamiltonian for a cubic co-ordination with [100] quantization is:

$$\mathcal{H} = B_4^0 (O_4^0 + 5O_6^4) + B_6^0 (O_6^0 - 21O_6^4) \qquad (2-27)$$

where B_n^m numerical coefficients

O_n^m Stevens operators.

In fact this is the quantum mechanical analogy of the pair model energy expression used in the previous treatment of magnetostriction.

At finite temperatures the value of the quantized angular momentum J_z will be a thermal average proportional to the induced magnetization. Thus Stevens operators, which are expressed in powers of $\hat{J}^2$ and $\hat{J}_z$ will now have a dependence on the reduced magnetization on which at low temperatures takes the convenient form of:

$$O_n^0 (T) = O_n^0 (O) M^{\frac{n(n+1)}{2}} \qquad (2-28)$$

The $O_n^0 (T)$ operators may be related to the usual anisotropy coefficients by expanding in terms of spherical harmonics. However we can see, for example, that the anisotropy determined by $B_4^0 O_4^0$ will be renormalised as $m^{\frac{4(4+1)}{2}} = m^{10}$. So in summary the final temperature dependence of the anisotropy energy depends on the relative magnitudes of the crystal field Hamiltonian terms.

Callen and Callen [6] and Callen and Shtrikman[7] have shown that the temperature

dependence of the magnetostriction follows the well known $m^{\frac{n(n+1)}{2}}$ power law for magnetic anisotropy[11] at low temperatures and the normalized hyperbolic Bessel function $\hat{I}_{n+1/2}(\mathcal{L}^{-1}(m))$ in the molecular field approximation at all temperatures. Here m is the reduced magnetic moment, $\mathcal{L}^{-1}(m)$ is the inverse langevin function, and n is the order of the spin operator in the magnetoelastic Hamiltonian. At low temperatures the hyperbolic Bessel function reduces to the power law.

CHAPTER III – The Measurement of Magnetostriction in Pulsed Magnetic Fields

3.1 Historical notes on high magnetic fields:

The history of the generation of magnetic fields is as interesting and exciting as that of any scientific development. It can be traced back to ancient Greece. The word 'magnet' in fact is derived from the name of the ancient town of Magnes (today Manissa near Smirne, Turkey), where a large deposit of lodstone was discovered. The peculiar properties of this material, such as attracting iron, became known as magnetism, and remained a curiosity for centuries.

In the pioneering first half of the 19th century, it became possible to study magnetic phenomena more systematically. It began with Oersteds discovery in 1819 that a compass needle is deflected if placed near a current carrying conductor. In 1820, Ampere extended both experimentally and theoretically the understanding of magnetic effects related to electric currents. For this work he can be considered the 'father' of the electromagnet. One year later (1821) Michael Faraday showed that "the rotation of a current around a magnet and a rotation of a magnet around a current are analogous". Ten years later he described the law of induction and introduced the concept of the magnetic field. In 1873, James Clerk Maxwell published "Treatise on electricity and magnetism". In 1898 Ch. Fabry[1] theoretically investigates the efficiency of air-cored galvanometer coils, and in 1914 H. Destandres and A. Perot produced a field of 50 KOe in about 4 cm^3 during many minutes by using for the first time, a watercooled, iron-free magnet[2] [3] [4].

P.L. Kapatiza[5] in 1924 discussed various methods of producing pulsed high magnetic fields. His experiments based on the use of an accumulator battery[6] and later of a motor generator[7]. T.F. Wall in 1926 used a capacitor bank of 3 KJ, 4KV to produce 200 KOe in 0.2 cm^3 with a multiturn solenoid.

More recently,[8] developments in the techniques of construction of large storage capacitors have enabled these to become the cheapest and simplest means of storing the electrical energy required to produce intense magnetic fields of short duration. Pulsed high magnetic fields are being used more and more in the laboratory. One reason is that pulsed fields can generally be produced much more easily than continuous ones, and modern time-resolved diagnostic techniques allow one to work in pulsed operation without difficulty. In fact the main point of using this technique is to get very high magnetic fields that is up to hundred Tesla. The cooling cost has limited the production of continuous fields to about 25 Tesla.

In pulsed systems, the magnet in almost adiabatic conditions, the total energy dissipated during the pulse is small enough to keep the final temperature of the magnet in the tolerable limits at much higher field levels. However, the total amount of dissipated energy has to be kept below the maximum amount that the coil can contain without damage.

Pulsed fields in a range of multi-hundreds of Tesla have been achieved by using explosive methods. In 1960, C.M. Fowler, W.B. Garn, and R.S. Caird published the first extensive paper on explosively generated megaoersted fields[9]. Now the countries which have (in 1969) their own explosive facilities for producing ultra high magnetic fields are U.S.A., U.S.S.R., and Italy.

3.2 The Pulsed Field Apparatus:

The system used in this work was that developed by McKinnon[10], Melville[11] and later modified by Mattocks[12], consisting of a 2.1×10^{-3} f capacitor bank for energy storage together with the necessary charging and discharging circuits[12]. The capacitor bank can be charged up to 6 KV. By triggering an electronic switch, the capacitor bank

is connected through an ignition to a wire wound solenoid. The current varies in the damped sinusoidal form associated with an RLC circuit. When the current is near its maximum value another ignition short circuits the coil (Fig. (3 – 1a)). This is the clamping process, so that the current (and the magnetic field which is proportional to it) decays exponentially to zero in a time depending mainly on the resistance of the coil (Fig. (3 – 1b)).

The equation representing the behaviour of the discharging circuit in terms of current, i, at time, t, is:

$$L\frac{di}{dt} + iR + \int_0^t \frac{idt}{c} = 0 \qquad (3-1)$$

At time t = 0, the capacitor bank with stored energy ½ CV^2, is connected to the coil.

With the boundary conditions of i being zero, and C being charged to a voltage, v, when t = 0, the solution for i is:

$$i = \frac{v}{L} e^{-tR/zL} \frac{\sin wt}{w} \qquad (3-2)$$

where $$w = \sqrt{\frac{1}{LC} - \frac{R^2}{4L^2}} \qquad (3-3)$$

$$w = (LC)^{-½} - (1 - d)^{½} \qquad (3-4)$$

where $d = \frac{R^2 C}{4L}$, and is called the damping constant.

If $d < 1$, w is real and the current i oscillates as a function of time.

If $d > 1$, w is imaginary and the current rises to a maximum and decreases to zero again without becoming negative.

If the coil is short-circuited at time $t = \frac{\tau}{2} (\tau \triangleq \frac{\pi}{w})$, when the voltage across the coil is zero, the capacitor is thus ineffective and the current in the coil decays exponentially in accord with the relationship:

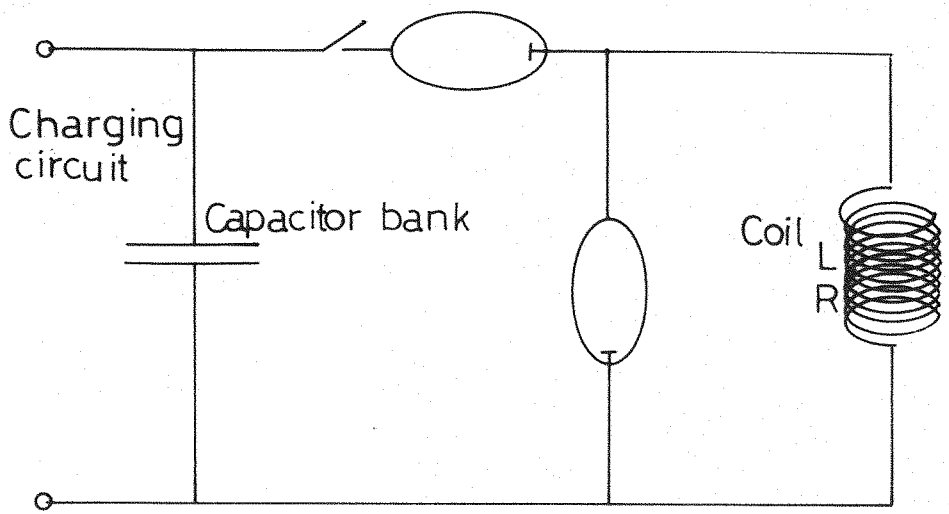

Fig. 3.1a The Capacitor discharge circuit.

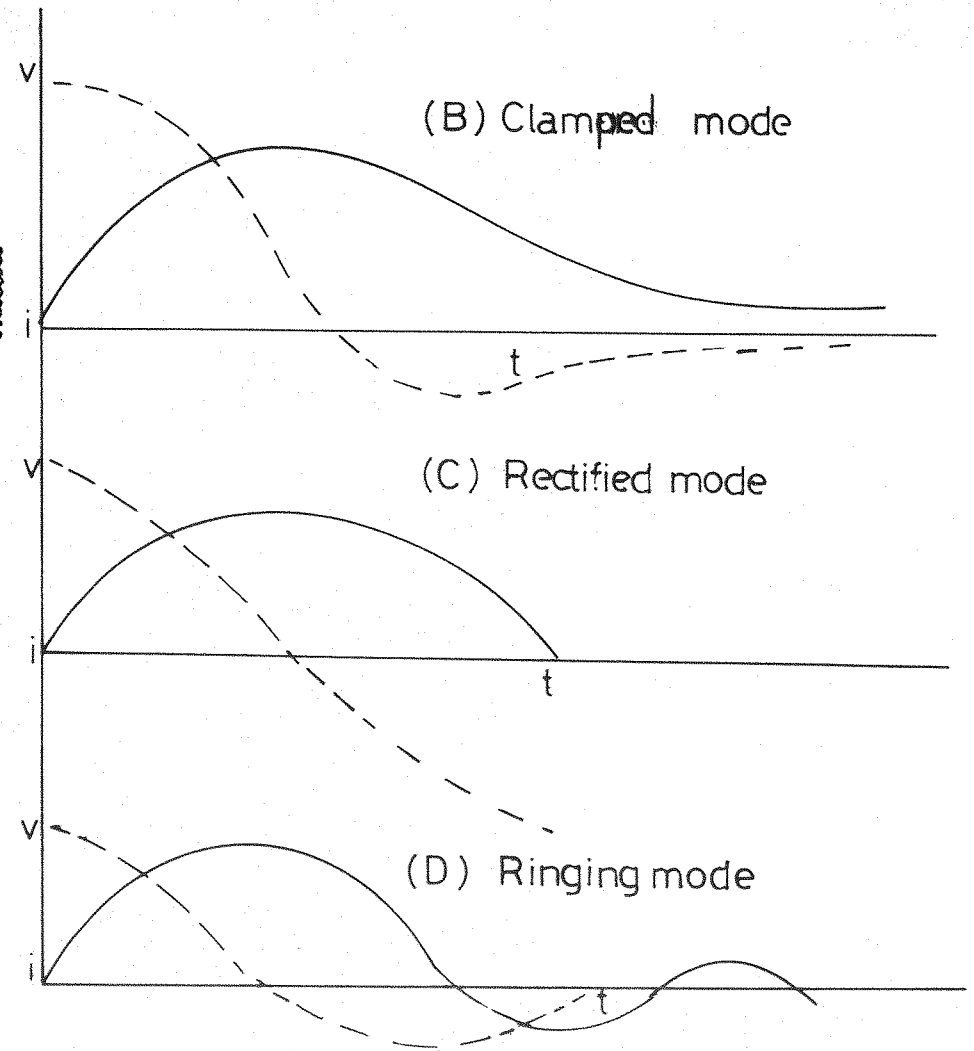

Fig. 3.1 The RLC and the current and voltage wave forms for the three modes of operation of a pulsed discharge circuit.

$$i = i_{\tau/2}\, e^{-\frac{Rt}{L}} \qquad (3-5)$$

and the voltage across the coil remains zero. The circuit is then said to be clamped.The second mode occurs when the circuit is not clamped and the main discharge switches are ignitrons (Fig. (3–1c)). The current and the voltage waveforms are shown in Fig. (3–1d) .

3.3 The Cryostat and the Vacuum system:

The Cryostat used in this work is that constructed by McKinnon[10], Melville[11] and later modified by Mattocks[12]. It has a narrow tail enabling it to be inserted into the base of a solenoid while the body is designed so that it can contain enough liquid gases for the experimental purposes.

The specimen chamber is a 10 mm. O.D. german silver tube with access from the top. This isolates the specimen and is supported from the refrigerant chamber which has a capacity of 300 ml. It is terminated at its lower end by a 12 mm. exhaust tube, concentric with the specimen chamber, while the liquified gases may be introduced via the 4 mm. vacuum jacketed tube leading off to the right. The whole of the cryostat is surrounded by a vacuum tight jacket.

The specimen, heater, and pick up coil are supported by a german silver rod connected to the hat-shaped chamber which, sealed by an 'O' ring, sits on the top of the cryostat.

Figure (3–3) shows the parts of the cryostat and the vacuum system in more detail.

3.4 The Specimen holder and specimen positioning:

Great care is required in the design of the specimen holder and its position inside the cryostat. To eliminate the eddy currents effects in the specimen holder, it had to be made from non-conducting materials. As shown in Fig. (3–3), the transducer assembly is simply

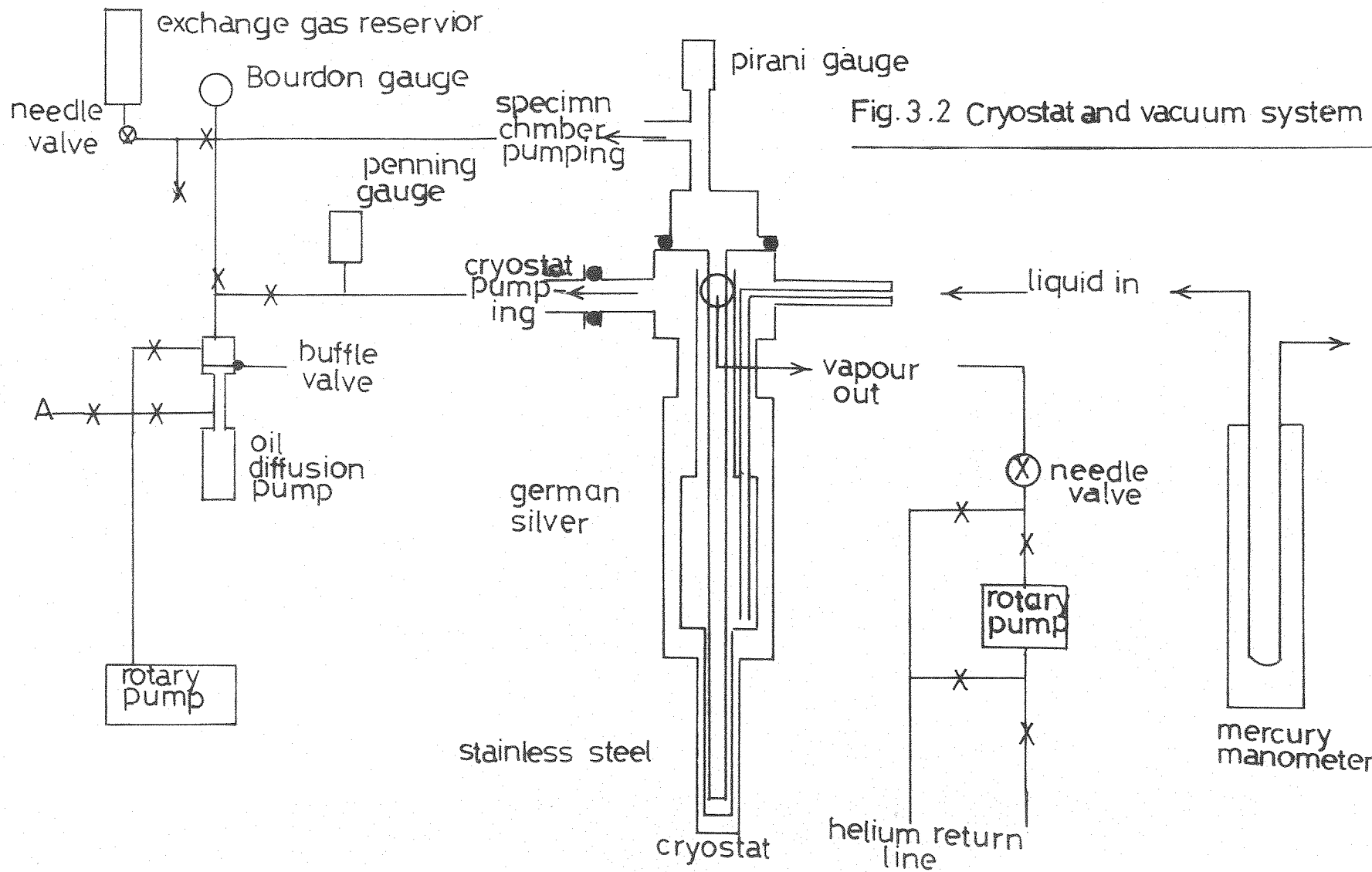

Fig. 3.2 Cryostat and vacuum system

a german silver tube of about 7 mm. diameter connected to the hat-shaped chamber which forms the cryostat head.

The cables and the thermocouple have to pass through this tube down to the transducer. They have to be screened so as to minimize pick-up.

The specimen holder is situated at the end of this tube, it contains the heater, search coil (for measuring the magnetic field) and the specimen with the strain gauge bonded on it (a dummy gauge was also used in most cases).

The upper part of the specimen holder is made of PTFE material which is not conductor, so that no eddy current problem arises. The lower part of the holder (where the sample and the search coil are situated) is made of tufnol because it is more rigid than PTFE, and is also not a conductor.

The homogeneity of the magnetic field near the centre of the coil can be found from the work of Milville [11]. W–3 is the coil which is used in this work. Table (3–1) gives the characteristics of this coil.

At 5 mm. away from the middle of the coil, the field is only 1% lower than at the centre. The radial variation of the field is less than 1% in the space inside the windings. The search coil and the specimen have to be in this region to avoid problems associated with a field gradient. For magnetostriction measurements on ferromagnetic materials, such a field gradient gives rise to a force able to displace the specimen holder which could induce capacitance changes in the strain gauge leads. Also it interacts with eddy currents. Thus it may effect the accuracy of the measurement, Figure (3–3a) shows the specimen holder design. Figure (3–3b) is the transducer assembly photograph.

3.5 The measuring system:

Figure (3–3c) shows the block diagram of the measuring system. The aim of the

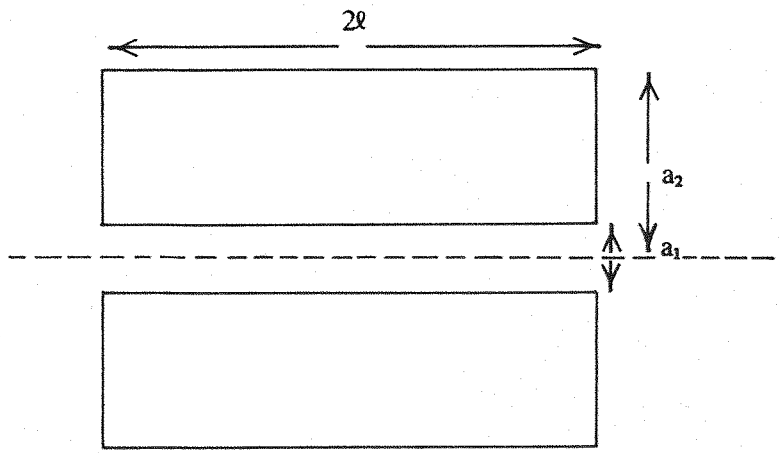

TABLE (3–1)

β	=	3.75		J	= 0.8946
α	=	4.59		s	= 0.421
N	=	560.9		B_{max}	= 16.69 Tesla
λ	=	1.9139×10^{-2}		I_{max}	= 1.7721×10^{3} amp
Ψ	=	29.34			
R/L	=	41.84	henry/ohm	v	= 169.458×10^{-6} m^3
L	=	4.8171×10^{-3}	henry	R	= 0.202 Ω
σ	=	1.0014×10^{-2}	sec	ΔT	= 10.2 K
				maximum voltage	= 3KV

$$\alpha = \frac{a_2}{a_1}$$

$$\beta = \frac{\ell}{a_1}$$

coil parameters

The Characteristics of Coil $w_3{}^{11}$,(calculated values)

experiment is to measure $\Delta R/R$, the relative change of resistance of the gauge, induced by a strain. A type Q-plug in unit was used for this purpose. It is an A.C. bridge with a 25 KHZ carrier[13]. It is made to be operated with strain gauges and other transducers. Excitation voltages for the strain gauge are provided by the plug-in unit. The output of the bridge can be calibrated for a finite amount of bridge unbalance by operating a calibration switch incorporated in the calibration circuit. (See section (3–12) for more details).

In figure (3–3c), a strain gauge is connected to one arm of the A.C. bridge. Stretching or compressing the strain gauge (depending on whether it is positive or negative magnetostriction) gives unbalance in the A.C. bridge. The output signal is an amplitude modulation of the 25 KHZ carrier. This signal is applied to an ac-coupled amplifier where the desired sidebands are amplified while unwanted frequencies are rejected. It is then applied to a phase sensitive demodulator which separates the carrier and the modulation envelope. The signal is filtered, amplified and then applied to the deflection paltes of the oscilloscope.

The field signal from the search coil, situated in the centre of the solenoid, was integrated and then amplified or attenuated by using a type O plug-in unit in the oscilloscope. Figure (3–3d) shows the integrating circuit.

Both the strain signal and the field signal were fed to two separate channels of a Datalab Unimac System (The Unimac will be described below). The two signals stored in the Unimac can be plotted out using a Farnell XY-recorder.

To increase the accuracy of the measuring technique, a digital microprocessor was used to record the data in preference to the existing method of photography oscilloscope traces. A Datalab Unimac/DL 450 microprocessing system was used. It is a modular

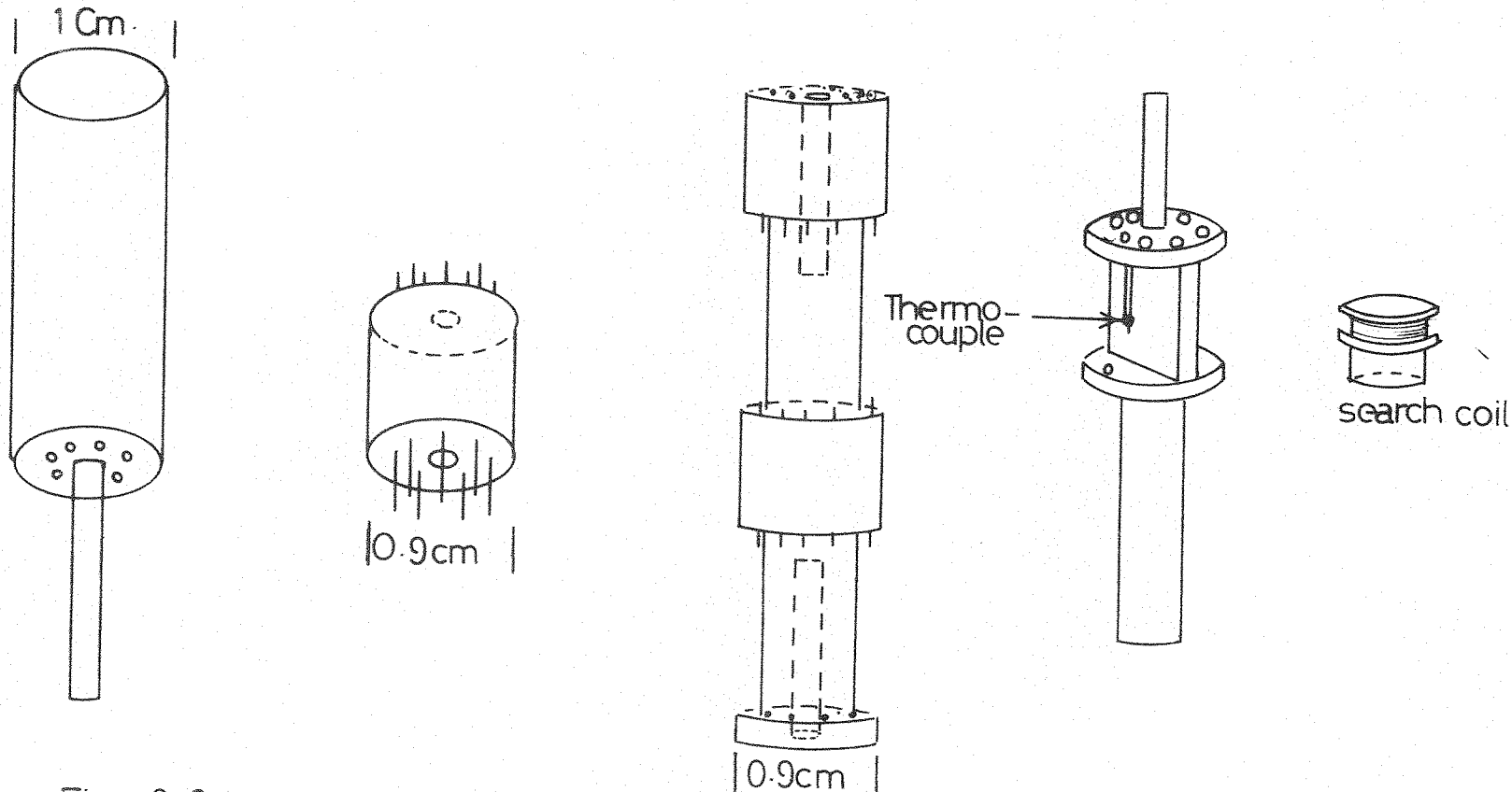

Fig. 3·3a

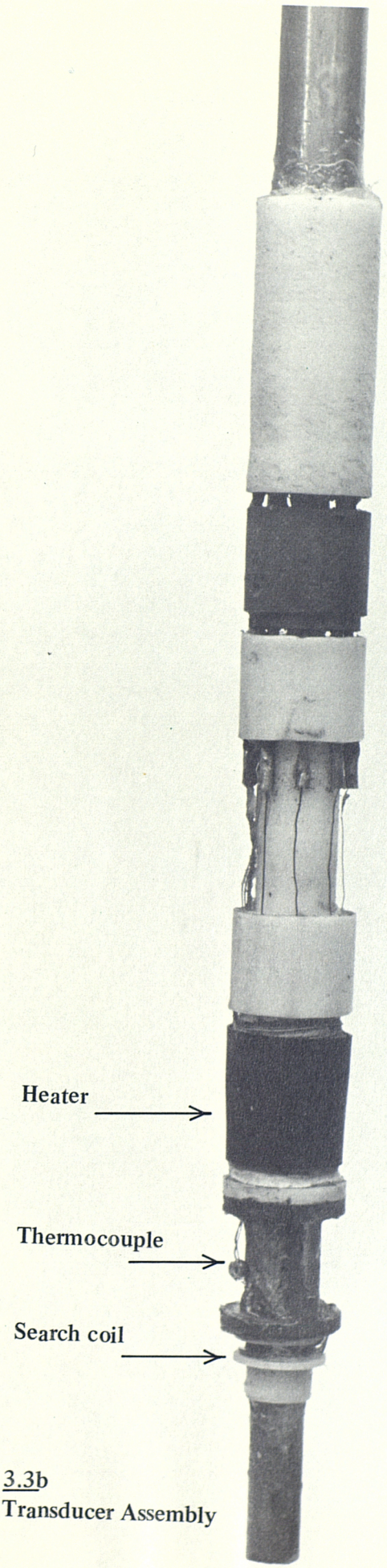

Fig. 3.3b
The Transducer Assembly

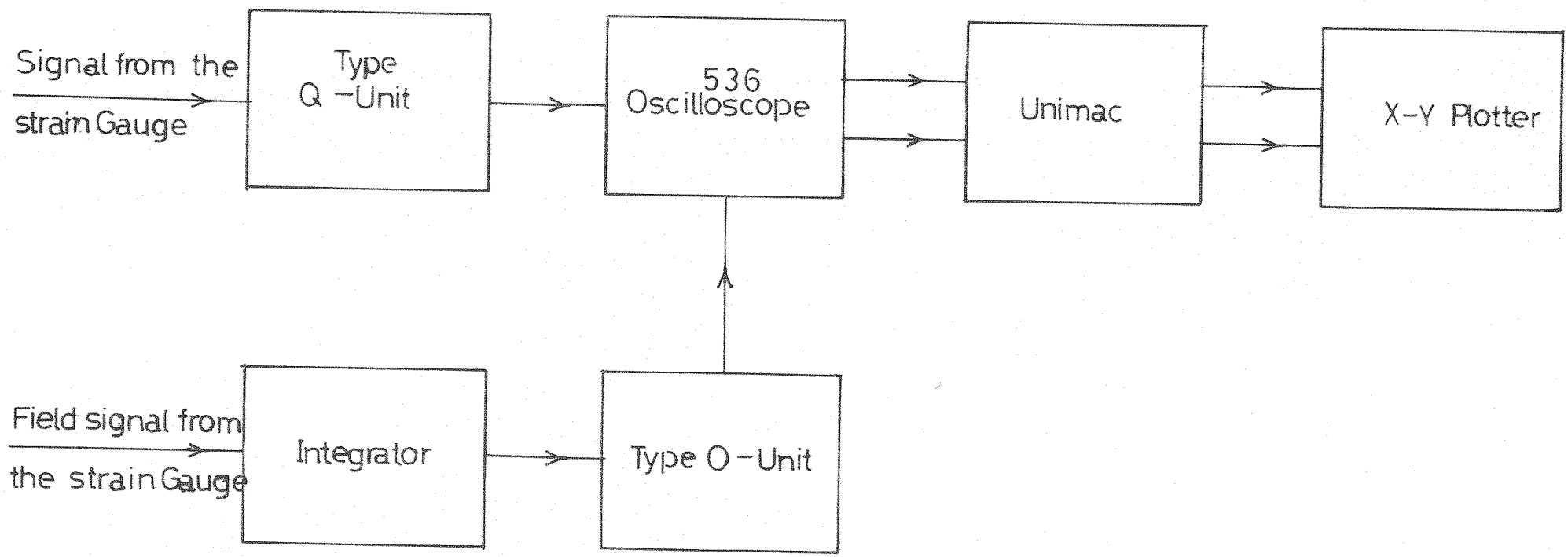

Fig. 3.3c The block diagram of the measuring system

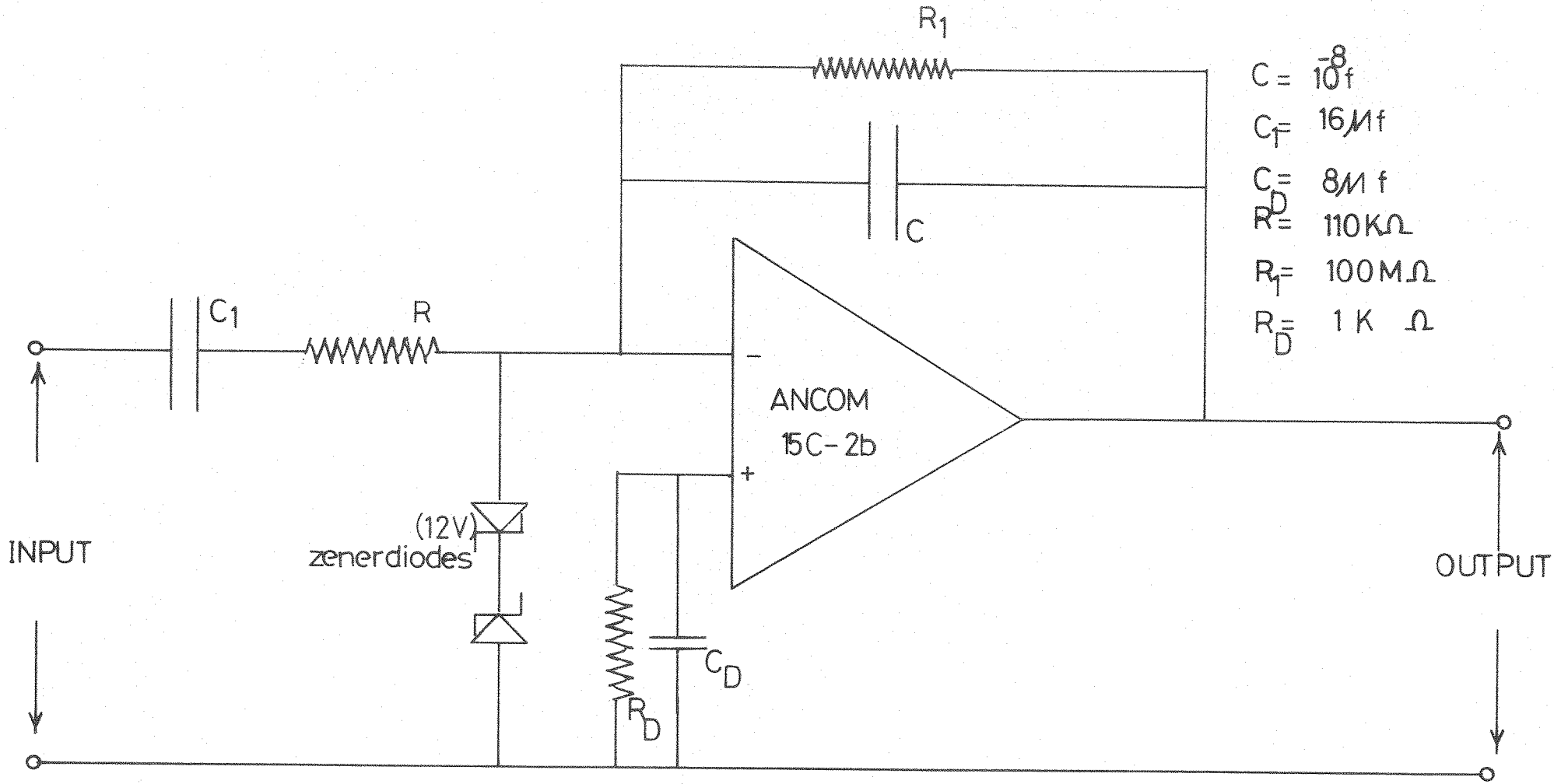

Fig. 3.3d The integrating circuit

system consisting of two parts: an on-line signal analysis crate and the microprocessor proper, the later incorporating a small oscilloscope display.

The signal analysis crate contains 2 channel signal conditioning amplifier, an analyser crate containing the ADC, a sweep timer, a display module, a 1024 word store and an interface to the DL 450 microprocessor. It can accept up to 4 signals simultaneously and these are multiplexed at a rate determined by the setting up of the sweep timer (minimum intersample time is 10 μs). The resolution is adjustable, being 8, 10 or 12 bits. The sweep timer can be used in a pretrigger mode so that pretrigger information can be stored and in this work it was found to be particularly useful. Another useful facility, was the displaying of one half of the memory against the other, so that magnetostriction versus magnetic field curves could be plotted directly.

The DL 450 microprocessor manipulates the information stored in the memory. It contains programmes which enable addition, multiplication, integration, differentiation and 3 point smoothing processes to be carried out on any part of the memory ; different signals can also be compared, added together, multiplied, etc. The memory contents are displayed on the oscilloscope screen together with an alphanumeric display, from which the desired data can be read by the use of a cursor. This was used to obtain peak heights, etc. and a permanent record of a curve could be made using an XY plotter.

3.6 The Problems involved in carrying out pulsed field magnetostriction measurements:

3.6.1 Introduction: Magnetostriction measurements in high pulsed magnetic fields involve many difficulties. The fact that we are using a time varying magnetic field creates a number of problems. For example, eddy currents in the sample, pick up in various parts of the apparatus, especially the specimen holder, magnetoresistance in the strain gauges, and mechanical noise, which tends to move the cryostat. Consequently great care must

be taken in designing the specimen holder.

The pick up, mechanical noise and magnetoresistance are explained in this section in detail while the eddy current is explained in section (3.6.2).

(i) **Pick up in the Q-unit**: The most serious problem encountered was stray pick up by the Q-unit which is plugged in to the oscilloscope. This pick up which is due to coupling between the pulsed magnetic field and the Q-unit gives rise to an additional signal of up to 20% of the whole signal. This additional signal increases as the oscilloscope is brought nearer to the coil, following approximately the law $1/r^3$ (r is the distance between the oscilloscope and the coil). Therefore in this work the measurements had to be done with the measuring system far away from the coil, (about four metres). Figure (3–4a) shows the unclamped field signal after it has been integrated. Figure (3–4b) shows the pick up signal by the Q-unit which is recorded during the pulse while there was no direct input to the Q-unit. The sign of this pick up signal changes by reversing the direction of the magnetic field (Fig. (3–4c)). Figure (3–4d) shows the loop obtained with a plot of pick up signal against the field.

Figure (3–5a) is the field signal while Fig. (3–5b) is the strain signal, λII, of the $TbFe_2$ compound (λII is the strain measured in the direction parallel to the field). It can be seen from Fig. (3–5b) that the pick up signal by the Q-unit adds to the first half of the strain signal while it is subtracted from the second half.

Figure (3–5c) is the strain signal when the direction of the magnetic field has been reversed. In this case the pick up signal subtracts from the first half of the strain signal and it adds to the second half.

Figure (3–6c) shows the loop obtained with a plot of the parallel magnetostriction against the field. Figure (3–7a) is the longitudinal magnetostriction signal of $TbFe_2$

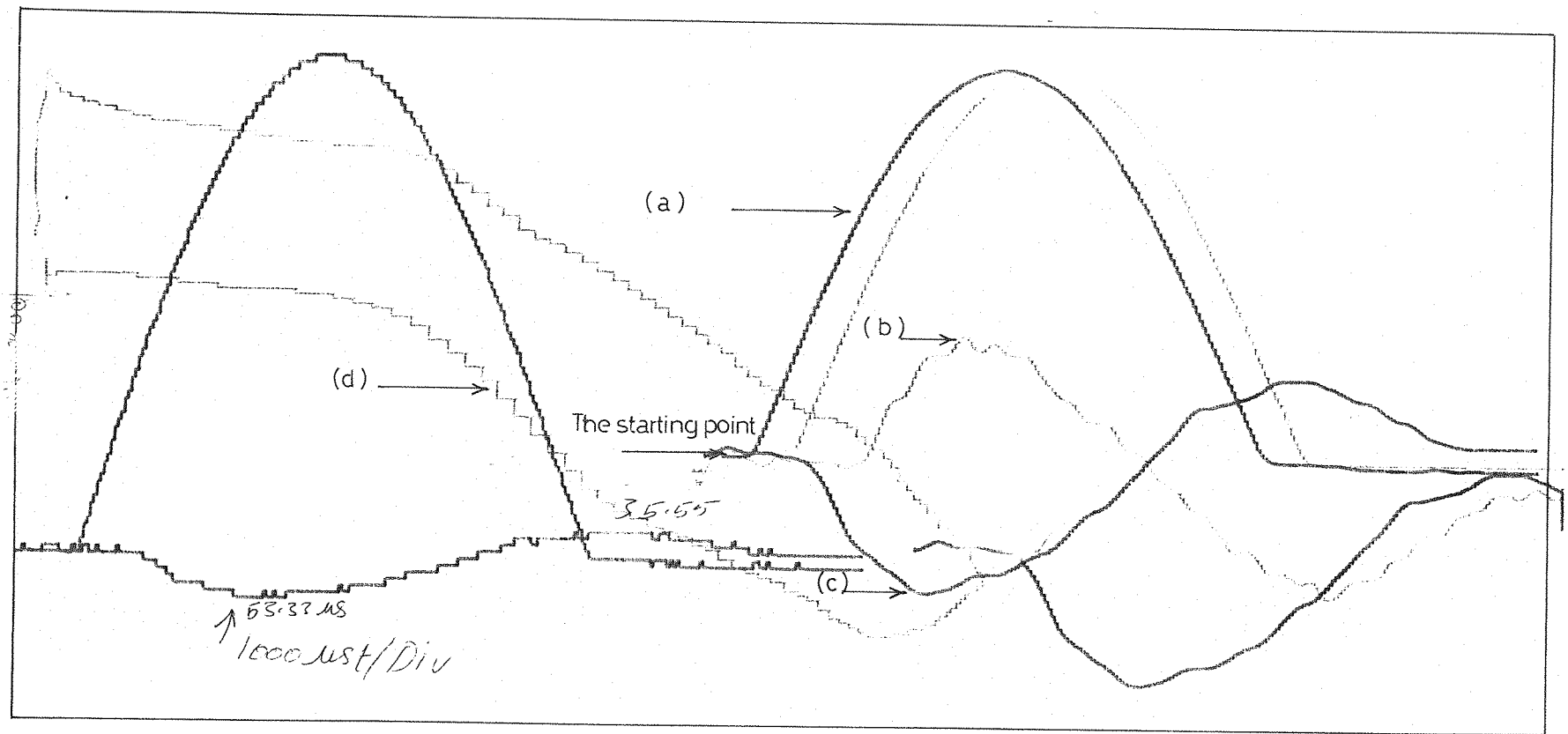

Fig. 3.4 (a) The field signal. (b) The pick-up by the Q-unit. (c) The pick-up by the Q-unit after reversing the magnetic field signal. (d) The loop obtained with a plot of the pick-up signal against the field.

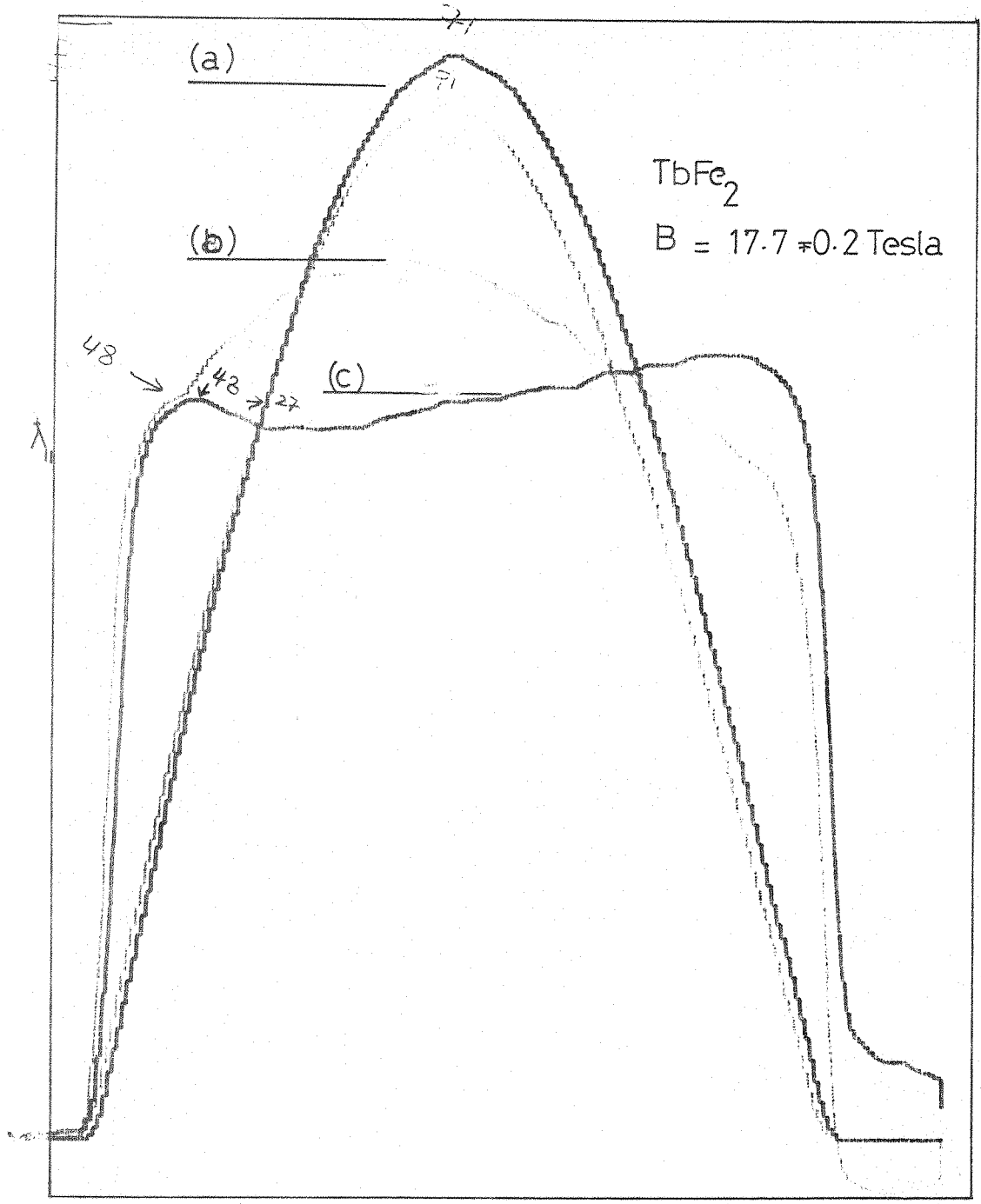

Fig. 3.5 (a) The field signal
(b) The longitudinl strain signal of $TbFe_2$.
(c) The strain signal after the field being reversed.

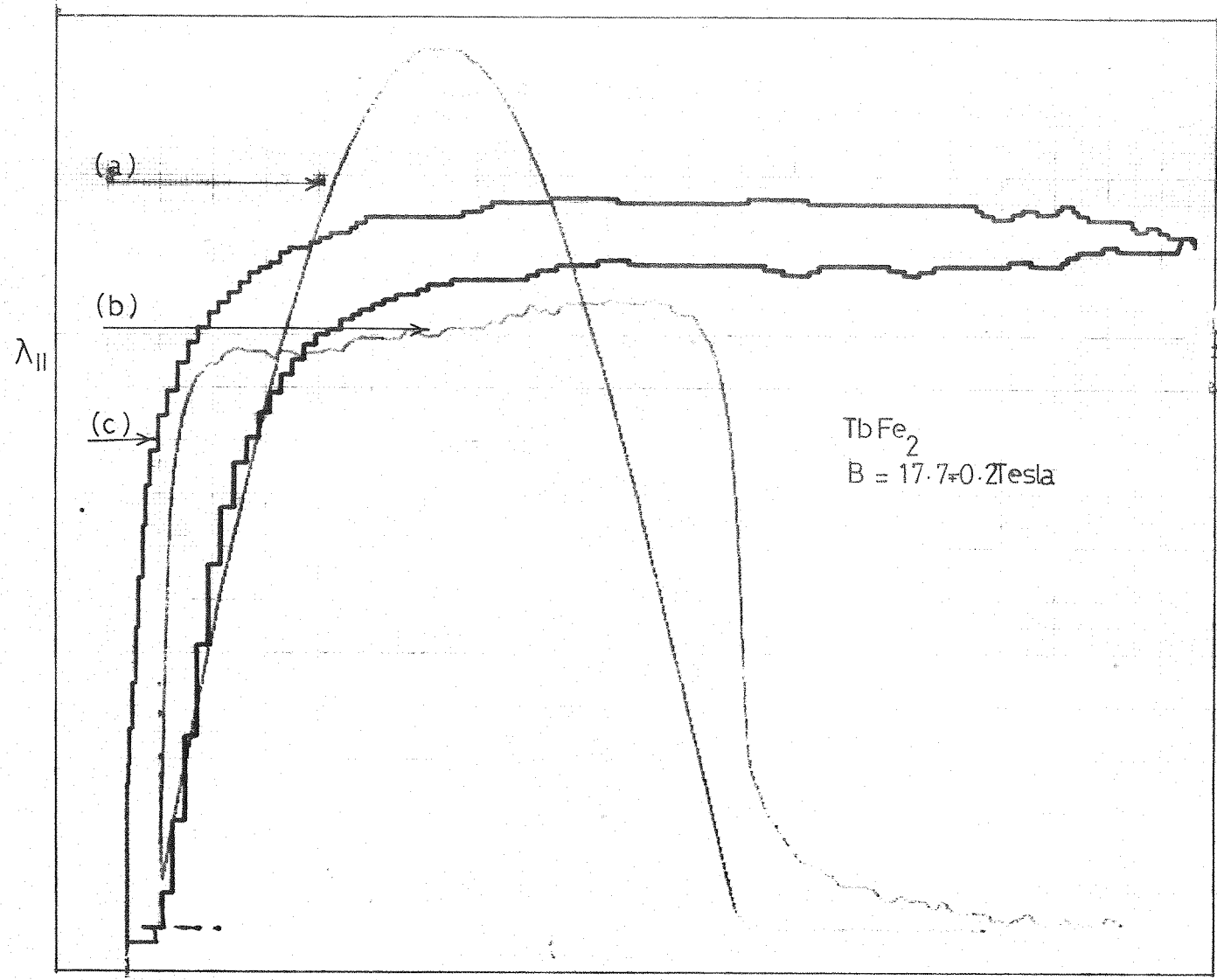

Fig. 3.6(a) The field signal against time. (b) The strain signal.
(c) The corresponding strain signal against the field.
(The loop is due to the pick-up).

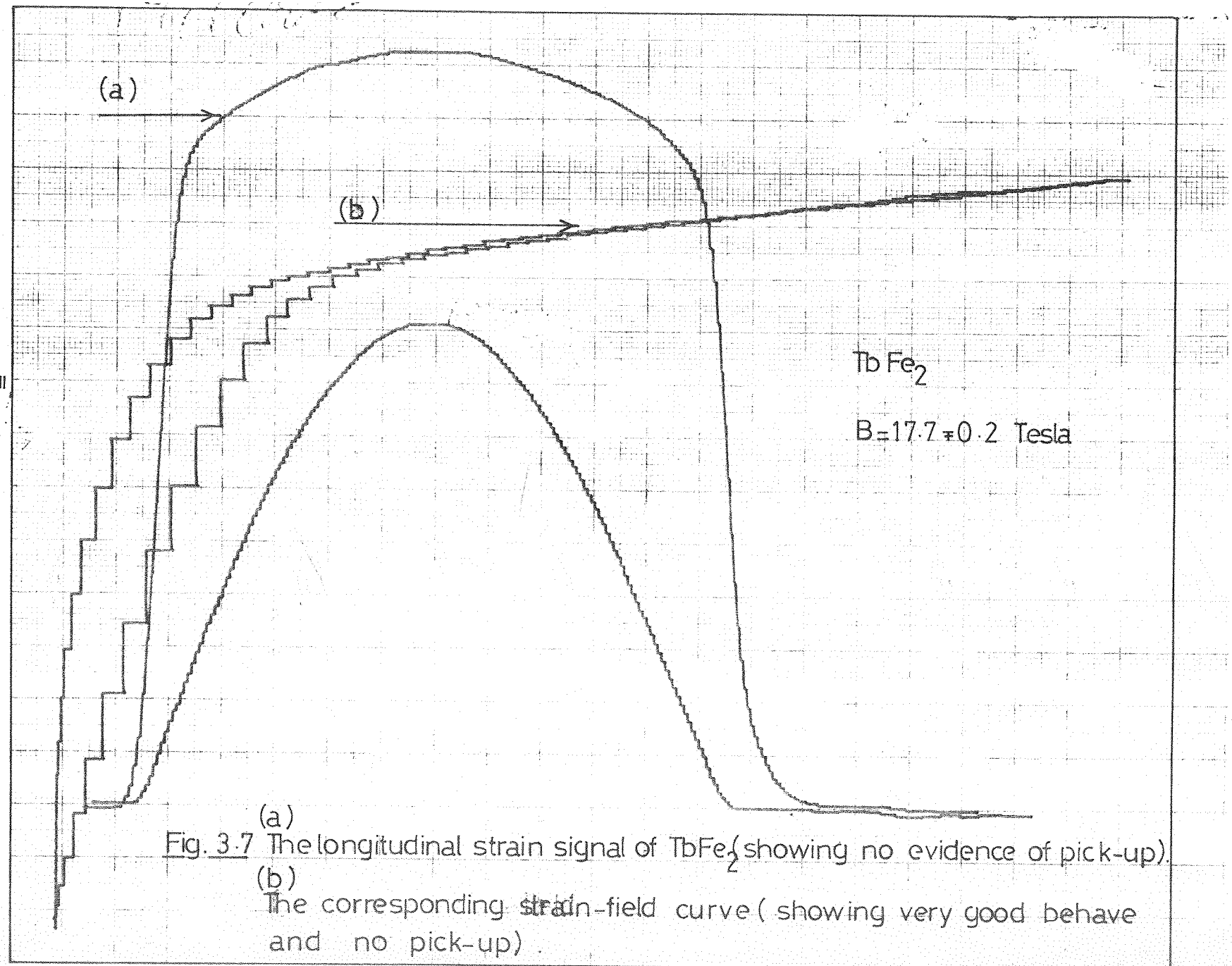

Fig. 3.7 The longitudinal strain signal of $TbFe_2$ (a) showing no evidence of pick-up. (b) The corresponding strain-field curve (showing very good behave and no pick-up).

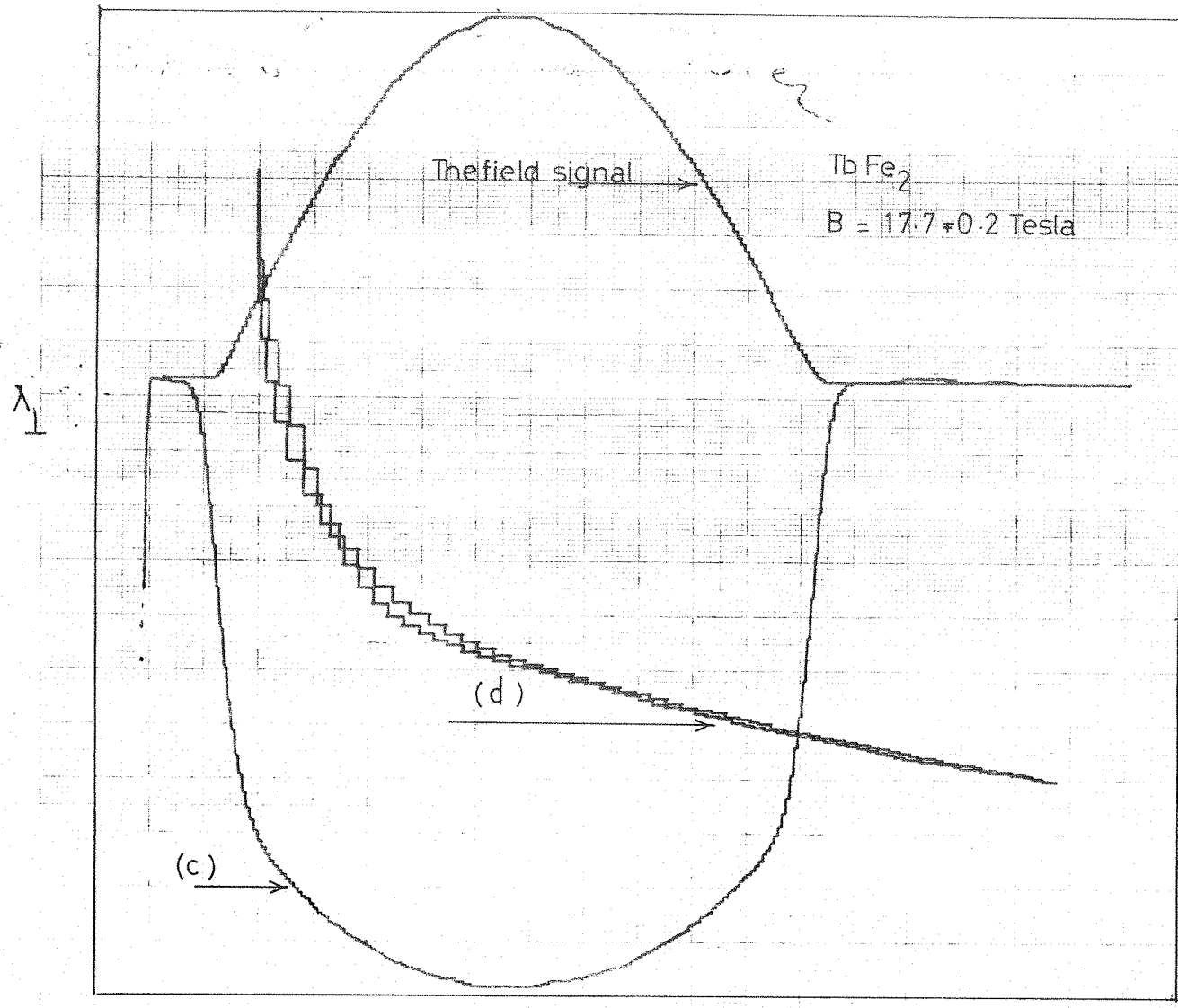

Fig. 3.7 (c) The transverse strain signal of $TbFe_2$.
(d) The corresponding strain-field curve.

showing no evidence of pick up while Figure (3–7b) is the corresponding strain field curve.

It was noticed that the pick up is due to coupling between the magnetic field and some transformers in the Q-unit, and by shielding these transformers with μ-metal (~ 1mm thickness) the pickup was reduced significantly.

(ii) Mechanical Noise: Another serious problem which appeared in this work was that due to physical noise. The net effect of the Lorentz forces produced during the field pulse has a tendency to vibrate the whole coil horizontally on its mounting. This mechanical movement produced spurious electrical noise which reduced to overall accuracy of the measurements. The mechanical coil supports were reinforced and the coil-cryostat system was centrally aligned to minimize these effects. The specimen holder was also designed so that it did not vibrate easily.

After these modifications, the physical noise was almost eliminated. This can be seen from Figure (3–7a) which shows no evidence of any physical noise in the strain signal.

In this work, only the transverse and the longitudinal strain for a given sample can be measured because the field direction with respect to the cryostat cannot be changed. Thus it is the orientation of the measuring device which must be varied.

(iii) Magnetoresistance of the strain gauges: When a magnetic field applied to a conductor the electrical resistivity changes its value. This phenomenon is called "magneto-resistance". Typically, it has values in the region of ($50 - 200 \times 10^{-6}$) at temperatures below liquid nitrogen and at high fields (~ 18 Tesla). Magnetoresistance in strain gauges has been extensively studied at low temperatures and moderate magnetic fields up to 2 Tesla, by Greenough and Lee [14], Asgar[15] and at high fields up to 15 Tesla by Del Moral and Melville[16]. One result of their work was that all the gauges behaved differently. The

factors controlling the variations in the magnetoresistance of these gauges may depend on the alloy composition, the metallurgical history of the gauge, and perhaps the content of the magnetic impurities.

However, because of the difficulty in finding two strain gauges having the same properties in the same environment it is seen that using a dummy gauge does not solve the magnetoresistance problem. Experimentally irregularities were obtained in the curves due to the dissimilarity of their behaviour. These have been avoided by using one strain gauge only which was bonded on the surface of the sample. However, here the strain gauge had to be calibrated before use and this will be explained later in this chapter, (see section 3.11.1)

3.6.2 Eddy Currents Effects: A serious problem, which must be considered very carefully in both magnetostriction and magnetization measurement arises due to eddy currents set up in the conducting specimens.

From Maxwell's equation, curl $E = -\frac{\partial B}{\partial t}$

Because of the time-varying field an electric field is established throughout the specimen causing eddy currents to flow.

There are three distinct effects in this measurement due to eddy currents which are now discussed. These effects have been previously discussed by Melville[11] and Ricodeau[17].

(i) Heating effects: During the pulse the temperature of the sample will rise due to joule heating produced by the eddy currents.

Consider an elemental ring of radius r, thickness dr, and length dz fig. (3-8), of a cylindrical sample radius a, length h.

The current density j, is given by:-

$$j = \frac{\pi r^2}{2\pi r\rho / drdz} , \frac{1}{dr\ dz} , \frac{dB}{dt}$$

where ρ is the resistivity of the cylindrical sample

$$j = \frac{r}{2\rho} , \frac{dB}{dt} dr\ dz$$

The current in the elemental ring,

$$di = \frac{r}{2\rho} \frac{dB}{dt}, dr\ dz$$

$$dw = (di)^2 , R$$

To get the heating effect we integrate the square of the current density over the specimen and the time of the field pulse.

$$w = \int_0^h \int_0^a \int_0^\tau \left(\frac{r}{2\rho} \frac{dB}{dt}\right)^2 \frac{2\pi r\rho}{drdz} (drdz)^2\ dt \qquad (3-1)$$

Assuming $B = Bo \sin wt$, where Bo is the maximum field,

$$\frac{dB}{dt} = BoW \cos wt$$

$$\left(\frac{dB}{dt}\right)^2 = Bo^2\ W^2\ \cos^2 wt$$

$$\cos^2 wt = \frac{\cos 2wt + 1}{2}$$

Substituting for $\left(\frac{dB}{dt}\right)^2$ in equation (3–1) and integrating

$$w = \frac{\pi a^4 h\ B_0{}^2 w}{16\rho} \tau$$

where τ is the pulse length $= \frac{\pi}{w}$, and the volume of the specimen $v = ha^2$

so $$w = \frac{\pi^2 a^2 B_0{}^2 v}{16\ \rho\tau} \text{ joule}$$

$$w = C\ .\ m\ .\ \Delta T$$

where w : is the quantity of heat in joule
c : is the specific heat ($J \cdot Kg^{-1} \cdot K^{-1}$)
m : mass (Kgm)

$m = V.D$

where V is the volume (m^3)
D is the density (Kgm/m^3)

$w = C.V.D.\Delta T$

so $$\Delta T = \frac{\pi a^2 B_0^2}{16 \rho .C.D.\tau} \qquad (3-2)$$

For $TbFe_2$ $C = 209 \quad J \cdot Kg^{-1} \cdot K^{-1}$ at room temperature[18]

$D = 9.056 \times 10^3 Kg \cdot m^{-3}$

$\rho = 59 \times 10^{-8} \Omega \cdot m$ at 300 K[19]

$\rho = 2.5 \times 10^{-8} \Omega \cdot m$ at 4.2 K[19]

$B_0 = 18$ Tesla

$\tau = 10^{-2}$ sec

If the magnetic field applied in the y direction:

$\pi a^2 = t \times b$

where a is the radius of a cylindrical sample
t is the thickness of the rectangular sample
b is the width

$a \approx 1.116 \times 10^{-3}$ m

$\Delta T \simeq 0.17$ K

If the magnetic field applied in the x direction:

$a \simeq 1.464 \times 10^{-3}$ m

$\Delta T \simeq 0.288$ K

For $DyFe_2$

$C = 159 \ J.K^{-1} Kg^{-1}$ [18]

$D = 9.256 \times 10^3 \ Kg/m^3$

$\rho \simeq 2.5 \times 10^{-8}$ Ω . m at 4.2 K

$B_0 = 18$ Tesla

$\tau = 10^{-2}$ sec

when B_0 in the y direction

$\Delta T \simeq 0.194$ K

when B_0 in the x direction

$\Delta T \simeq 0.382$ K

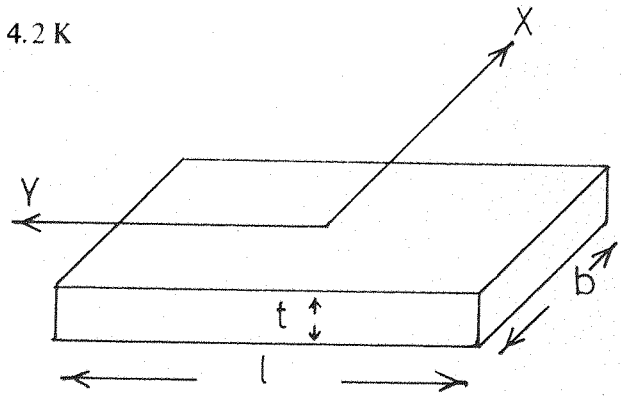

(ii) Shielding effect: A magnetic field is also created by the eddy current, this magnetic field according to Lent's law tends to counteract the effect of the variation of the external field. The result is that the internal field in the specimen is different from the applied field, both in magnitude and phase. This effect becomes more important for a short duration pulsed field.

The diffusion equation describing the distribution of the field in the specimen is[20]

$$\Delta^2 H = \frac{\mu}{\rho} \frac{\partial H}{\partial t}$$ where ρ = resistivity and μ = permeability.

Now to solve this equation consider a cylinder of a finite length along the Z-axis with electrical resistivity ρ and magnetic permeability μ, which is assumed to be a constant. A homogenous and time-dependent magnetic field, B_0, is applied along the Z-axis. This field will give rise to an induced emf and hence to eddy current in the cylinder, resulting in a magnetic field opposing the applied field. The field is a function of radius a, and the time, t. The field at the centre of the cylinder is given by[20]

$$\frac{H(o, t)}{H(a, t)} = (ber^2 xo + bei^2 xo)^{-\frac{1}{2}} \qquad (3-3)$$

where H (o, t) is the field at the centre, H (a, t) the field at the surface and $xo = a(\mu w/\rho)^{1/2}$,

where w is the frequency and a is the radius of the sample.

The Kelvin functions ber and bei are given by Lowell[21].

To avoid the effects of the eddy current we require $\frac{H(o, t)}{H(a, t)}$ to be as near to unity as possible.

Suppose the field variation throughout the specimen is no more than 1%, this implies $\frac{H(o, t)}{H(a, t)} \geqslant 0.99$, for this condition $x_0 \leqslant 0.9$. Using the value of w equivalent to $\tau = 10$ msec and putting $\mu = 4\mu \times 10^{-7}$ and the liquid helium temperature value of $\rho = 2.5 \times 10^{-8}\ \Omega.\ m$ it is found that the maximum specimen radius allowable is ~12 mm. From this we understand that this effect is negligible in this case, because the radius of the specimen is less than 2 mm.

(iii) The strain arising due to the interaction of the applied field with the eddy currents: Due to the interaction between the applied field and the eddy current generated in the specimen, there is a resultant Lorentz forces acting radially inwards and leading to a strain in the specimen.

For a cylindrical specimen of radius 'a' (radial variable r, and axial variable z), the varying magnetic field induces eddy currents.

The strain resulting in a solid cylindrical specimen due to eddy currents in a pulsed field, has been calculated by Melville as follows:

In fig. (3–8) the current density in elementary ring is

$$j = \frac{\pi r^2}{\rho\, 2\pi r/drdz}\ ,\ \frac{dBz}{dt}\quad \frac{1}{drdz}$$

where ρ is the resistivity of the cylindrical specimen.

The force $Fr = j \times B_0$

Assuming $Bz = B_0 \sin wt$ where B_0 is the maximum field,

$$\frac{dBz}{dt} = B_0 \, w \cos wt$$

$$j = \frac{r}{2\rho} \frac{dBz}{dt} = \frac{r B_0 w}{2\rho} \cos wt \text{ , } \rho \text{ is the resistivity}$$

so $$Fr = r \frac{B_0^2 w}{2\rho} \sin wt \cos wt = r \frac{B_0^2 w}{2\rho} \frac{\sin 2wt}{2}$$

$$Fr = Ar \quad \text{where } A = \frac{B_0^2 w}{4\rho}$$

The stress equation in the radial direction is[22]

$$r\frac{\partial \sigma_r}{\partial r} + \sigma_r - \sigma_\theta + rfr = 0 \qquad (3\text{–}4)$$

σ_r, σ_θ are the stress in the radial and the azimuthal direction respectively. Also for strain compatability.

$$\epsilon_r = \epsilon_\theta + r\frac{\partial \epsilon_\theta}{\partial r} \qquad (3\text{–}5)$$

ϵ_r : is the radial strain
ϵ_θ : is the azimuthal strain

And Hooke's law gives

$$\epsilon_r = \frac{1}{E}(\sigma_r - v\sigma_\theta)$$
$$\epsilon_\theta = \frac{1}{E}(\sigma_\theta - v\sigma_r) \qquad (3\text{–}6)$$

where E is the young modulus and v is the poisson's ratio of the conductor.

Substituting equation (3–6) into equation (3–5) gives

$$\sigma_r - v\sigma_\theta = \sigma_\theta - v\sigma_r + r\frac{\partial \sigma_\theta}{\partial r} - vr\frac{\partial \sigma_r}{\partial r}$$

ie. $$vr\frac{\partial \sigma_r}{\partial r} - r\frac{\partial \sigma_\theta}{\partial r} + (1-v)(\sigma_r - \sigma_\theta) = 0 \qquad (3\text{–}7)$$

$$r\frac{\partial \sigma_r}{\partial r} + (\sigma_r - \sigma_\theta) + A r^2 = 0 \qquad (3\text{–}4)$$

From equation (3–4)

$$\sigma_\theta = r\frac{\partial \sigma_r}{\partial r} + \sigma r + A r^2 \qquad (3-8)$$

and $$\frac{\partial \sigma_\theta}{\partial r} = r\frac{\partial^2 \sigma_r}{\partial r^2} + 2\frac{\partial \sigma_r}{\partial r} + 2Ar \qquad (3-9)$$

Substituting (3–9) and (3–8) into (3–7) gives

$$r^2\frac{\partial^2 \sigma_r}{\partial r^2} + 3r\frac{\partial \sigma_r}{\partial r} = -(3+v)Ar^2$$

$$\frac{1}{r^2}\frac{d}{dr}\left(r^3\frac{\partial \sigma_r}{\partial r}\right) = -(3+v)Ar$$

$$(r^3\sigma_r') = -(3+v)\frac{Ar^4}{4} + B$$

$$\sigma_r' = -(3+v)\frac{Ar}{4} + \frac{B}{r^3}$$

$$\sigma_r = -(3+v)\frac{Ar^2}{8} - \frac{B}{2r^2} + C \qquad (3-10)$$

Boundary conditions 1) $\sigma_r \neq -\infty$ as $r \to 0$
2) $\sigma_r = 0$ at $r = a$

So B should equal zero and

$$C = \frac{3+v}{8}A\,a^2$$

Then $$\sigma_r = \frac{3+v}{8}A(a^2 - r^2) \qquad (3-11)$$

Substituting equation (3–11) in (3–4) gives

$$\sigma_\theta = \frac{3+v}{8}A(a^2 - r^2) - 2r^2\frac{3+v}{8}A + Ar^2$$

$$\sigma_\theta = \frac{A}{8}[(3+v)a^2 - (1+3v)r^2] \qquad (3-12)$$

At $r = a$, $\sigma_r = 0$ and equation (3–4) gives

$$\sigma_\theta(a) = \frac{A}{4}(1-v)a^2 \qquad (3-13)$$

From equation (3–6)

$$\epsilon_\theta = \frac{1}{E}(\sigma_\theta - v\sigma_r)$$

$$\epsilon_\theta(a) = \frac{1}{E}\sigma_\theta$$

$$\epsilon_\theta(a) = \frac{A}{4E}(1 - v)\, a^2 \qquad \left(A = \frac{w}{4\rho} B_0{}^2\right)$$

$$\epsilon_\theta(a) = \frac{w}{16\rho E} \cdot B_0{}^2 a^2 (1-v) \tag{3–14}$$

$$\epsilon_r = \frac{1}{E}(\sigma_r - v\sigma_\theta) \tag{3–6}$$

$$\epsilon_r(a) = \frac{-v\sigma}{E} = -\frac{Av}{4E}(1 - v)\, a^2$$

$$\epsilon_r(a) = \frac{w}{16\rho E} \alpha\, B_0{}^2 a^2 (1-v) \tag{3–15}$$

In case of $TbFe_2$

$$E = 9.4 \times 10^{10}\ N/M^2 \quad [19]$$

$$\rho = 2.5 \times 10^{-8}\ \Omega \cdot m \quad \text{at } 4.2\ K \quad [19]$$

$$\tau = 10^{-2}\ sec$$

$$B_0 = 17.6\ Tesla$$

$$\nu \simeq 0.35 \quad , \quad a = 1.116 \times 10^{-3}\ m$$

$$\epsilon_\theta(a) = \frac{w}{16\rho E} B_0{}^2 a^2 (1-v)$$

$$\epsilon_\theta(a) \simeq 2 \times 10^{-6}$$

$$\epsilon_r(a) \simeq 0.74 \times 10^{-6}$$

These values are almost the same for $DyFe_2$.

Compared with the magnetostriction of $DyFe_2$ and $TbFe_2$ ($> 3000 \times 10^{-6}$), these values are negligible.

(iv) Forces due to non-uniform field: The eddy currents also leads to forces which tend to displace the specimen. The origin of these forces is due to the interaction between the eddy currents and the radial component of the field.

For a cylindrical specimen with radius a and height h placed with its axis parallel to the magnetic field, the current density induced in an elementary ring of radius r (Fig. (3–8)) is:

$$j = \frac{r}{2\rho}\frac{dBz}{dt} \qquad (3-16)$$

where ρ is the resistivity of the material.

The force on the element depends on the radial component of the field Br and is:

$$dfz = j\,(dr\,dz)\,(2\pi r)\,Br \qquad (3-17)$$

In (3–16) and (3–17) the field was assumed to be constant throughout the specimen and the effect is negligible.

For small values of r and for a field of cylindrical symmetry [23]

$$Br \triangleq -\frac{r}{2}\frac{dBz}{dz} \qquad (3-18)$$

Assuming $Bz = Bz(max)\sin wt$

equation (3–17) becomes:

$$dfz = \frac{\pi r^3}{2\rho} w\, Bz(max)\frac{dBz(max)}{dz}\sin wt\cos wt\, drdz \qquad (3-19)$$

And by integrating over the whole cylinder equation (3–19) gives:

$$fz = \frac{a^2 v}{8\rho} w\, Bz(max)\frac{dBz(max)}{dz}\sin wt\cos wt \qquad (3-20)$$

where $v = \pi a^2 h$

A plot of fz as a function of time is shown in Fig. (3–9).

In fig. (3–9), fz = 0 at B = B(max), and is equal in magnitude, but opposite in sign

for equal values of B on either side of B(max).

From equation (3–20), $Fz \alpha a^2$, so that the effect of eddy currents can be minimised by using specimens of small radius.

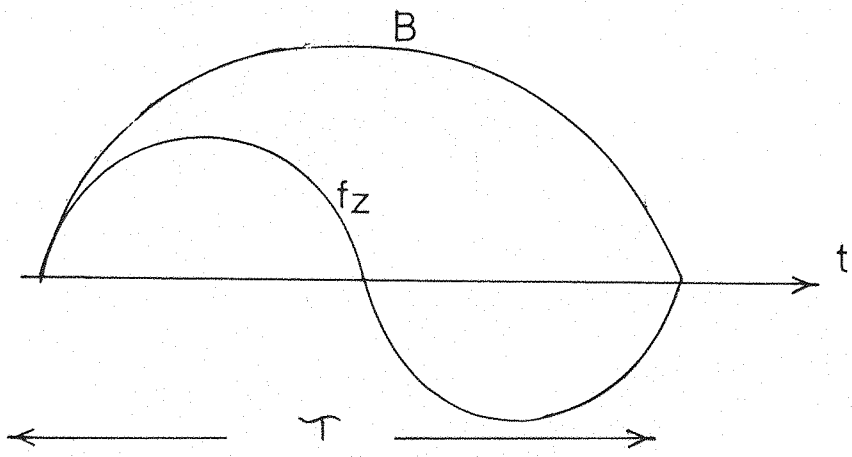

Fig. (3–9)
The force fz exerted on the specimen due to eddy currents in a field, B.

3.7 The Demagnetizing Field:

When a body of finite size is magnetized, it can be considered to have free magnetic poles induced on both of its ends, These poles give rise to a magnetic field in a direction opposite to the applied field, so the effective field is the sum of the applied field and the field produced by the specimen. If the body is homogeneous and has the shape of an ellipsoid of revolution, the demagnetizing field is uniform. It depends on the dimensional ratios of the ellipsoid and proportional to the magnetization of the body. To estimate the demagnetizing field, a knowledge of the shape and the magnetization of the magnetic body is required.

From Zijlstra[20] the average of the demagnetizing field for a cylindrical specimen can be calculated from the following formula:

$$Hd = NM \qquad (3–21)$$

where N is the demagnetizing factor and M is the magnetization ($A.m^{-1}$).

The specimen was rectangular in shape of dimensions 5.9 x 3.4 x 1.13 mm. It is assumed that this shape gives a demagnetizing factor similar to that of a cylinder of length 5 mm. and diameter 3 mm. with uniform magnetization. From Zijlstra[20], the parallel and the perpendicular demagnetizing factors are $M_{\parallel} = 0.15$ and $N_{\perp} = 0.4$ respectively.

Magnetization measurement for $DyFe_2$ and $TbFe_2$ have been carried out by A.E. Clark [19] and A.E. Clark and J.R. Callen[24] with magnetic fields up to 12 Tesla. Saturation magnetization for these compounds has not been achieved. The demagnetizing field for $TbFe_2$ and $DyFe_2$ was calculated by using the magnetization values of the above authors. For $TbFe_2$ it was found to be 0.162 Tesla at room temperature for the parallel direction, while it was 0.43 in the perpendicular direction. In addition the values for $DyFe_2$ at room temperature were found to be 0.122 and 0.325 Tesla for the parallel and perpendicular directions respectively. It is necessary to subtract the calculated values from the measured field.

3.8 The Magnetocaloric Effect:

In addition to the effects of eddy currents, the magnetocaloric effect can lead to a temperature rise and hence to an extra strain which may add or subtract from the original value.

This phenomenon arises due to the heating effect accompanying the magnetization processes. When a magnetic field is applied to a magnetic substance, there will be an increase in the magnetic order of the system. In other words, the entropy of the spins has decreased. If the magnetic material were thermally isolated from the surroundings, the decrease in the entropy of the spins will lead to an increase in the entropy of the lattice; thus the temperature of the lattice will rise. The magnetocaloric effect forms

the basis of the "magnetic cooling" method for obtaining temperature lower than 1K.

In this work the sample is thermally isolated from the surroundings, so that the process is adiabatic, ie. there will be no change in the entropy of the system and therefore no change in the temperature of the sample will be expected in the end of the magnetic field pulse. This is because the spins and the lattice take a very short time to reach thermal equilibrium. At room temperature it might be 10^{-6} sec.[25]

The temperature rise due to the magnetocaloric effect can be determined as follows:

Consider the entropy 's' as a function of temperature 'T' and the field is 'H'.

$$S = f(T, H)$$

$$dS = \left(\frac{\partial S}{\partial T}\right)_H dT + \left(\frac{\partial S}{\partial H}\right)_T dH \qquad (3-21)$$

$$TdS = T\left(\frac{\partial S}{\partial T}\right)_H dT + T\left(\frac{\partial S}{\partial H}\right)_T dH \qquad (3-22)$$

The heat capacity C_H of a system at constant field is defined as

$$C_H = \left(\frac{\partial Q}{dT}\right)_H = T\left(\frac{\partial S}{\partial T}\right)_H \qquad (3-23)$$

Equation (3-22) becomes

$$Tds = C_H dT + T\left(\frac{\partial M}{\partial T}\right)_H dH \qquad (3-24)$$

For an adiabatic process, that is when there is no change in entropy S, equation (3-24) gives

$$C_H dT = -T\left(\frac{\partial M}{\partial T}\right)_H dH$$

A finite adiabatic change in field thus produces a temperature change given by

$$\Delta T = -\frac{T}{C_H}\left(\frac{\partial M}{\partial T}\right)_H \Delta H \qquad (3-25)$$

$\Delta T = 0.12$ K at 4.2 K

3.9 The Spin-Spin and Spin-lattice relaxation times:

By applying a magnetic field to a system of spins, the spins will align themselves in the direction of the applied field. The spin-spin relaxation time, $\tau s - s$, is due to the interaction between spins of the system and is a measure of the time taken for the spin system to come to equilibrium. It is usually very short (of the order of 10^{-10} sec.)[25] and it is independent of the temperature of the system. The energy released during this interaction must be absorbed by the surroundings, i.e. the remaining electrons, the crystal lattice and the temperature controlled environment.

Due to the applied field there is no longer a state of equilibrium between the magnetic system and the lattice, so that an atom whose state has been raised in energy, decays into a lower state by emitting a phonon. For this to occur there must be coupling between the spins and the phonon system. The time for this interaction to occur is called the spin-lattice relaxation time, $\tau s-L$, and can be defined as a measure of the period required for the spins to give up their energy to the lattice. It is a rapidly varying function of temperature. At room temperature it might be 10^{-6} sec. [25]

Relaxation with the environment usually takes several seconds to complete, but this does not affect the measurements.

The pulse length of the magnetic field used in this work was 10^{-2} sec. Hence, spin-spin and spin-lattice relaxation effects could be neglected.

3.10 The Calibration of the field:

In the experiment, a search coil was used to measure the magnetic field. It was calibrated by rotating it in a steady magnetic field whose value was determined using NMR.

For an atomic nucleus, the relation between the magnetic moment m and the spin angular momentum is given by:

$$m = \gamma s \hbar \qquad (3-26)$$

where γ is a positive or negative scalar quantity, called the gyromagnetic ratio.

If such a moment is placed in a magnetic field B_0 along Z-axis, the potential energy is given by:

$$U = - m_z B_0 \qquad (3-27)$$

where B_0 is the magnitude of the applied field
and m_z is the moment along field direction.

Then $$U = - \gamma \hbar B_0 S_z \qquad (3-28)$$

where S_z is the projection of S along the Z-axis.

Hence in a magnetic field a nucleus with S = ½ has two energy levels corresponding to $S_z = \mp$ ½. The energy difference between the two levels is $\Delta E = \gamma \hbar B_0$.

If the system is excited with radiation of frequency wo such that $\hbar$ wo = ΔE then:

$$wo = \gamma B_0 \qquad (3-29)$$

This is the fundamental condition for magnetic absorption. For the proton $\gamma = 2.675 \times 10^8$ rad. sec.$^{-1}$ Tesla^{-1}.

By using this formula a steady magnetic field of an electromagnet was measured with a percentage of error up to ± 0.08%.

3.11 The strain gauge, strain gauge calibration, and the gauge factor:

3.11.1 The Strain gauge and Strain gauge calibration: The change of length of a magnetized body can be measured by using strain gauges after an idea of Goldman (1947). The use of strain gauges is based on the fact that any strain characteristic of the specimen on which the gauge is bonded is transmitted to the electrically sensitive zone of the gauge and is observed as a resistance change.

A strain gauge consists of a folded metal wire as illustrated in Fig. (3–10). The wire rectangle is covered on either side by a thin paper sheet or embedded in a thin strip of

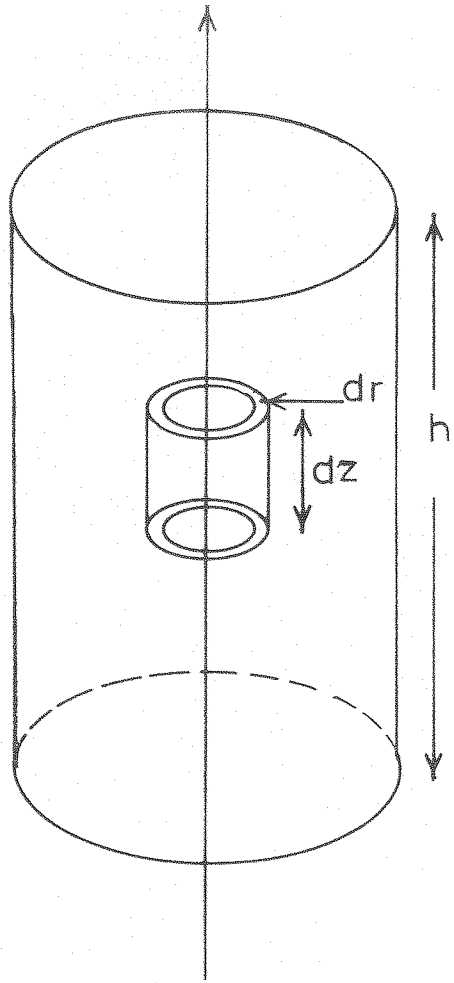

Fig. 3.8

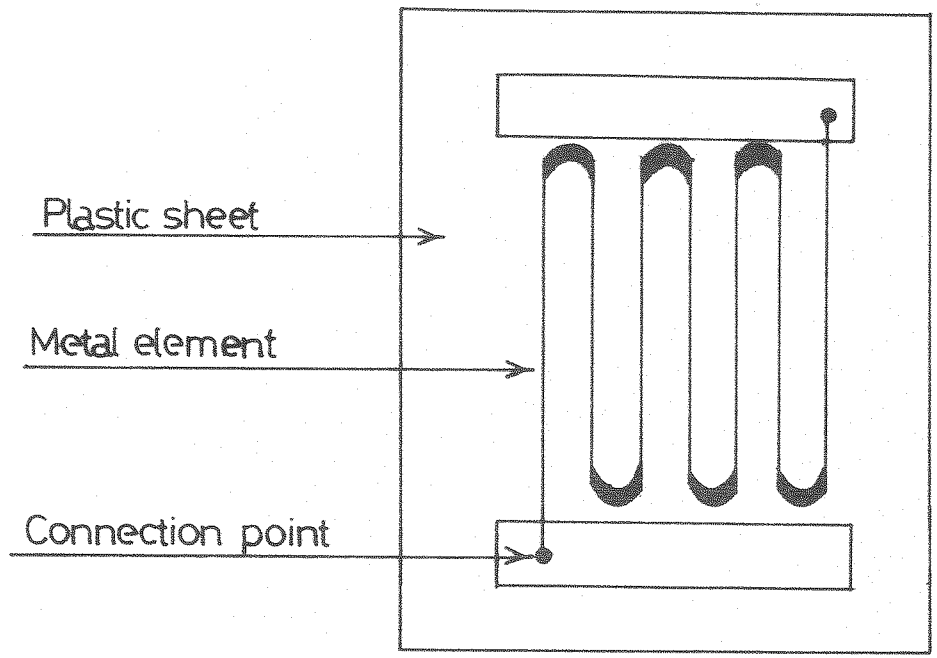

Fig. 3.10 Strain gauge (schematic).

plastic, and provided with two connection points. If the strain gauge is extended or compressed along the wire direction its electrical resistance increases or decreases.

The gauges used in this work were micromeasurements type SK–09–031–DE–350 with M–600 bonding agent, the dimensions of these gauges are 3 x 7 mm. and they are strong and stable over a large temperature range (4.2K to 520 K). They are thermally self compensated so that when they are bonded on to a material, the signal corresponding to the thermal expansion is minimized. The magnetoresistance of these strain gauges at room temperature is about 5×10^{-6} strain equivalents at 18 Tesla. The magnetoresistance increases slowly down to liquid nitrogen temperature, and increases rapidly from liquid nitrogen to liquid helium temperature as shown in Fig. (3–11). (All magnetoresistance curves are plotted in terms of equivalent strain). It shows a quadratic behaviour with magnetic field as shown in Fig. (3–12).

It is very difficult to find two gauges having the same characteristics. It was found experimentally that the magnetoresistance of these gauges have values between 40×10^{-6} to 200×10^{-6} strain equivalents at 18 Tesla and at 16 K. It was not possible to go lower than 16K because of the heat dissipation through the strain gauges. However, it might be possible to go further down by reducing the current passing through the strain gauge which was 10 m Amp in this work.

The magnetoresistance parallel to the applied magnetic field for the same kind of strain gauges have been measured by Adel Moral and D. Melville between near 8K and 100K and pulsed fields up to 14.5 Tesla. The largest magnetoresistance was found to be $\Delta R_{11}/R_{11} \approx 5.5 \times 10^{-4}$ at 11 Tesla and 8K which is in good agreement with the above values.

The gauges used in these measurements had to be calibrated from room temperature

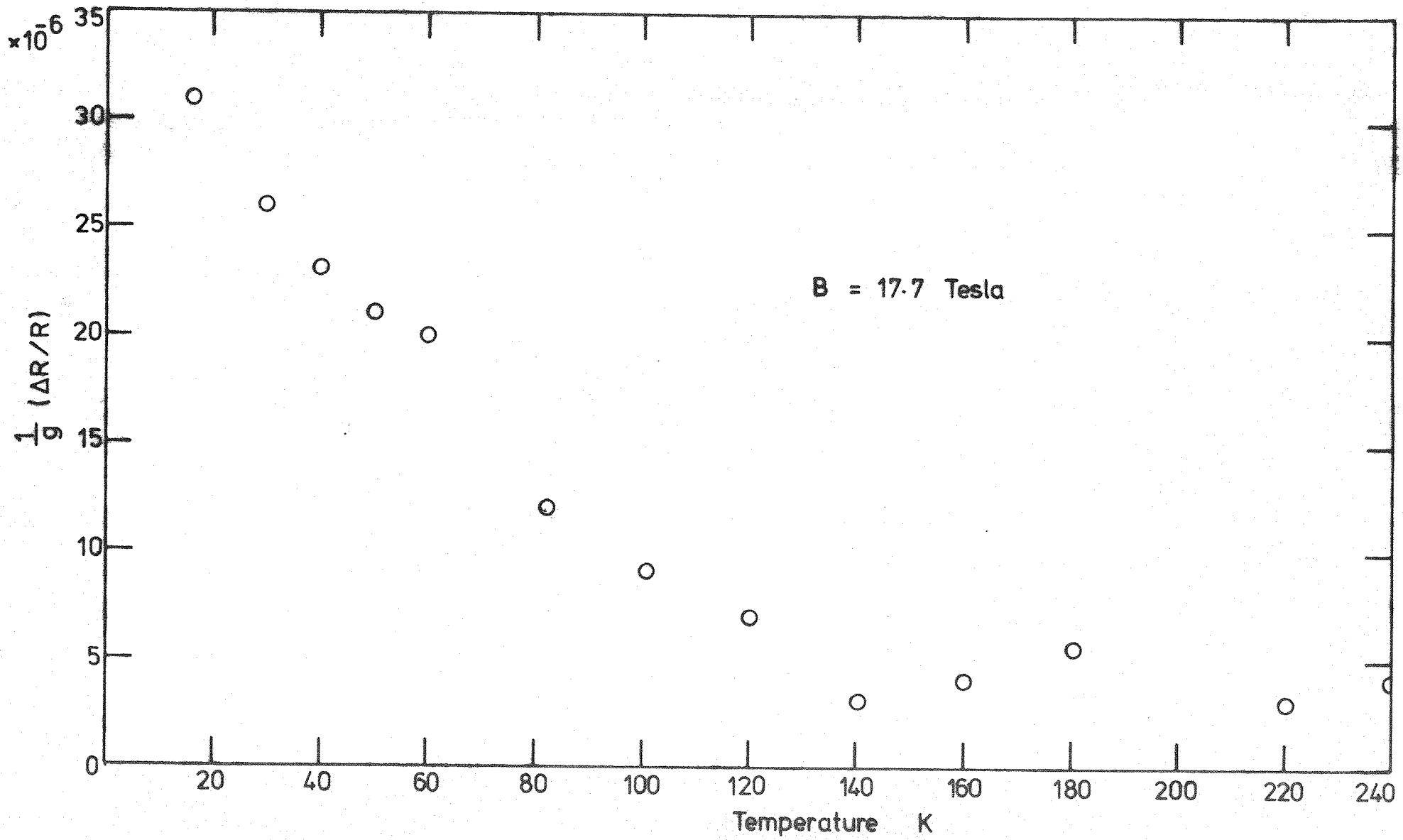

Fig. 3.11a Magnetoresistance of the strain gauge (K3) parallel to the applied field

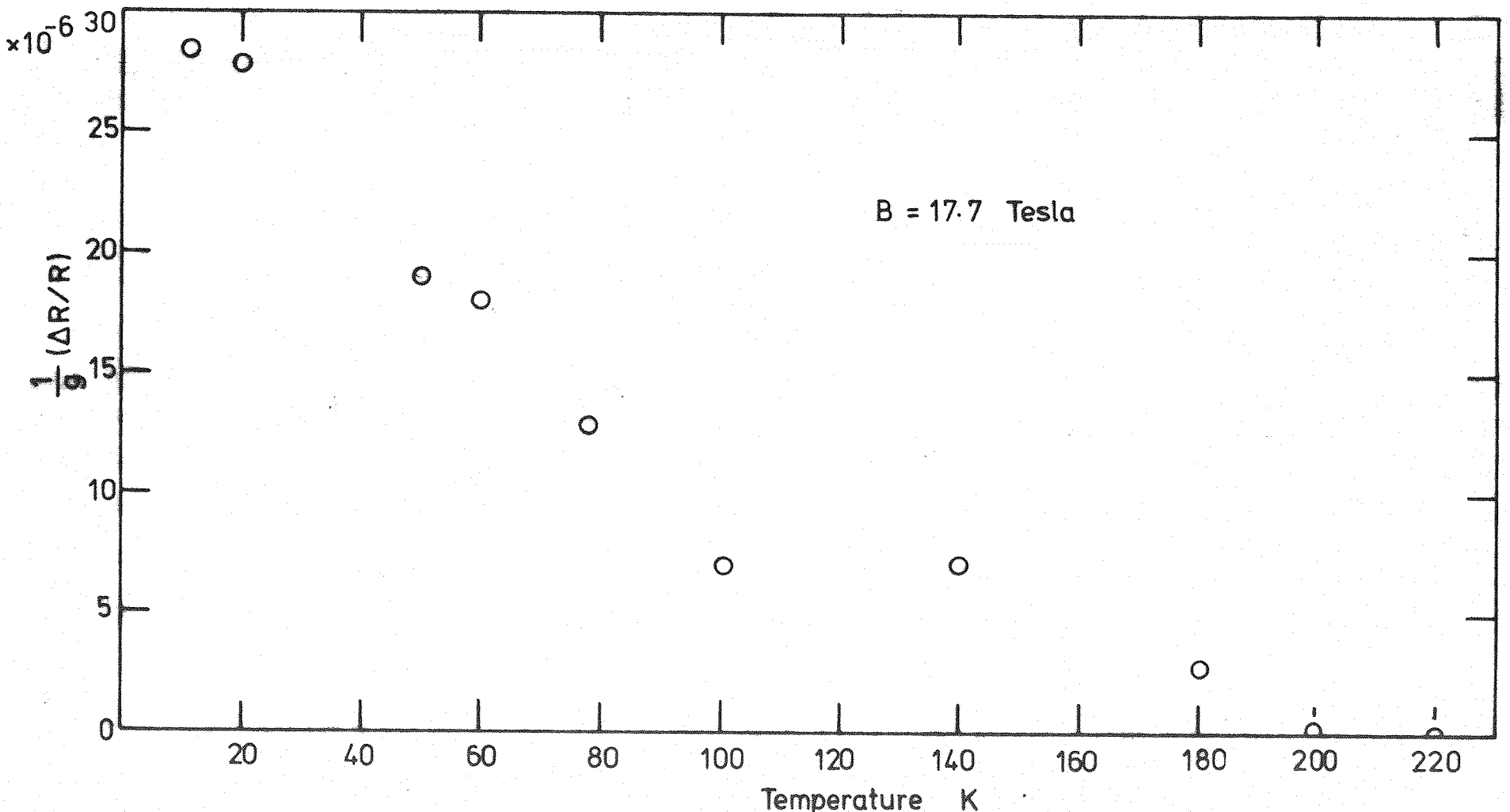

Fig. 3.11b Magnetoresistance of the strain gauge (K 3) perpendicular to the applied field

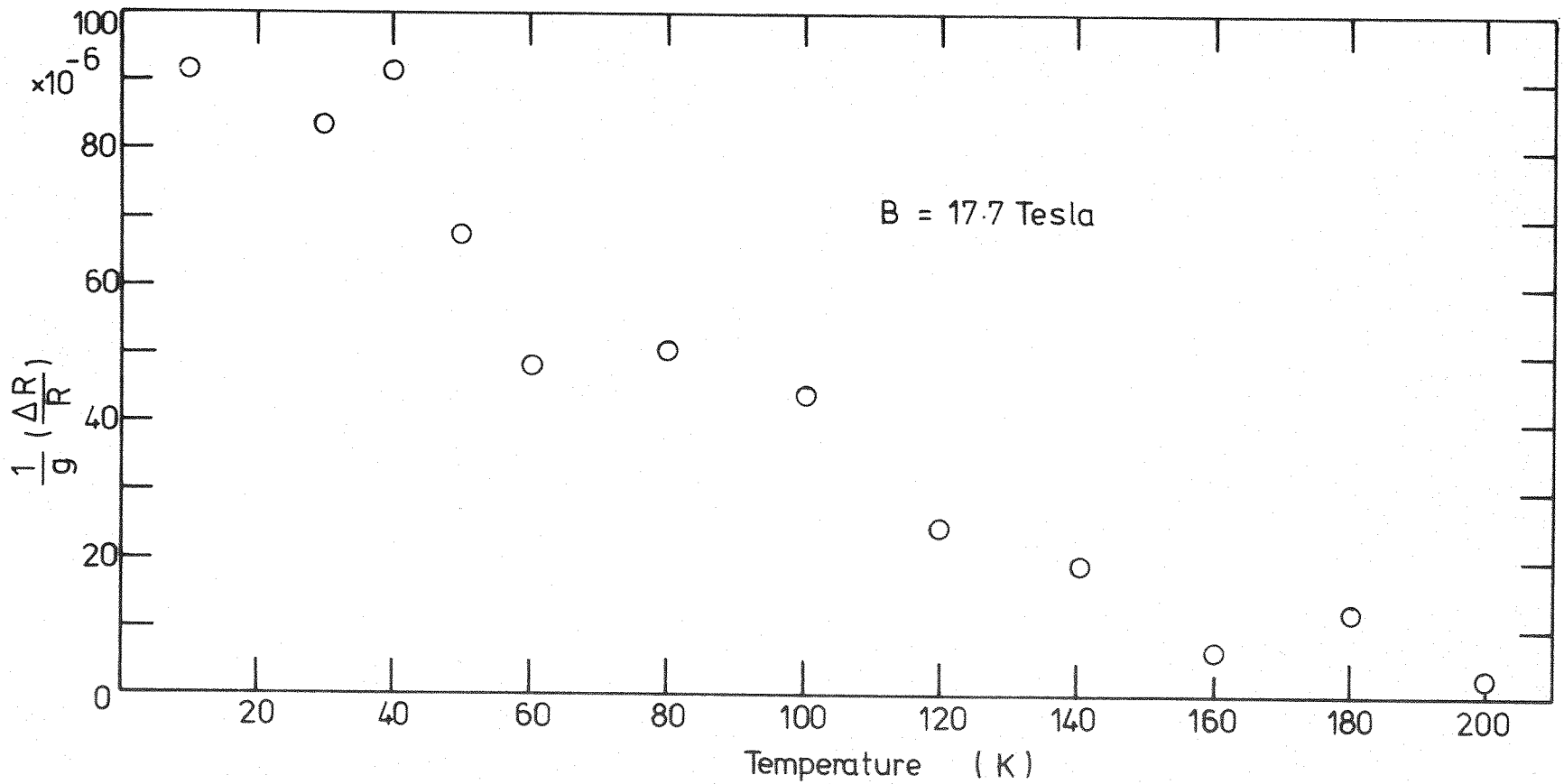

Fig. 3·11 c Magnetoresistance of strain gauge (K1) parallel to the applied field

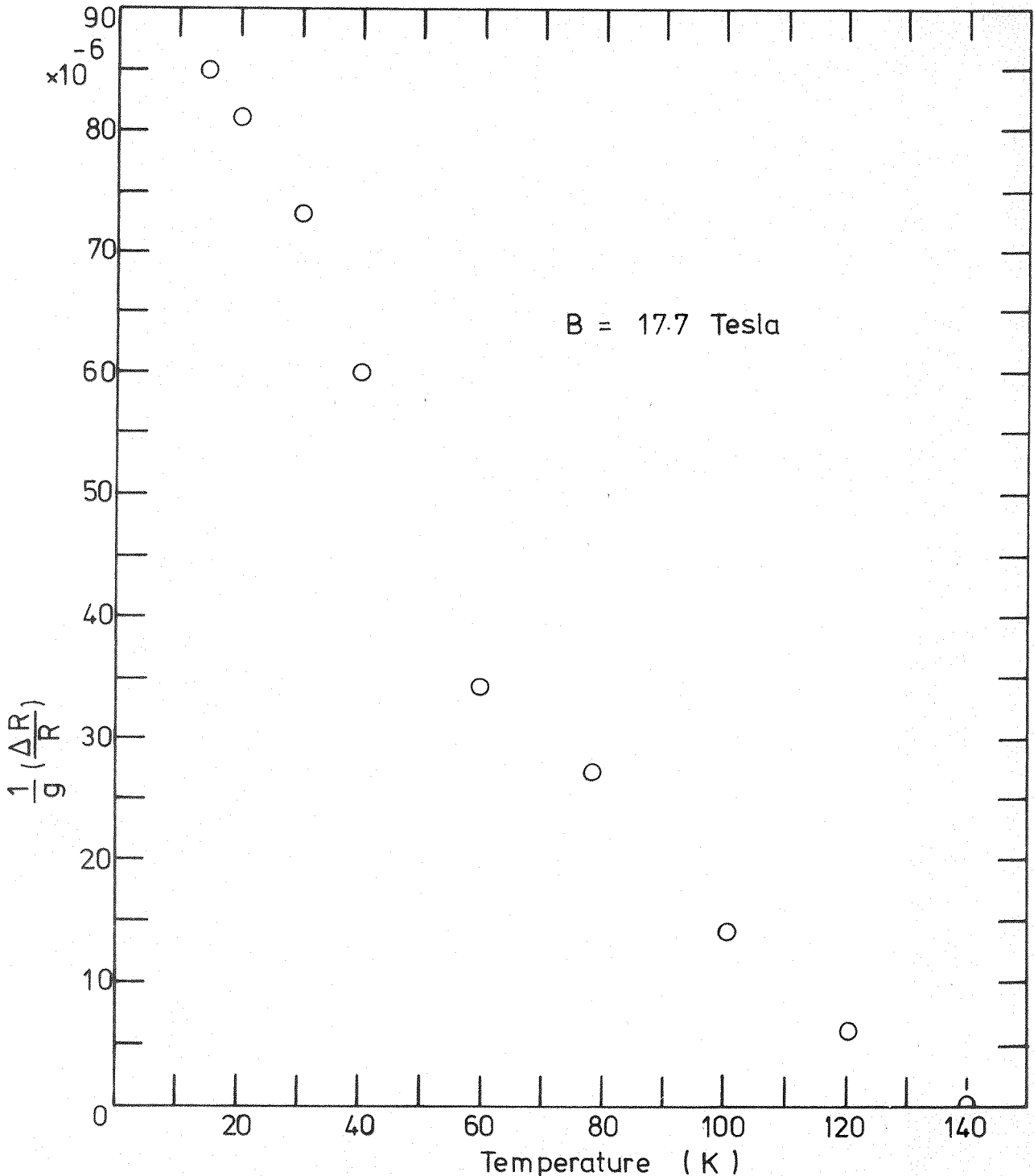

Fig. 3.11 d Magnetoresistance of strain gauge (K1) perpendicular to the applied field

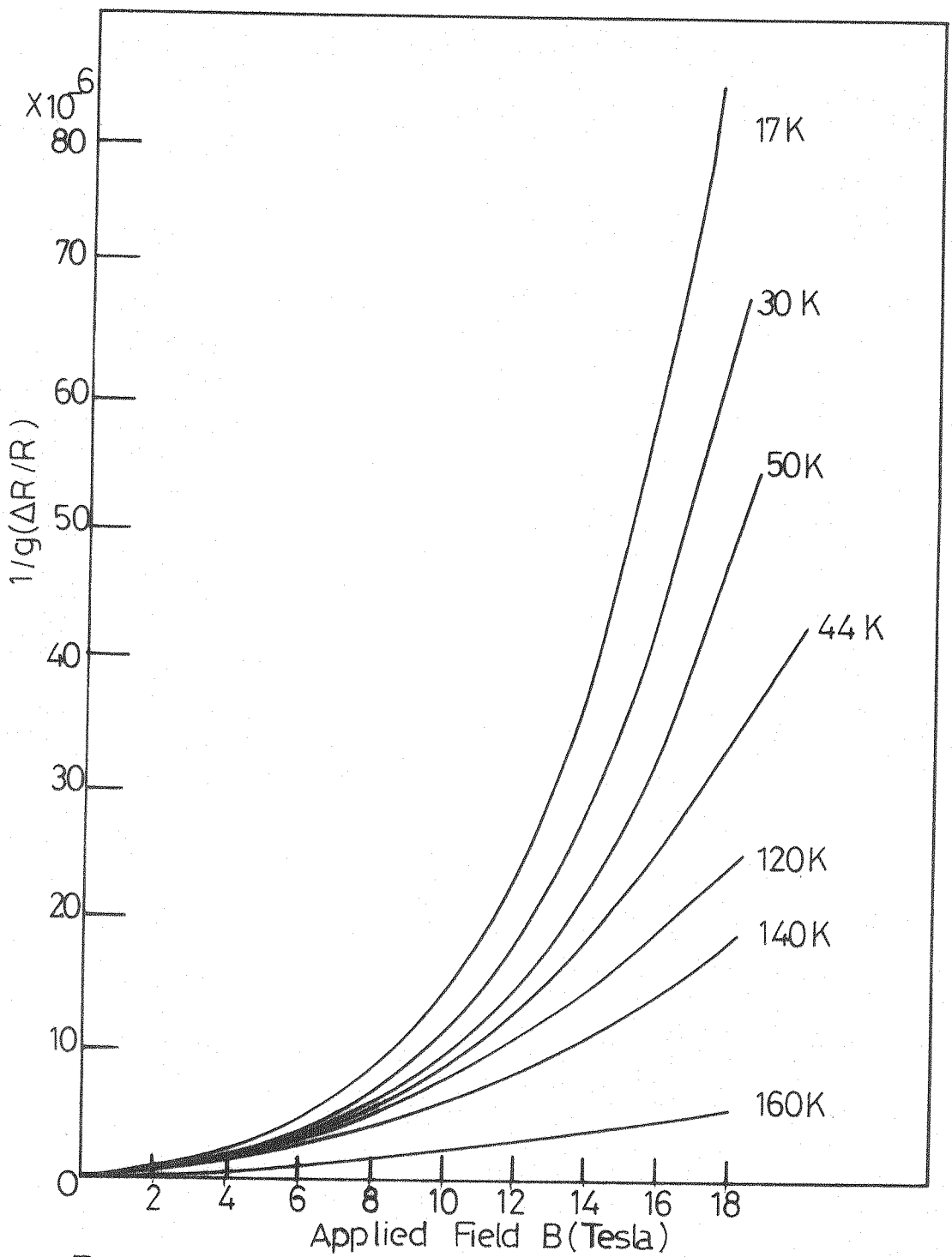

Fig. 3.12 The magnetoresistance of strain gauge, K_1, in terms of strain measured while the strain gauge was parallel to the applied field.

down to 16K at fields of 18 Tesla. They were bonded on to a piece of pyrex, since pyrex has a small thermal expansion coefficient ($\sim 50 \times 10^{-7} K^{-1}$). Durofix was used to attach the strain gauge on to pyrex so that it could be taken off easily.

In this work no dummy gauge was used and therefore the experiment utilised only one arm of the bridge. Ideally one would like to use identical active and dummy gauges so that magnetoresistance effects are automatically compensated during the experiment, but unfortunately no two strain gauges were found to have the same characteristics. However, by using one arm of the bridge and calibrating one gauge it was possible to obtain a satisfactory set of magnetoresistance, temperature curves from which the correction could be made easily.

The actual magnitude of the strain gauge magnetoresistance was not troublesome since when compared to the large measured magnetostriction of the RFe_2 compounds, it represented only a small correction ($\sim 2\%$).

Figures (3–11b), (3–11c) and (3–11d) are the magnetoresistance-temperatures curves for strain gauges K_1 and K_3 in the parallel and perpendicular direction to magnetic field.

3.11.2 **The gauge factor:** It has been established experimentally that the resistance of a thin wire varies proportionately to the strain to which it is subjected, provided the temperature is constant and the applied strain is small.

$$\frac{\Delta R}{R} = g \frac{\Delta \ell}{\ell} \qquad (3-30)$$

And g, the proportionality factor is defined as the gauge factor, which is the fractional change in resistance per unit strain.

This effect of resistance variation in resistance per unit strain as has been discussed by

Biermasz and Hoekstra (1949/50), who calculated it as follows:

Let the length of the wire be 'h' and it is diameter 'a'. The resistance of the wire then is:

$$R = \frac{h}{\pi a^2}\rho = \frac{h^2}{v}\rho \qquad (3-31)$$

where ρ is the resistivity and v is the volume of the wire .

Now if the strain gauge is stretched elastically by a relative elongation $\frac{\delta \ell}{\ell}$ where ℓ is the length of the strain gauge,

$$\frac{\delta h}{h} = \frac{\delta \ell}{\ell}$$

The resistivity and the volume will also change during this process therefore the change in the resistance is:

$$\frac{\delta R}{R} = 2\frac{\delta h}{h} + \frac{\delta \rho}{\rho} - \frac{\delta v}{v} \qquad (3-32)$$

At constant temperature the resistivity of a metal may be assumed to be a function of the volume only:

$$\frac{\delta \rho}{\rho} = C\frac{\partial v}{v} \qquad (3-33)$$

where C is a coefficient independent of elastic strain. The change in volume related to change in length by

$$\frac{\delta v}{v} = (1 - 2\nu)\frac{\delta h}{h} \qquad (3-34)$$

where ν is the poisson's ratio.

$$\text{Finally } \frac{\delta R}{R} = [\, 2 + (C - 1)(1 - 2\nu)\,]\frac{\delta \ell}{\ell} = g\frac{\delta \ell}{\ell} \qquad (3-35)$$

The factor g has a value of about 2.

Although the gauge factor is not very temperature sensitive, calibration for use at other temperatures remains necessary. Mclintock devised an apparatus for this purpose which essentially consists of a triangular cantilever beam to ensure constant strain along the entire length of the beam by maintaining constant stiffness-to-bending ratio. The calibration can be done in the temperature range between 4K and 300K and higher.

Strain gauges manufactured by H. Tinsley and Co. Ltd., were examined by Birss and Lee (1960) who found an increase of g of less than one percent when going from room temperature to 77K. Above room temperature g decreased by 0.01% per degree until failure of the gauge occurred at about 600 K.

Asgar [15] has used a miniature bending beam to calibrate the gauge factor, which could be deflected within the cryostat by rotating a cam, to which a small magnet was attached, using an external magnetic field.

In this work the gauge factor assumed to be constant $\simeq 2$.

3.12 The Type Q-plug-in Unit:

The Q-unit[13] is an A-C bridge with a 25 KHZ carrier, the output of which is applied to a synchronous phase-sensitive detector. It permits any Tektronic type 530, 540, or 550 series oscilloscope to be used for strain analysis. An excitation voltage of 5Vrms is provided by a 25 KHZ oscillator coupled to the bridge through a transformer. The unit provides high gain, low noise, an extremely low drift. Suppressed carrier amplitude modulation is produced by unbalancing the A-C bridge with the strain gauge or other transducers. It has ten calibrated steps from 10 microstrain per major graticule division to 10,000 microstrain per division.

Figure (3–12) shows the block diagram of the Q-plug-in unit while Figures (3–13) and (3–14) show the simplified schematic diagram of the bridge with the bridge balance

circuit and the calibration circuit respectively.

Depressing the "calibrate" button on the Q-unit front panel connects a calibration resistor in parallel with one arm of the input bridge. The calibration resistor supplied with the Q-unit simulates a $-400\,\mu$ strain unbalance of the bridge, when a 120 Ω strain gauge with a gauge factor 2 is used. In this experiment strain gauges of 350 Ω with gauge factor 2 were used and so the calibration resistor supplied with the Q-unit no longer simulated a $-400\,\mu$ strain unbalance. Therefore either the calibration resistor must be changed or a change in calibration strain allowed for when adjusting the GAIN ADJ. The calibration resistor was kept constant, and the gain changed to $-1{,}120\,\mu$st. This value was calculated from the following formula:

$$R_{cal} = \frac{Rs.G}{-(G.F.)(strain)} - Rs.G \qquad (3-36)$$

where R_{cal} is the calibration resistor
G.F. is the gauge factor
Rs.G is the resistance of the strain gauge.

In operation the bridge circuit modulates the 25 KC carrier in accordance with the bridge unbalance produced by the transducer.

Under no signal conditions, the bridge is balanced and the carrier is suppressed. The amplitude of the output signal from the bridge is determined by the amount of unbalance. The modulation sideband from the bridge circuit are applied to an A-C-coupled amplifier where the desired sidebands are amplified while unwanted frequencies are rejected.

To demonstrate the action of the unit, and the function of the filters, the signal was photographed at the output of the bridge, after the low frequency filter, and before demodulation (Fig. (3–13)). These photographs show that the bridge output consists of an unwanted magnetic field signal which completely swamps the desired modulated

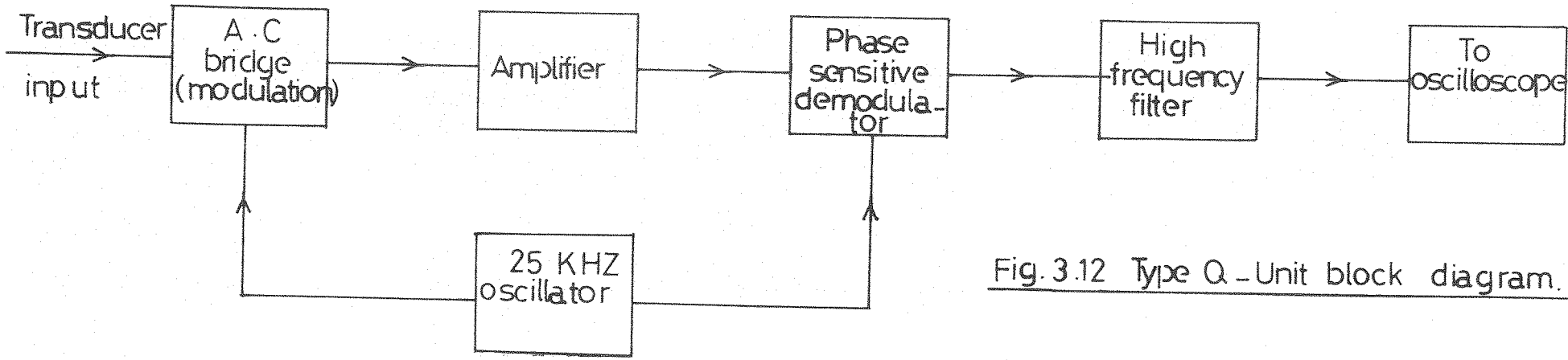

Fig. 3.12 Type Q - Unit block diagram.

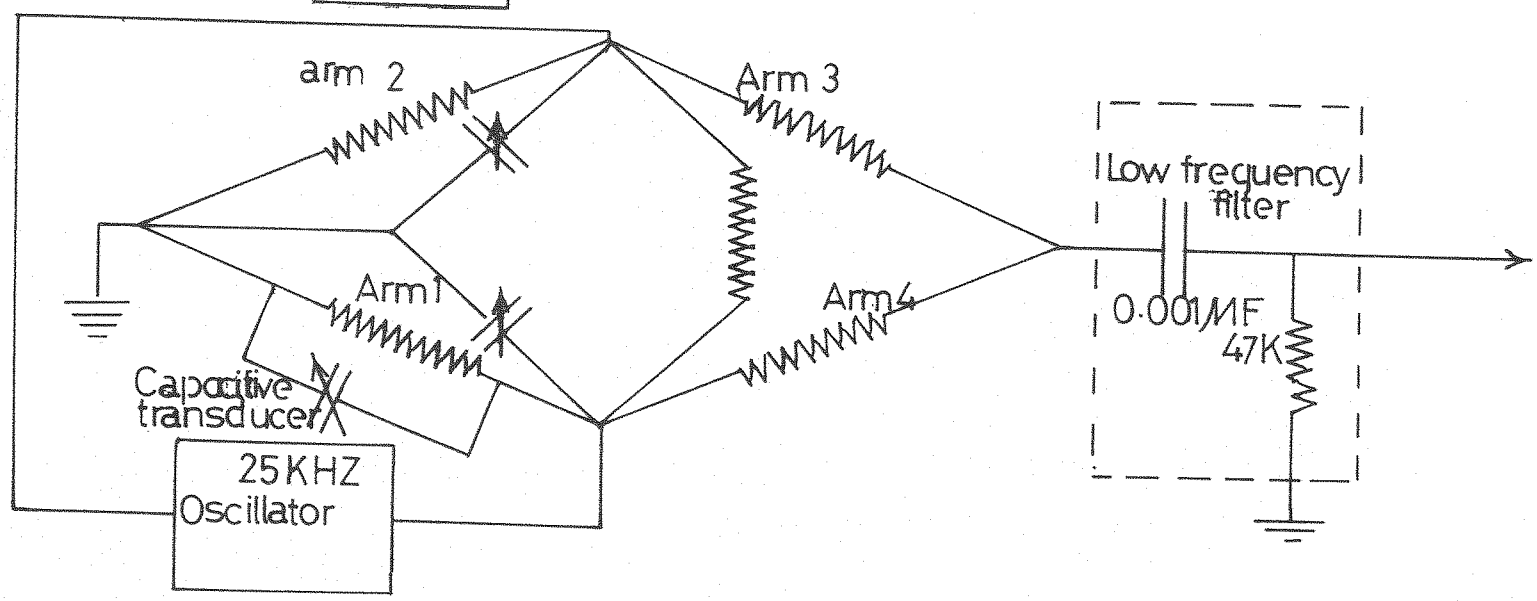

Fig. 3.13 Simplified schematic diagram of the bridge showing the bridge balance circuit and the low frequency filter.

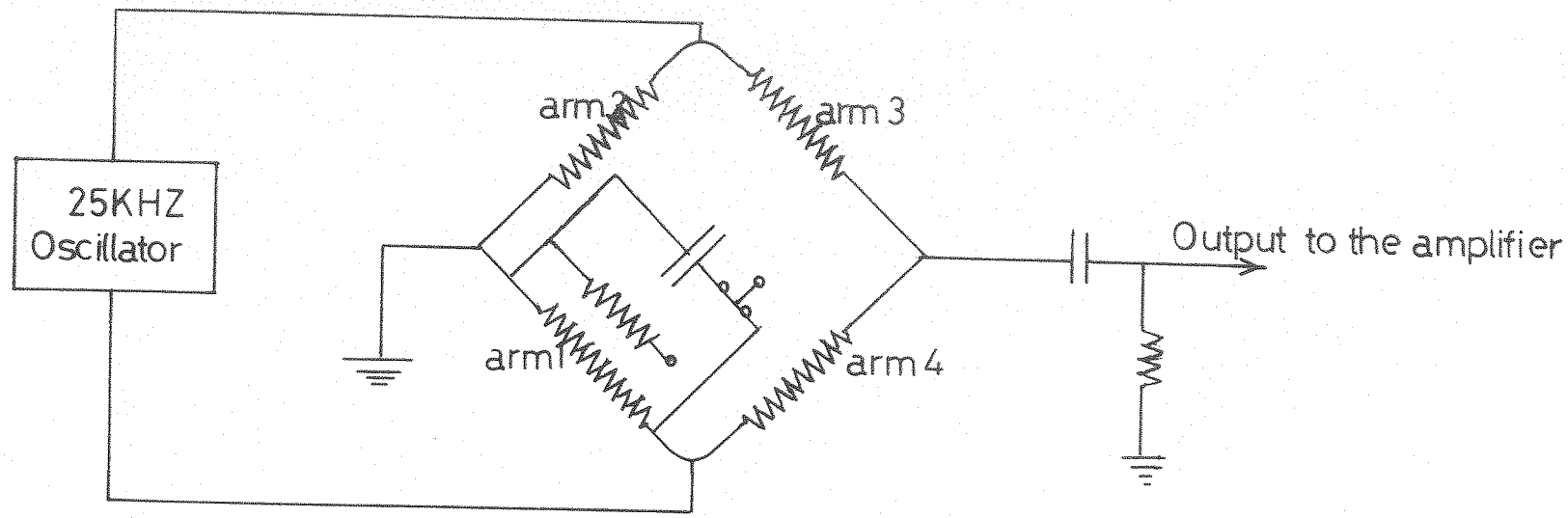

Fig.3.14 Simlified digram of the calibrating circuit.

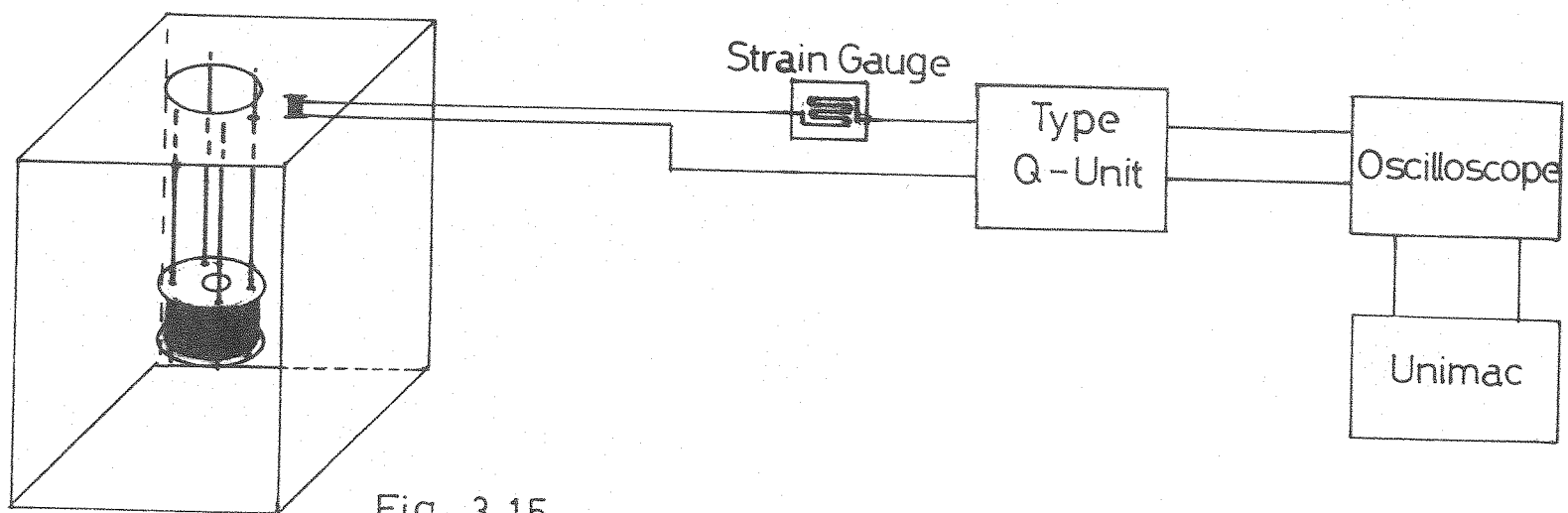

Fig. 3.15

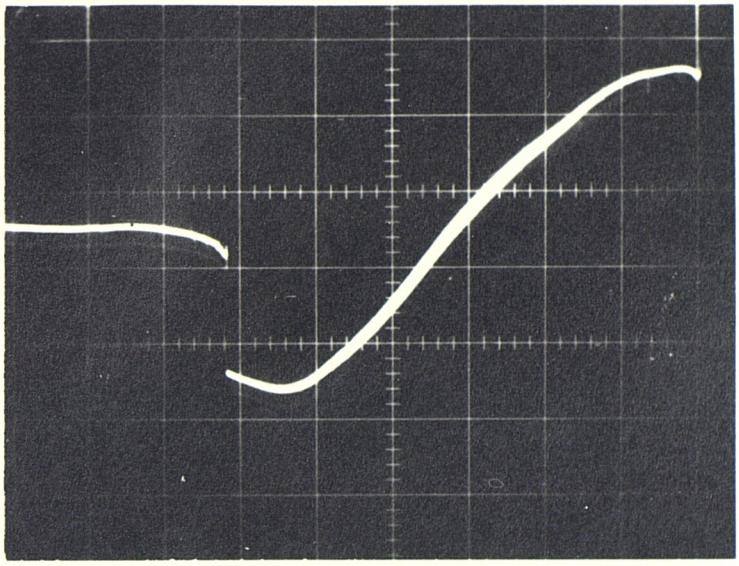

Fig. 3.16a The output of the A.C bridge before the short time constant filter. The unbalance is due to the magnetoresistance of the strain gauge (5 m. volt/cm.)

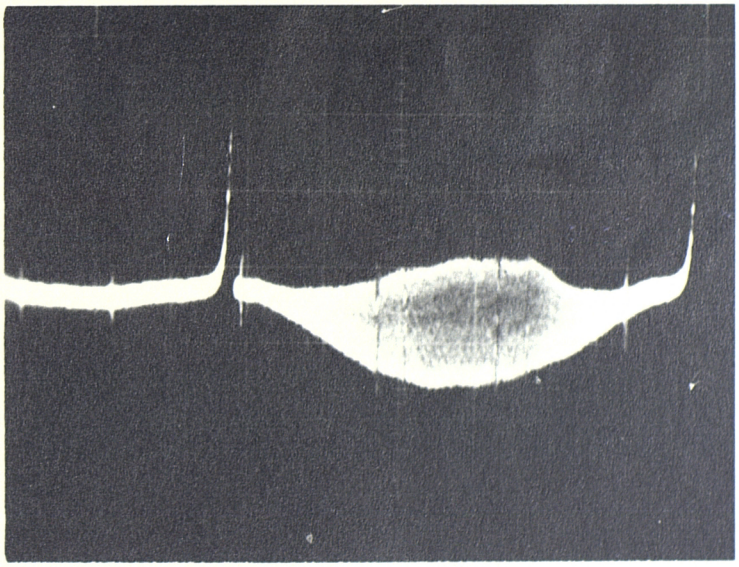

Fig. 3.16b. The output after the filter (1 m. volt/cm.)

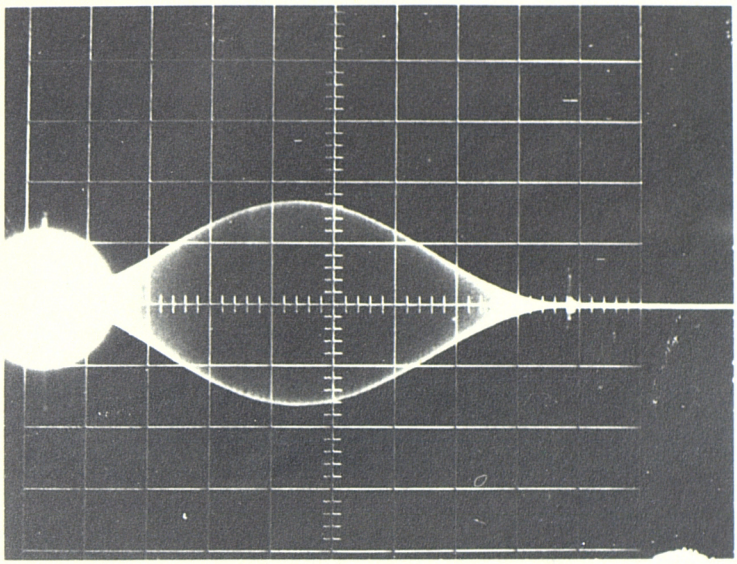

Fig. 3.16C. The output of the Q-unit before demodulation

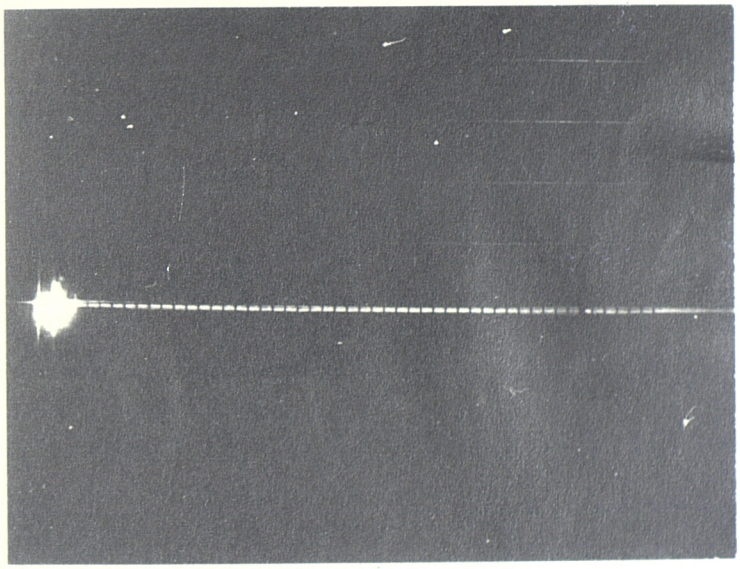

Fig. 3.16d. The output of the Q-unit when a search coil was connected to the arm one of the A.C bridge while a strain gauge was connected in series with the search coil to keep the bridge in balance.
(Scale 10 μst./Div.)

signal. The action of the filter is to get rid of this unwanted field signal and other pickup signals of low frequency.

The mains hum in the photograph (3–16b) is an artifact of the measurement. The signal is of very low amplitude (order of one millivolt) and so this part of the circuit is very sensitive to the influence of the measuring equipment.

The efficiency of the filter was shown by connecting a search coil to the A-C bridge, and pulsing the field; the unit recorded nothing as shown in Fig. (3–16d). In order to avoid measuring the magnetoresistance of the search coil itself, it was placed about ½m. away from the centre of the magnetic field coil. In this position the e.m.f. induced in the search coil was equal to that observed in the strain gauges when in the centre of the coil, but the magnetoresistance was zero.

CHAPTER IV – Results and Discussions

4.1 Introduction:

The cubic rare earth (R) – iron laves compounds RFe_2, have been subject to many structural and magnetic investigations. These compounds exhibit extremely large magnetostrictive strains ($> 10^{-3}$), and magnetic anisotropies at room temperature and down to liquid helium temperature. They also have very high magnetic ordering temperatures (570K – 800K)[1], and high saturation magnetisations which makes them attractive for various applications, including magnetostrictive transducers and permanent magnets.

Magnetostriction measurements at room temperature and magnetic fields up to 2.5 (Tesla) have been reported by many authors (2–7). Koon et al.[6] have measured the magnetostriction of a polycrystalline sample of $DyFe_2$, $ErFe_2$ and $HoFe_2$ over the temperature range 77–300K. They found that the magnetostriction for $DyFe_2$ at 300K in a field of 1.75 (Tesla) was 220×10^{-6}, which was the largest room temperature value observed at that time. While $(\lambda_{11} - \lambda\perp)$ for $HoFe_2$ is $\sim 100 \times 10^{-6}$ and $\sim -100 \times 10^{-6}$ for $ErFe_2$. In the same year (1972) Clark and Belson[5] measured the magnetostriction of $TbFe_2$ and $DyFe_2$ using polycrystalline samples at room temperature and in fields up to 2.5 (Tesla). They found that $(\lambda_{11} - \lambda\perp)$ for $TbFe_2$ was 2630×10^{-6}, while for $DyFe_2$ it was $\sim 600 \times 10^{-6}$. They also extrapolated to get $(\lambda_{11} - \lambda\perp)$ at 0K which they found to be $\sim 5100 \times 10^{-6}$. In their work the magnetostriction of $TbFe_2$ and $DyFe_2$ appear similar in some respects, but $DyFe_2$ was far from saturation. This led to an unusual temperature dependence of the magnetostriction in which $(\lambda_{11} - \lambda\perp)$ was increasing with increasing temperature in contrast to the usual negative $\delta\lambda/\delta T$. While the magnetostriction of $TbFe_2$ was near saturation in the same field and at the same temperature. The origin of this high magnetostriction in these compounds is thought to be the large

strain-dependent amisotropy of the rare-earth ions situated at cubic sites in the RFe_2 lattice. The magnetostriction of these compounds remains large at room temperature because of the large rare-earth-iron exchange interaction which aligns the rare earth spins even at room temperature.

More investigations have been carried out recently on the RFe_2 series by the same authors, Clark[2], Clark and Callen[3] and Koon[7]. Clark[2] has measured $(\lambda_{11} - \lambda\perp)$ for $TbFe_2$, $SmFe_2$, $DyFe_2$ and $TmFe_2$. The slow increase in magnetostriction with field (particularly for $DyFe_2$) indicates a large magneto-crystalline anisotropy with values of $K \sim 10^7$ ergs/cm^3 at room temperature. Mossbauer measurements by Wertheim et al.[8] and Bowden et al.[9] show that the heavy rare earth compounds Tb, Er, and Tm, have an anisotropy constant $K_1 < 0$ and Dy and Ho can be grouped together with $K_1 > 0$. The change in sign is because the rare earth 4f charge cloud changes from oblate to prolate as one proceeds across the periodic table from Ho to Er. The easy axis of magnetization for $ErFe_2$, $SmFe_2$ and $TbFe_2$ is the [111] direction and [100] for $DyFe_2$ and $HoFe_2$. There is a striking difference between the field dependence of the magnetostriction of these compounds with [111] easy direction and [100] easy direction. A rapid rise to a value close to saturation was found for (111) easy materials, while a slow approach to saturation was noticed for the [100] materials[2], this is very clear in the case of $DyFe_2$. Therefore, Clark[2] suggested that $\lambda 111$ is probably much greater than $\lambda 100$, so the magnetostriction of $TbFe_2$, $ErFe_2$, $SmFe_2$ and $TmFe_2$, arises directly from $\lambda 111$, while for $DyFe_2$ it arises from the rotation of the magnetization away from the easy [100] axes, causing $\lambda 111$ to contribute. The magnetostriction of a single crystal of $ErFe_2$ also has been measured, which showed that $\lambda 111 \sim 300 \times 10^{-6}$ with field up to 2.5 (Tesla), while $\lambda 100$ could not be detected[2]. Clark also believes the magnetostriction of $DyFe_2$, $TbFe_2$,

$ErFe_2$, etc. is due to domain wall motion alone, but as it is well known, domain wall displacements are an easy process and it should be completed at fields ~ 1 Tesla. Also his suggestion that $\lambda 111 >> \lambda 100$ is not always true, and the reason that he did not detect $\lambda 100$ for $ErFe_2$, is because he did not use a high enough magnetic field.

More recently work by Clark and Callen [3] on a single crystal and polycrystal of $TbFe_2$ and $ErFe_2$ have been reported. They found that $\lambda 111 = 2400 \times 10^{-6}$ for $TbFe_2$ and at room temperature and $K_1 = -7.6 \times 10^6$ J / m^3, while for $ErFe_2$ $\lambda 111 = -300 \times 10^{-6}$.

Atzomony et al. [10 11] have determined the easy direction of magnetization of the ternary compounds $Ho_xTb_{1-x}Fe_2$, $Ho_xEr_{1-x}Fe_2$, $Dy_xTb_{1-x}Fe_2$ and $Ho_xTm_{1-x}Fe_2$, by means of the mossbauer effect. They have also shown that the composition-temperature plane (x, T) is divided into two or three regions, in each of which the easy direction of magnetization is along a different major crystal axis. For $TbFe_2$, $ErFe_2$ and $TmFe_2$, [111] is the easy direction while for $DyFe_2$ and $HoFe_2$ it is [100].

The magnetic properties of several series of iron compounds are currently the subject of investigations in several laboratories. The RFe_2 compounds exhibit very interesting magnetic behaviours. The electrons responsible for the magnetism of the rare earth ions are the well localized 4f electrons which are enveloped by 5S and 5P shells, so they are insensitive to the interactions with neighbouring atoms. For transition metals the correlations between the 3d electrons are strong and give rise to important short range magnetic interactions. Therefore when increasing the rare earth content in a compound a decrease of the mean value of the magnetic moment of Fe, Co, or Ni takes place[12 13 14]. The magnetic anisotropy of the rare earth containing alloys and compounds is related mainly to the interaction between the crystal field and the 4f electrons of the rare earth ions.

Nesbitt et al.[15] in 1959, studied the bulk magnetic characteristics of a series of Gd–Fe alloys, including $GdFe_2$ and he concluded that they are ferrimagnetic materials. More work was done later in 1964 [16] [17] [18]; these and many other studies[19]–[27] showed that R–Fe coupling is antiferromagnetic when R is a heavy rare earth, and coupled ferromagnetically when R is light rare earth. The mossbauer data of Werthiem and Wernick[8] and magnetization data of Crangle and Ross[20] showed that the iron in these compounds carries a magnetic moment of 1.7 $\mu\beta$. Crangle and Ross have also found an anomalous break occuring in the magnetization temperature curves for all members of RFe_2 and RCo_2 series. However there is clear indication that the anomolous breaks in RCo_2 series are due to a second phase in these compounds[28].

Nikiten and Bisliev[29] have calculated the effective exchange field acting on the rare earth ions. It is equal to 260 (Tesla) for $ErFe_2$, $HoFe_2$ and $DyFe_2$ at 300 K, and 280 (Tesla) for $GdFe_2$. These are the highest known values of the exchange field acting on the rare earth side of rare-earth ferromagnets, ferrimagnets (in case of rare-earth iron garnets H_{eff} = 30 (Tesla), and in orthoferrites, H_{ef} = 1 Tesla). The high values of H_{eff} are responsible for the magnetic ordering of the rare-earth sublattice at high temperatures.

4.2 **The magnetic properties of R–M Compounds** (R and M represents a rare earth and 3d element respectively):

The magnetic characteristics of rare earth intermetallic can not be fully appreciated without understanding of the nature of the magnetic interactions. There are three types of interactions which are responsible for the magnetic properties of R–M compound: R–R, M–M, and R–M interactions. This mechanism is called (RKKY) interaction (Ruderman–Kittel–Kasuya–Yosida).

The R–R interaction is believed to be the weakest in this group, because the 4f

electrons are localized inside the 5S, 5P electrons, so that the overlap between f orbitals centred on adjacent atoms is very small or negligible. Hence the exchange interaction and the dipole dipole interaction is very small and does not contribute to the total magnetic interactions. The dominant influence is the indirect interaction proceeding via the conduction electron spin polarization[30]. The polarization of the conduction electrons decreases as the distance from the magnetic ion increases in a damped oscillatory fashion, and it can lead to ferromagnetic as well as antiferromagnetic coupling.

Magnetization measurements on RFe_2 compounds indicate that R–R interaction is very weak and the M–M is the dominant interaction[1 20 31 32]. Magnetization measurement on RNi_2 and RCo_2[16 17 18 33–36] showed that for different transition metals this is not necessarily true.

The dominance of M–M interaction is because the 3d electrons are less localized than the 4f electrons. So they overlap a good deal and the interaction between two intermetallic ions is a direct exchange interaction. This interaction can be studied very well in compounds in which the R component is non-magnetic, ie. for compounds in which R represents La or Y. The R–M interaction is expected to be the intermediate one.

4.3 The Crystal Structure of RFe_2 Compounds:

The RFe_2 compounds (R = rare earth atom) are cubic laves phase compounds and have $MgCu_2$ type structure. The laves phase denote a large group of related intermetallic compounds AB_2 having one of the following structure types[36 37 38]:

(a) $MgCu_2$ (b) $MgNi_2$ (c) $MgZn_2$

The $MgCu_2$ structure is cubic, while the $MgNi_2$ and $MgZn_2$ structures are hexagonal on the basic of a hard sphere packing model. The ideal ratio of the atomic diameter

dA/dB for the formation of the laves phases is 1.225. Most of the compounds however have ratios which vary between 1.1 and 1.6 and because of this geometrical requirements, homogeneity ranges in these compounds are generally small. Dwight (1961), suggests that the Goldschmidt radii of the pure elements are not an important factor in detecting which of the three structure form. It is only necessary that the A atom be larger than the B atom and that they be able to contract or expand to achieve nearly the ideal ratio of 1.225.

The $MgCu_2$ structure has 8 formula of RFe_2 per unit cell. It can be regarded as being made up of two interpenetrating lattices of A and B atoms. The B atoms lie at the corners of tetrahedra and the tetrahedra are joined at points. Although the co-ordination to an A atom is four other equidistant A atoms, there are twelve B atoms at a somewhat smaller distance. Each B atom is surrounded by 6B and 6A atoms. There is an A atom at each cube corner of the crystal lattice.

The crystallographic properties of RFe_2 (R = Gd, Tb, Er, Ho, Dy, Tm) and YFe_2 intermetallic Compounds have been studied by various authors.[39–47]

Owing to a different electronic configuration there is a considerable difference between the dimensions of the two types of atoms forming the compounds, the rare earth element having a greater ratio than the iron. The most compact arrangement of hard spheres of two sizes within the cell is 1.225. As the radius ratio of the constituent atoms is greater than the above value[48], some changes occur in order to approach the ideal value. Thus the R atoms contract and Fe atoms expand. The effort has to be made to obtain a single phase material. Figure (4–17) shows the $MgCu_2$ structure.

4.4 The Compound preparation and identification

The two samples $TbFe_2$ and $DyFe_2$, were prepared in this laboratory in a water-

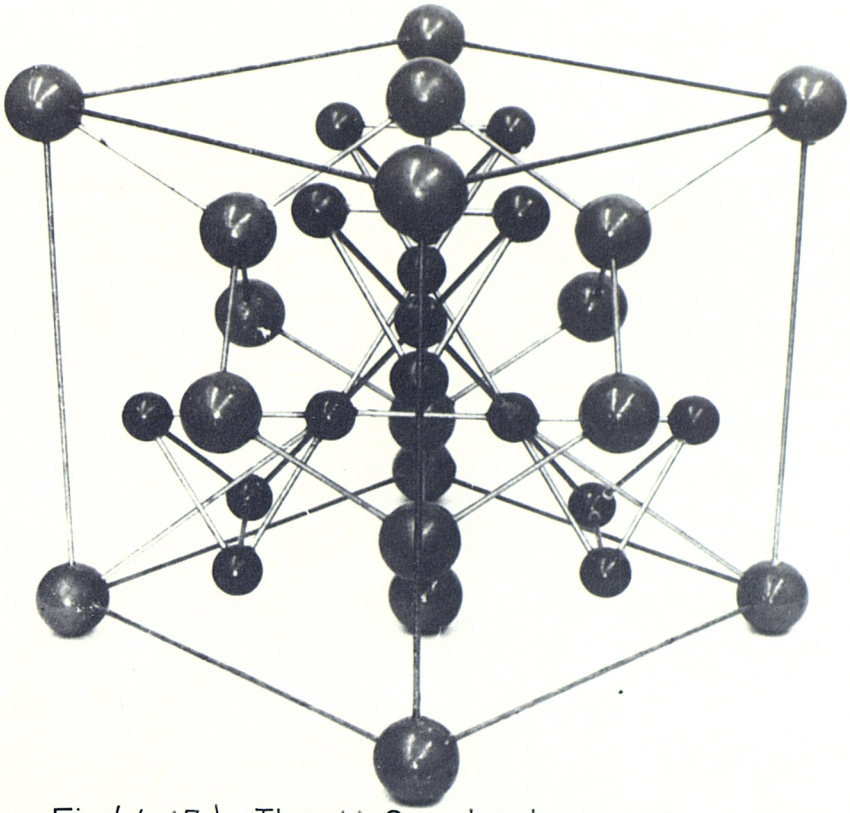

Fig (4.17) The $MgCu_2$ structure

Rare earth element

Transitional element

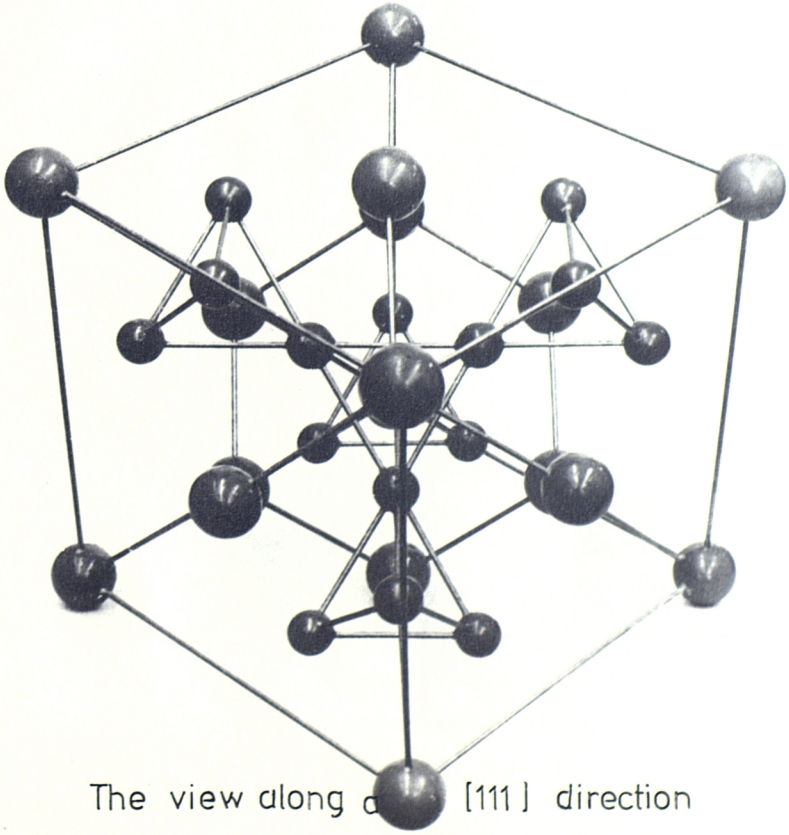

The view along a [111] direction

cooled argon arc furnace. The constituent elements were melted. The process of inverting and melting of the button was repeated five times. The purity of the starting material was 99.9% in the case of Dy and Tb and 99.99% in the case of iron.

The specimen was then taken out and weighed again. In $TbFe_2$ and $DyFe_2$ the losses were 0.06% and 0.65% respectively. The specimens were then sealed in silica tube and annealed for four weeks.

The lattice parameters of these two samples were determined by x-ray diffractometer study. By using the Nelson-Riley[49] extrapolation function the result agreed quite well with the previously reported results.

For $TbFe_2$: a = 7.348 $\mp$ 0.002, while for $DyFe_2$: a = 7.328 $\mp$ 0.002, at room temperature.

4.5 Form of magnetostriction – field curves of $DyFe_2$ compound:

The magnetostriction of $DyFe_2$ compound in the directions parallel and perpendicular to the field has been measured between 16K and 300 K, and at pulsed magnetic fields up to ~ 18 Tesla.

Figures (4–18) and (4–19) show the isotherms of λ_{11} and $\lambda\perp$ against applied field. It is clear that the magnetostriction is very far from saturation at the highest applied fields. The curves show that there is a domain wall displacement which takes place at room temperature and it decreases rapidly by decreasing the temperature, until ~ 150K the magnetostriction curves take a linear form, hence the domain wall displacements disappear. This leads to a suggestion that, $DyFe_2$ compound may have only 180° domains at low temperatures which is unusual for the cubic compounds which have 180° and 90° domains if [100] is the easy direction of magnetization.

Therefore, the linearity of the magnetostriction field curves is believed to be due

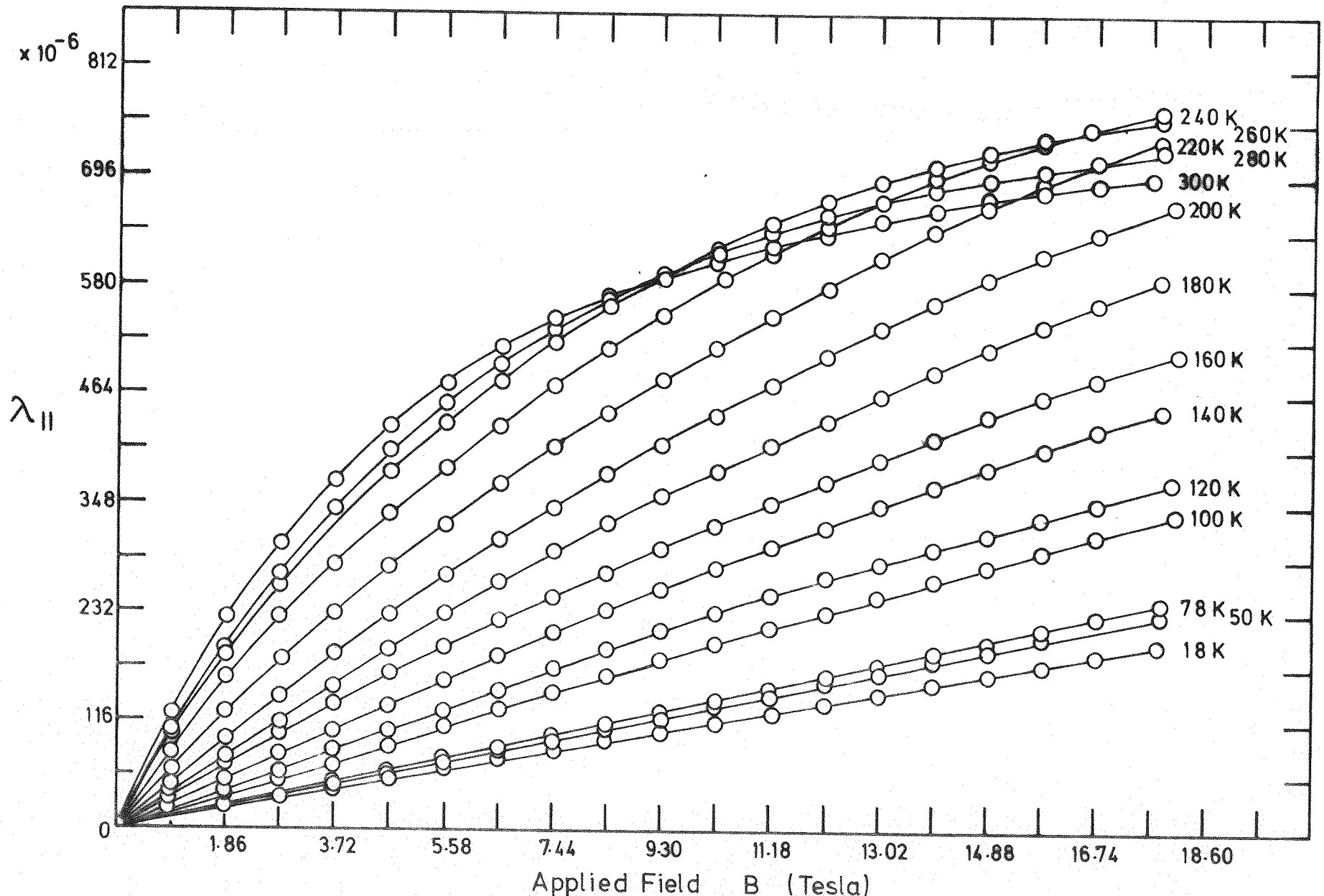

Fig. 4·18 The Magnetostriction of $DyFe_2$ parallel to the applied field direction

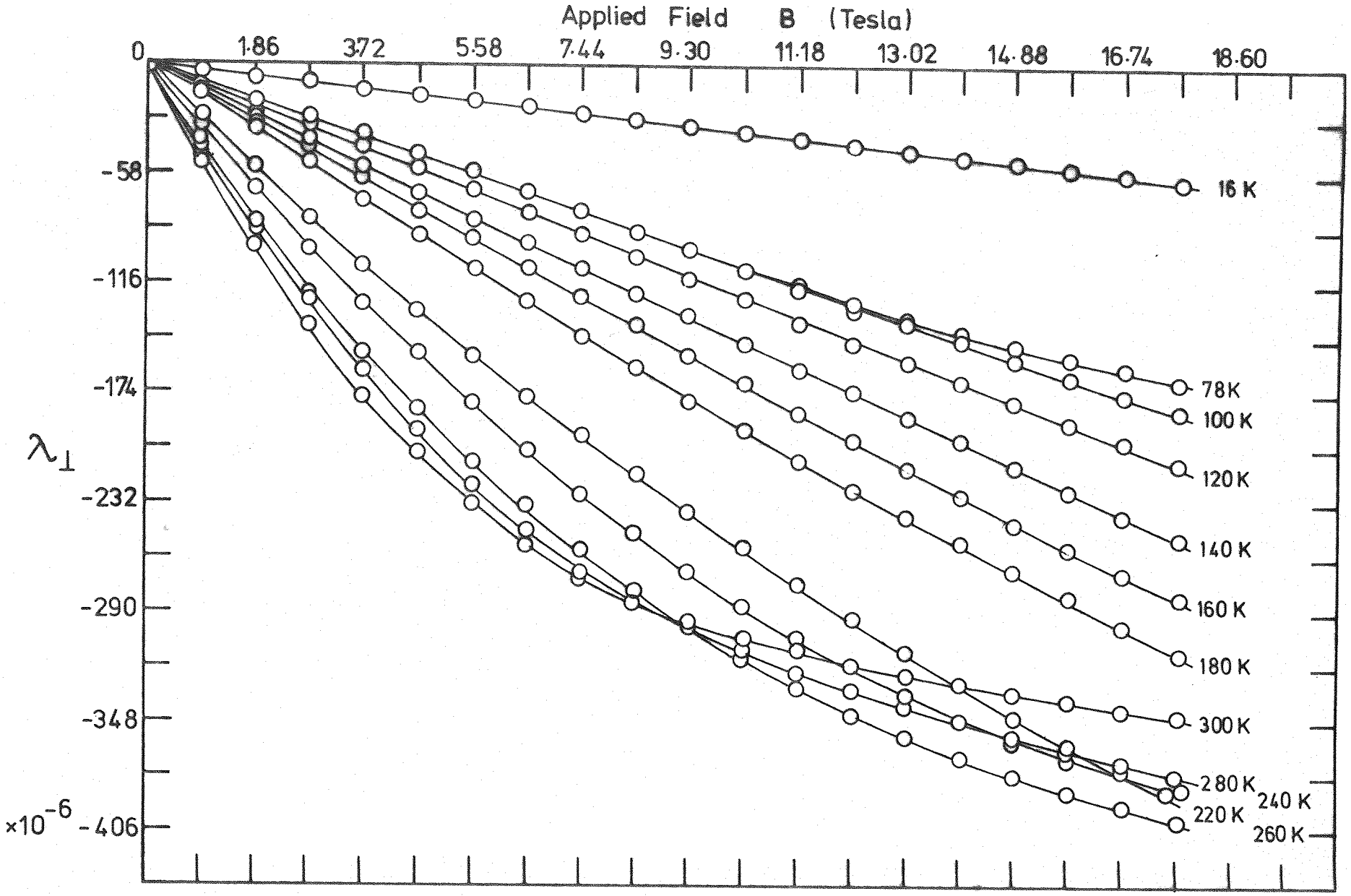

Fig. 4·19 The Magnetostriction of $DyFe_2$ perpendicular to the applied field direction

to the rotation of magnetization against anisotropy. It remains far from saturation up to 18 Tesla because $DyFe_2$ is a highly anisotropic compound. It has been found that K_1 Fo $DyFe_2 \simeq 2.1 \times 10^6$ J /m^3 [2], 2.7×10^6 J / m^3 [11] and 7.2×10^6 J/m^3 [10] at room temperature and it increased dramatically by decreasing the temperature: it is $\simeq 84 \times 10^6$ J/ m^3 at 4K[11]. The value of $K_1 = 7.2 \times 10^6$ J/ m^3 is more acceptable than the other values. By using this value the anisotropy field for $DyFe_2$ becomes ~17 Tesla. Experimentally it was noticed that 17 Tesla was not high enough to achieve saturation at room temperature.

To find out whether $DyFe_2$ can have only 180° domain walls as a preferred configuration or both 180° and 90° domain walls, calculations for the total energy in both cases may be made as follows:

In figure (4–20a) the magnetostatic energy $E_{mag.st.}$ can be given:

$$E_{mag.st.} = 1.704\, M_S^2\, d \quad (50) \quad \text{(cgs)}$$

where d is the width of the domains, M_S is the saturation magnetization.

$$E_{mag.st.} = 0.136\, \mu_0\, M_S^2\, d \quad \text{(SI Unit)} \qquad (4\text{–}37)$$

where M_S (A/m)
d (m)
μ_0 $4\pi \times 10^{-7}$ H. m^{-1} .

The total energy:

$$Et_1 = E_{mag.st.} + Ew \qquad \text{where Ew is the wall energy.}$$

$$Ew = \frac{\gamma t}{d} \quad (50) \qquad (4\text{–}38)$$

where γ is the surface energy of the wall
t is the thickness of the plate.

The equilibrium value of d is determined by minimizing the total energy

$$Et_1 = 0.136\, \mu_0\, M_S^2\, d + \frac{\gamma t}{d} \qquad (4\text{–}39)$$

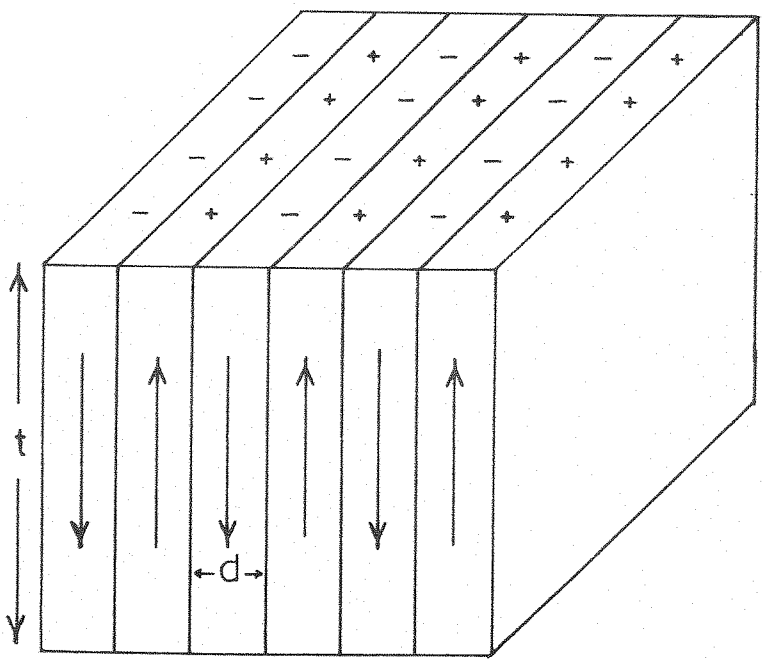

Fig. 4.20a 180° Domain walls

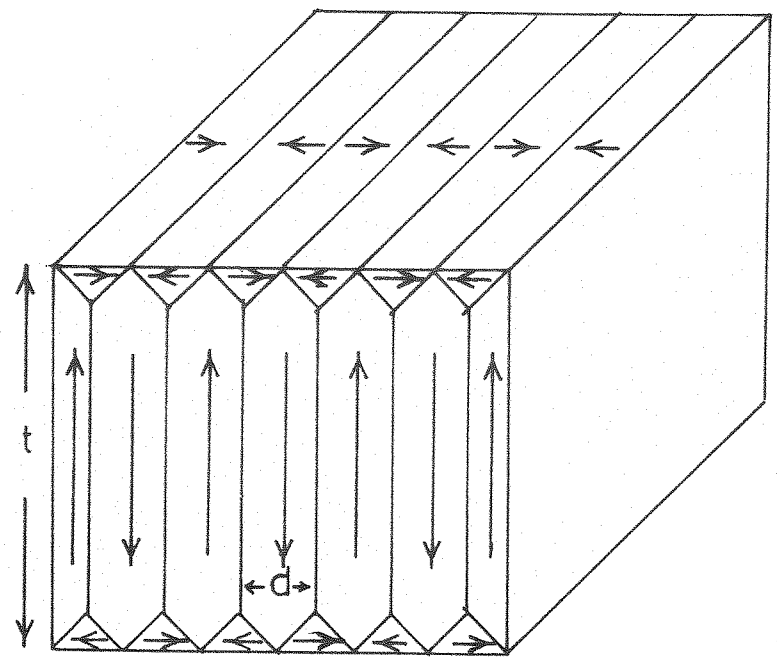

Fig. 4.20b 180° and 90° Domain walls

$$\frac{\partial Et_1}{\partial d} = 0.136\,\mu_0\,M_s^2 + \left(-\frac{\gamma t}{d^2}\right) = 0$$

or $$d = \sqrt{\frac{\gamma t}{0.136\,\mu_0\,M_s^2}}$$

From Fig. (4–20b)

The magnetoelastic energy $E_{mag.el.}$ is given:

$$E_{mag.el.} = \frac{9}{16}\lambda_{100}^2\ C_{11}\ d \qquad (4–41)$$

where λ_{100} is the elongation along [100] direction
C_{11} is the elastic moduli (N/m^2)

The total energy $Et_2 = E_{mag.el.} + Ew$

$$Et_2 = \frac{9}{16}C_{11}\,\lambda_{100}^2\,d + \frac{\gamma t}{d} \qquad (4–42)$$

By minimizing the energy

$$\frac{\partial Et_2}{\partial d} = \frac{9}{16}C_{11}\lambda_{100}^2 - \frac{\gamma t}{d^2} \qquad (4–43)$$

or $$d = \frac{4}{3}\sqrt{\frac{\gamma t}{\lambda_{100}^2 C_{11}}}$$

From equation (4–39) and (4–42), the magnetoelastic and the magnetostatic energy can be compared as follows:

$$\frac{E_{mag.st.}}{E_{mag.el.}} = \frac{0.136\,\mu_0 M_s^2 d}{\frac{9}{16}\lambda_{100}^2 C_{11} d} \qquad (4–44)$$

$C_{11} = 9.4 \times 10^{10}\ N/m^2$

$M_s = 620 \times 10^3\ A/m$ at 300K

$\lambda_{100} = 850 \times 10^{-6}$

$M_s = 1295 \times 10^3\ A/m$ at 0K

$\lambda_{100} = 3200 \times 10^{-6}$

Substituting the values of M_S and λ_{100} at room temperature in equation (4–44) it gives:

$$\frac{E_{mag.st.}}{E_{mag.el.}} = \frac{2d}{1d} \qquad (4–45)$$

Equation (4–45) shows that the magnetoelastic energy is less than the magnetostatic energy.

By using the minimized equilibrium value of 'd' equation (4–39) and (4–42) becomes:

$$Et_1 = 2\sqrt{0.136\,\mu_0\,\gamma t\,M_S} \qquad (4–46)$$

$$Et_2 = \frac{3}{2}\sqrt{C_{11}\,\gamma t}\qquad \lambda_{100} \qquad (4–47)$$

or

$$\frac{Et_1}{Et_2} = \frac{512\quad\sqrt{\gamma t}}{390\quad\sqrt{\gamma t}} \qquad (4–48a)$$

Substituting for λ_{100} and M_S at 0K

$$\frac{Et_1}{Et_2} = \frac{107\quad\sqrt{\gamma t}}{147\quad\sqrt{\gamma t}} \qquad (4–48b)$$

Equation (4–48a) shows that the total energy in Fig. (4–20b) is less than the total energy in Fig. (4–20a) therefore $DyFe_2$ might have 180° and 90° domains at room temperature, while equation (4–48b) shows that at low temperature the 180° domains may be the preferred configuration.

To understand the magnetostriction curves in more detail, the magnetization of $DyFe_2$ compound has also been measured at pulsed magnetic fields up to 18 Tesla and at temperatures between 4.2K and 300K. The magnetization was measured in the cooling direction of the sample and on the direction perpendicular to the cooling direction.

These measurements show that there is a degree of alignment in the cooling direction, eg. the specific magnetization, σ, at 18 Tesla and 4.2K was ~121 A.m^2/Kgm in the cooling direction, while it was ~84 A.m^2/Kgm in the direction perpendicular to the cooling direction, Fig. (4–21).

Figures (4–22) and (4–23) show the magnetization field curves in the parallel and perpendicular to the cooling direction. The sharp jump in the beginning of each magnetization curve is believed to be due to the 180° domain walls displacements which do not appear in the magnetostriction curves because 180° domain walls displacements do not contribute to the magnetostriction. The linear part of the magnetization curves is due to the rotation of the magnetization against the anisotropy. It is very clear that $DyFe_2$ is still very far from saturation at the highest fields, and there is a great similarity in the linear part of the magnetization and magnetostriction curves.

In the case of the magnetostriction measurements, the sample used in the experiment was cut so that the cooling direction was perpendicular to the plane of the sample. The strain gauge was bonded on the surface of that plane. That means that the magnetostriction was measured in the harder direction (the direction perpendicular to the cooling direction).

The linear variation of the magnetostriction can be accounted for as follows: Suppose the magnetization in this region to be $M = M_k + XhfH$ [51]. For anisotropy constant $K_1 > 0$, where M_k is the magnetization at the knee of the magnetization curve and Xhf is the high-field volume susceptibility.

For a single crystal, after 180° walls displacement have completed,

$$\frac{\partial \ell}{\ell} = 0 \qquad \text{for} \frac{M}{M_s} \leqslant \frac{1}{3}$$

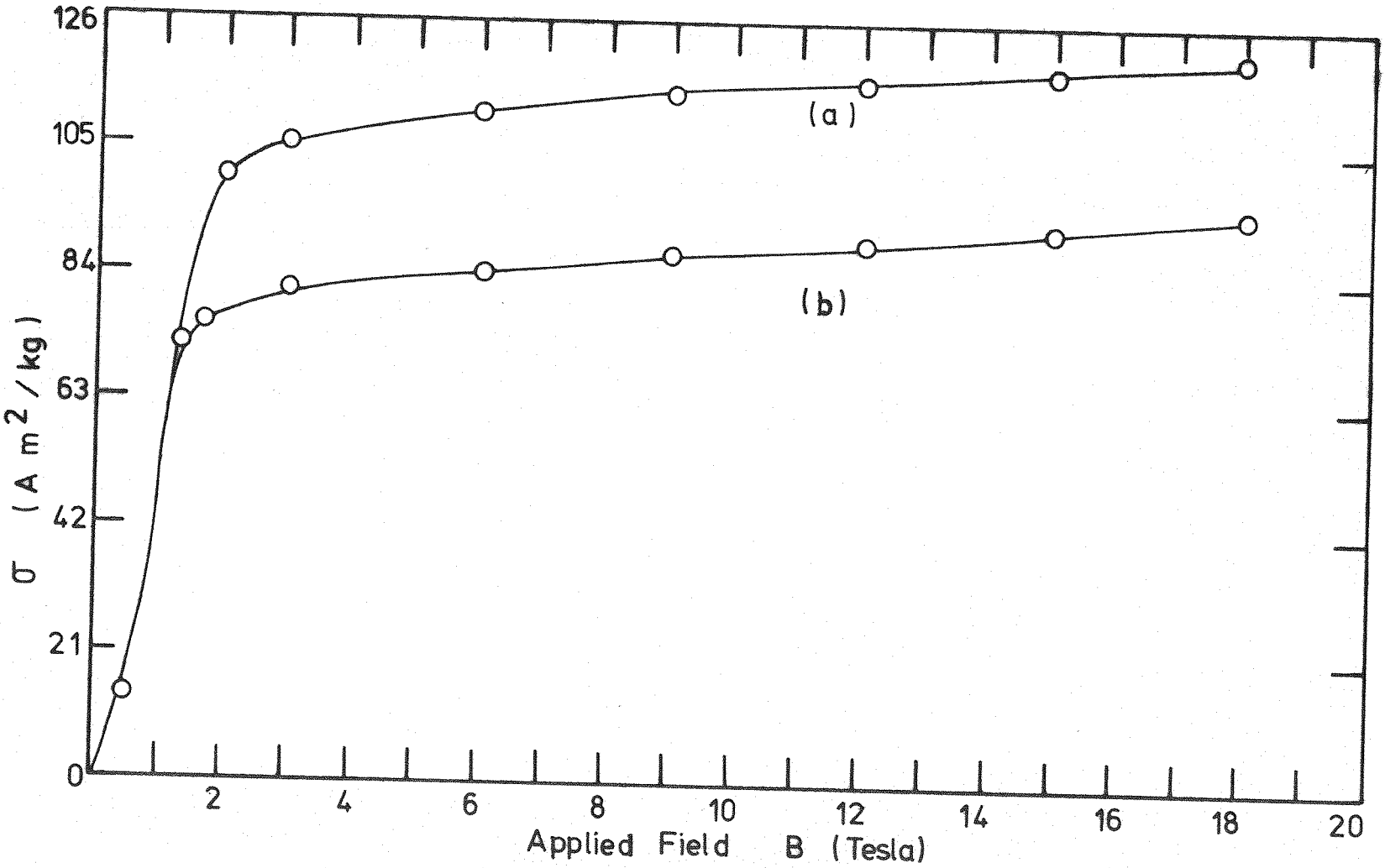

Fig. 4·21 Specific Magnetization versus Field for $DyFe_2$ at 4·2 K
(a) Applied field parallel to the cooling direction of the sample
(b) Applied field perpendicular to the cooling direction of the sample

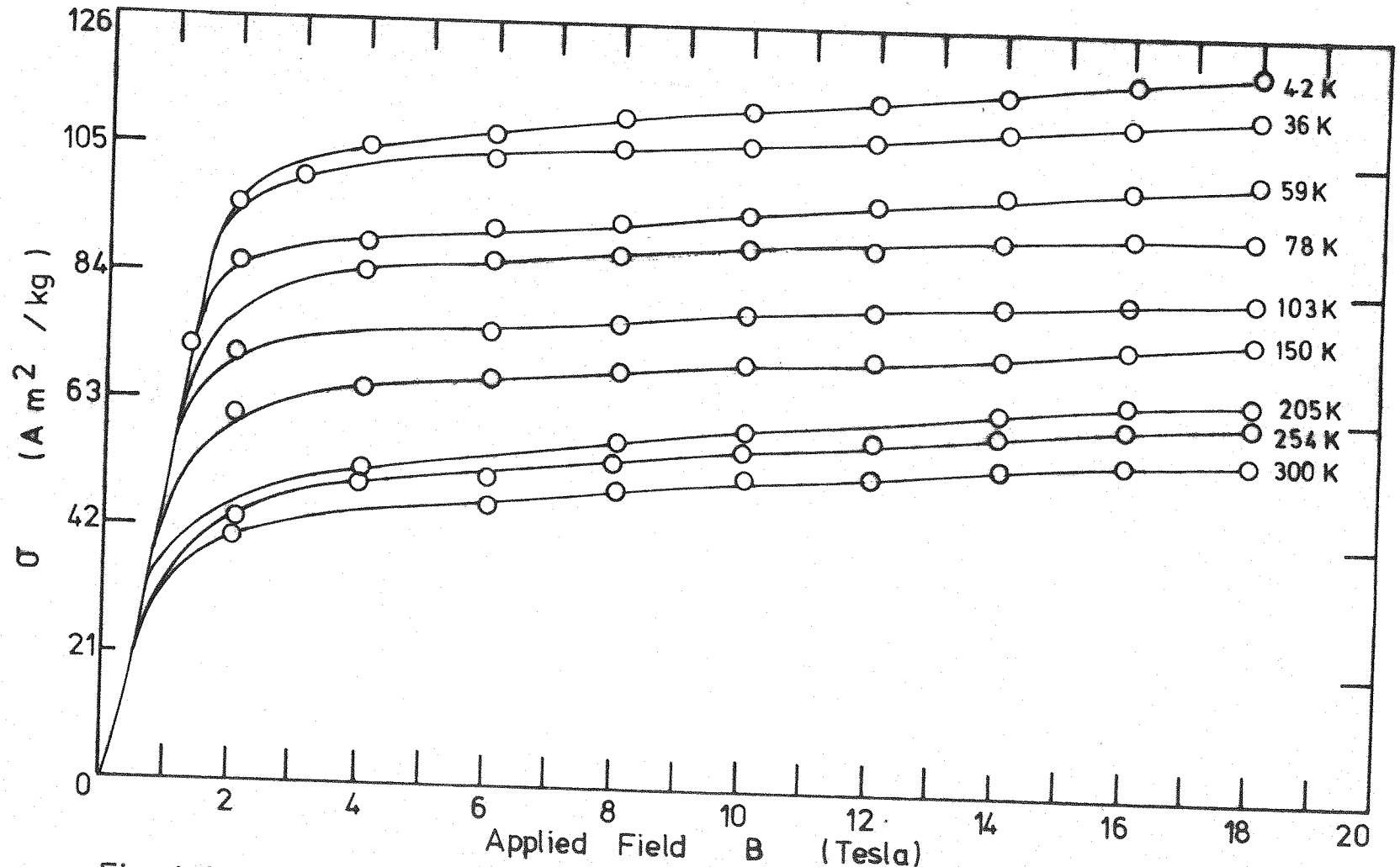

Fig. 4.22 Specific Magnetization of $DyFe_2$ parallel to the cooling direction of the sample

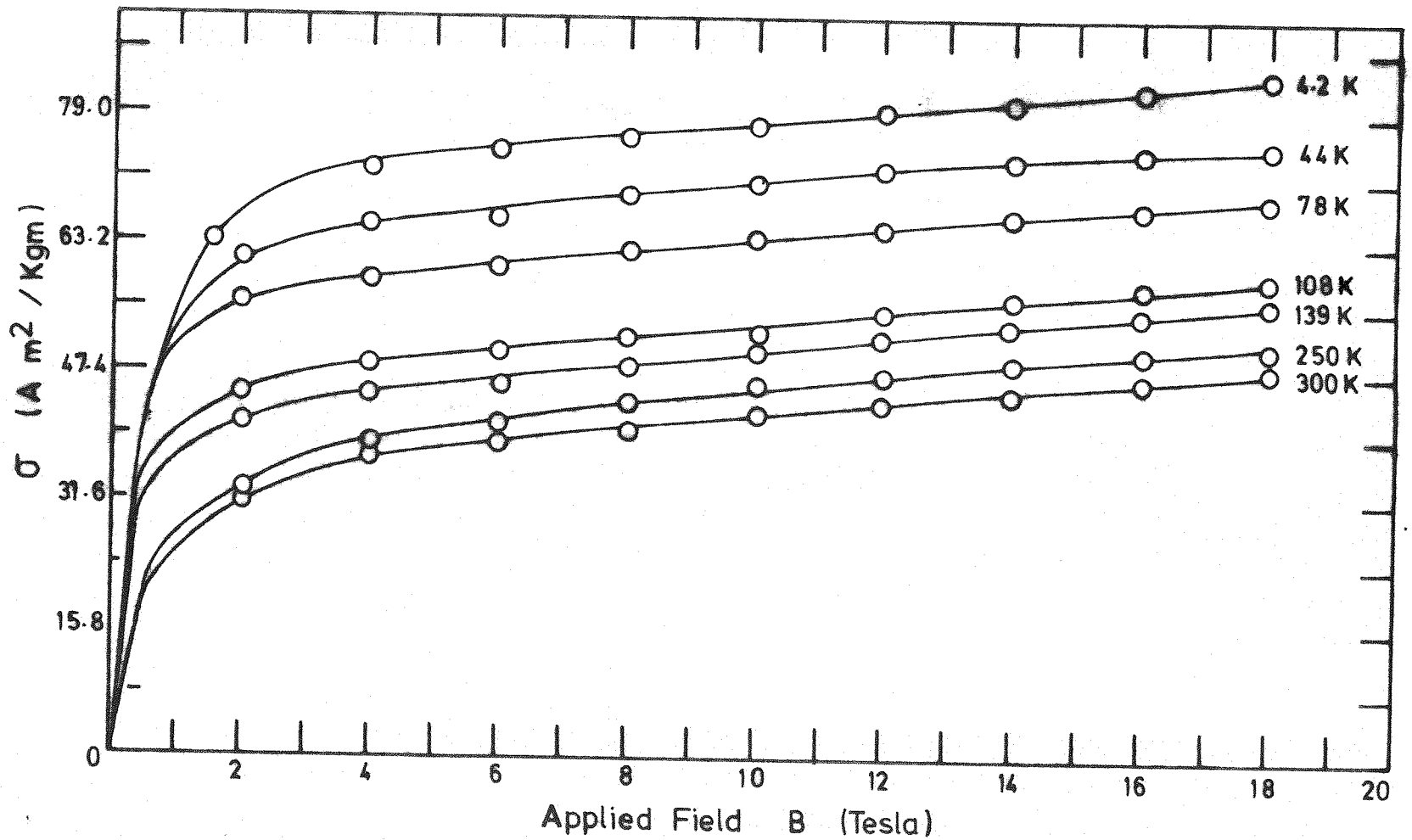

Fig. 4.23 The Specific Magnetization of $DyFe_2$ perpendicular to the cooling direction of the sample

$$\frac{\partial L}{L} = \frac{3}{2}\lambda s \left(\frac{M}{M_s} - \frac{1}{3}\right) \qquad \text{for} \frac{M}{M_s} \geqslant \frac{1}{3}$$

It is easy to show that for a single crystal the magnetostriction along (100) will take the form:

$$\lambda_{11} = \frac{3}{2}\lambda s\ (100)\ \left(\frac{Xhf\,(100)\ H}{M_s}\right)$$

or $$\lambda_{11} = \lambda s\,(100)\ \left(\frac{M_k}{M_s} + \frac{Xhf\,(100)\ H}{M_s}\right)$$

depending on whether there was initially only 180° wall displacements or 90° ones too.

Similarly for the magnetostriction along (111) direction we have

$$\lambda_{11} = \frac{3}{2}\lambda s\,(111)\ \left(\frac{1}{\sqrt{3}}\ \frac{Xhf\,(111)\ H}{M_s}\right)$$

assuming $Xhf\,H << M_s$.

In a polycrystalline material the magnetostriction will be some average value between these two and the intermediate direction.

It is possible to write[51]

$$\frac{\partial \lambda_{11}}{\partial H} = N\ \lambda s\ Xhf/M_s \qquad (4\text{–}49)$$

where N is a numerical factor of the order of unity [51] and Xhf is the polycrystalline high-field susceptibility.

From the magnetization curve XHf = 1.5 A. m²/Kgm . Tesla:

$\lambda s = 3200$ and $M_s \simeq 150$ A. m²/Kgm. Substituting the values in equation (3–49),

$$\frac{\partial \lambda_{11}}{\partial H} = 1.42 \times 10^{-5}\ \text{Tesla}^{-1}.$$

Experimentally $\frac{\partial \lambda_{11}}{\partial H} = 1.13 \times 10^{-5}$ Tesla^{-1} . Therefore equation (4–49) is reasonably in good agreement with the experimental result. This result indicates that

the linear regions in the magnetostriction curves come from the rotation of the magnetization vector.

4.6 The temperature variation of the magnetostriction:

Figures (4–24) and (4–25) show the variation of λ_{11}, $\lambda\perp$ and λt with temperature, where λt is the total magnetostriction equal $\lambda_{11} - \lambda\perp$ at applied field $\simeq$17.7 Tesla.

The magnetostriction initially increases then starts to decrease as the temperature decreases. This behaviour can be understood by looking at Fig. (4–26).

By decreasing the temperature the anisotropy increases and a higher magnetic field has to be applied to reach saturation. Therefore if the applied field is B(1) then the magnetostriction of $DyFe_2$ will increase with increasing temperature in contrast to the usual negative $(\partial\lambda/\partial T)$. If the applied field is B(2) then the case will be similar to the behaviour of Fig. (4–24). At applied field B(3) the saturation magnetostriction increases by decreasing temperature as usual.

The linearity of the magnetostriction curves makes extrapolation procedures useless except for room temperature. By extrapolation to $H \to \infty$ at room temperature, $\lambda_{total} \simeq 1270 \times 10^{-6}$, therefore $\lambda s = \frac{2}{3}\lambda t = 846 \times 10^{-6}$.

Figures (4–18) and (4–19) show that the magnetostriction field curves at room temperature down to ~ 260 K might be due to domain wall displacements in the initial excursion of the magnetostriction curve. While the linear part may be due to the domain rotation process. This leads to a suggestion that $DyFe_2$ might have 90° and 180° domains at room temperature, and the 90° domains disappear as the temperature is decreased. Hence at low temperatures $DyFe_2$ may have 180° domains only. This is believed to be due to the large contribution of the magnetoelastic energy at low temperature, which makes the 180° domains the preferred configuration for $DyFe_2$ compound.

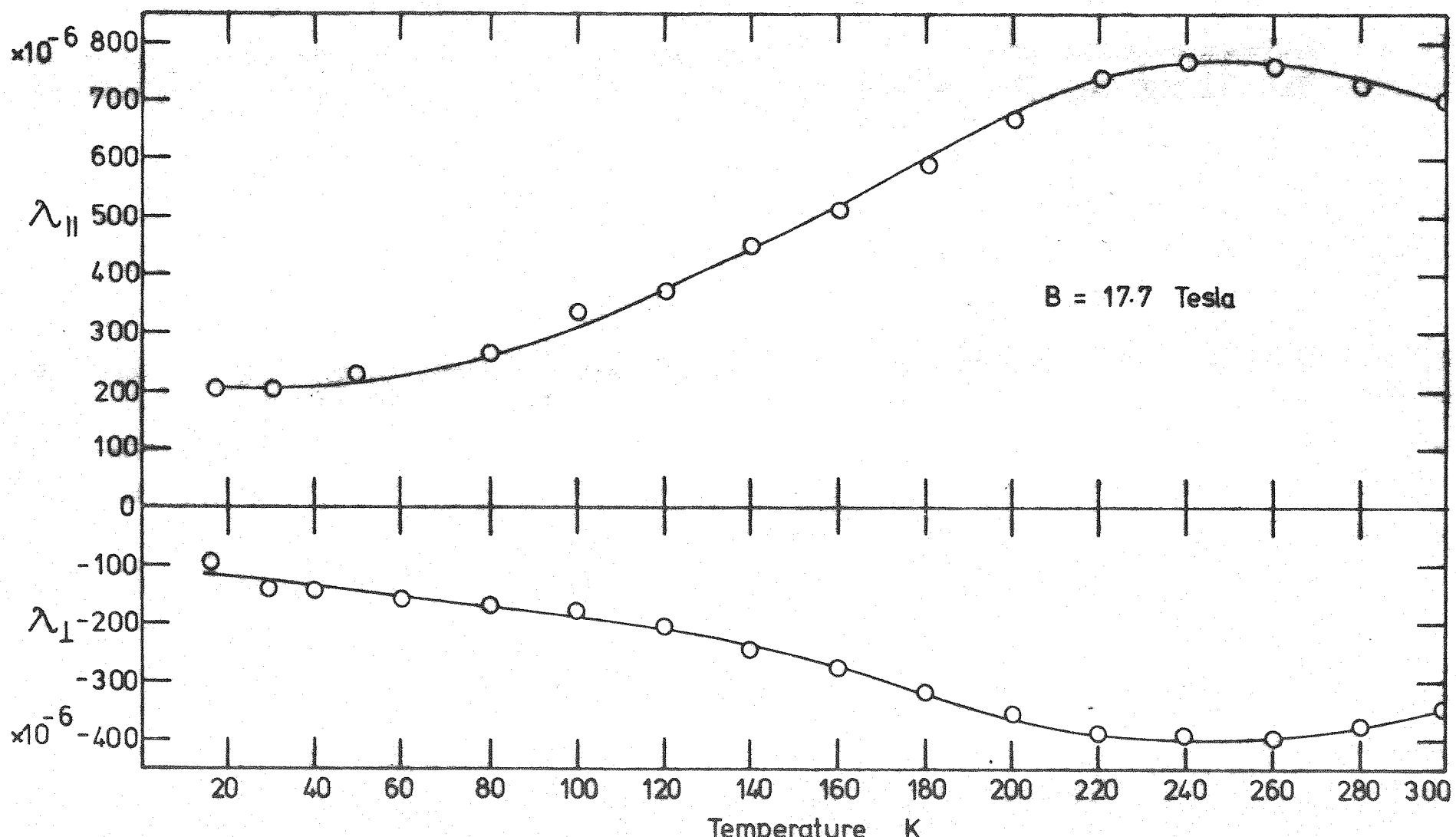

Fig. 4.24 Variation of the magnetostriction of $DyFe_2$ ($\lambda_{\parallel}$ and $\lambda_{\perp}$) with temperature

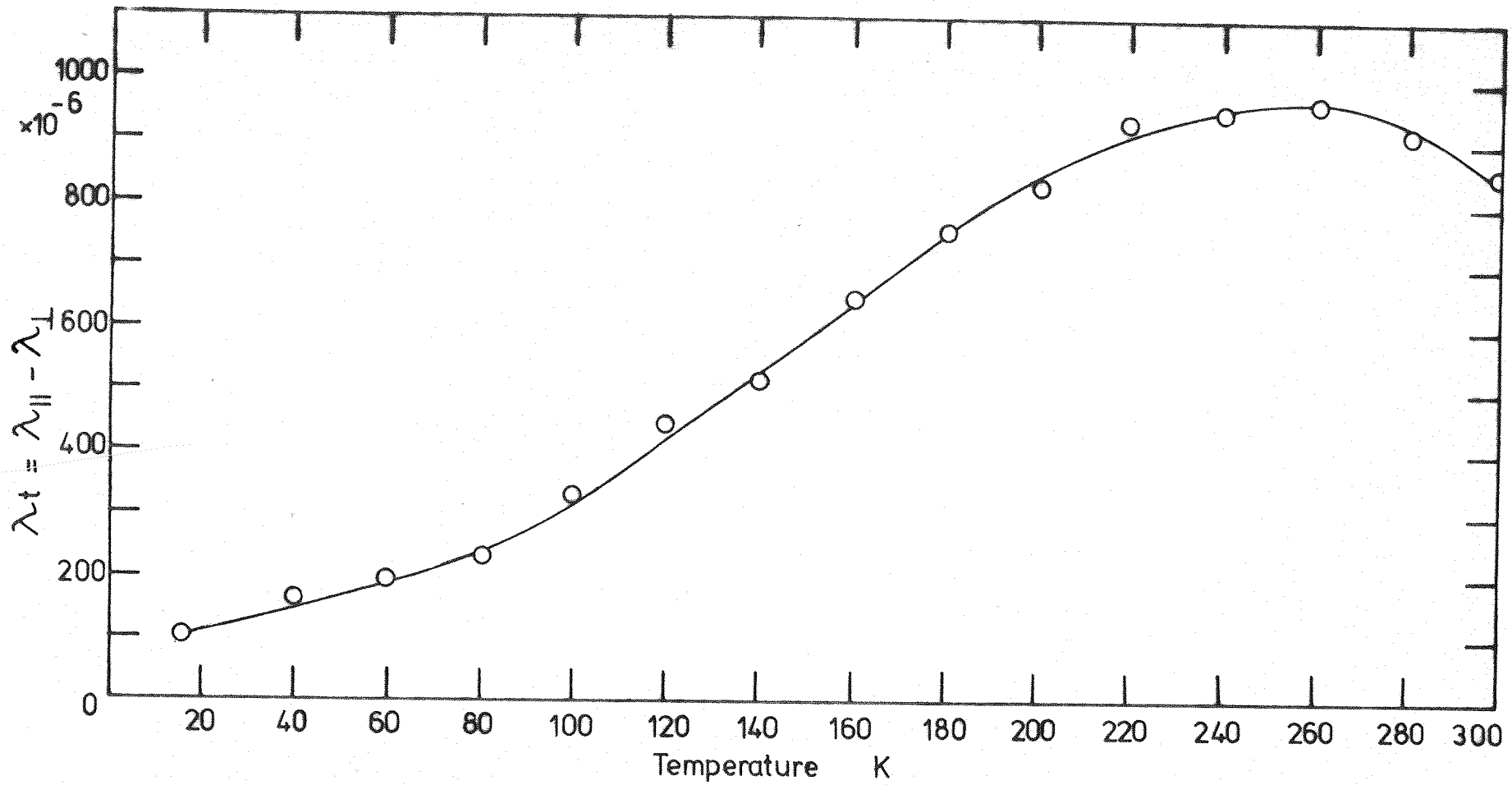

Fig. 4·25 Variation of the total magnetostriction (λt) of $DyFe_2$ with temperature

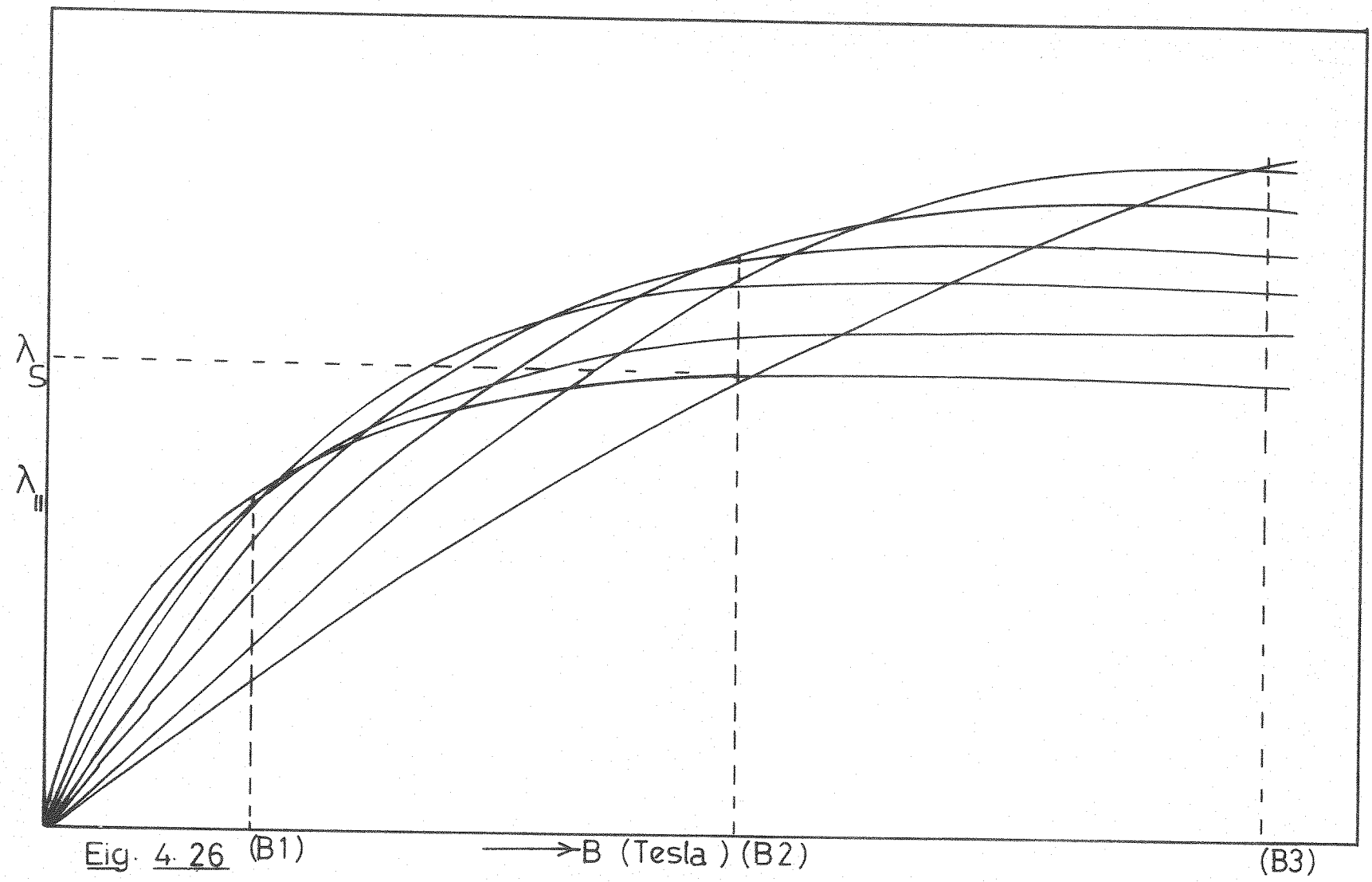

Eig. 4.26

Assuming that the $DyFe_2$ polycrystalline sample is an aggregate of single domain particles without interactions it can be shown that for $K_1 > 0$, $\lambda = h_1 (C_1 - \frac{1}{3}) + h_2 C_2$, where the h_1's are the single crystal magnetostriction coefficients and the C_1's are the constants obtained from the averaging procedure. λ is the strain measured parallel to the applied field.

Now if we suppose that domain wall displacements take place during the initial part of the magnetostriction curves, then from Lee and Bishop (1966)[54] it can be shown that $C_1 - \frac{1}{3} = 0.37$ and $C_2 = 0$ for $K_1 > 0$.

At the end of the domain wall process:

$$\lambda = h_1 (C_1 - \frac{1}{3}) + 2h_2 C_2 \qquad (4-40)$$

By extrapolation the magnetostriction field curve at room temperature to $H = 0$, λ was found to be $= 520 \times 10^{-6}$.

Substituting for C_1 and λ in equation (4–40) gives:

$$h_1 = 1400 \times 10^{-6}$$

$$\lambda_{100} = \frac{2}{3} h_1 = 930 \times 10^{-6}$$

By extrapolation of the magnetostriction curves, λ_{11} and $\lambda\perp$ to $H \to \infty$ at room temperature gives: $\lambda_{11} - \lambda\perp = 1270 \times 10^{-6}$

$$\lambda s = \frac{2}{3} (\lambda_{11} - \lambda\perp)$$

Therefore $\lambda s = \frac{2}{3} (\lambda_{11} - \lambda\perp) = h_1 (C_1 - \frac{1}{3}) + h_2 C_2$ (4–41)

At saturation $C_1 = 0.6$, $C_2 = 0.2$

Substituting these values in equation (4–41) gives:

$$h_2 = 2370 \times 10^{-6}$$

$$\lambda_{111} = \frac{2}{3} h_2 = 1580 \times 10^{-6}$$

These calculations show that $\lambda_{111} > \lambda_{100}$

The magnetostriction curves given an indication that the domain wall displacements may not exist at low temperatures, which means that by extrapolation to $H = 0$, $\lambda \rightarrow 0$. Substituting $\lambda = 0$ and $C_2 = 0$ in equation (4–40):

$$h_1 = 0$$

Hence $\lambda_{100} = 0$

Therefore as the temperature decreases the remanence may decrease and hence $\lambda_{100} \rightarrow 0$. Therefore the magnetostriction at low temperatures may be due to the rotation of the magnetization away from the easy axis.

In fact substituting for $\lambda = 0$ in equation (4–40), is not quite right because equation (4–40) is only valid for a single crystal containing 90° and 180° domains.

At 0K ($\lambda_{11} - \lambda\perp$) at saturation was calculated to be = 3920×10^{-6}. Suppose ... $h_1 = 0$, as found above,

then by substituting for $h_1 = 0$, $C_1 = 0.6$ and $C_2 = 0.2$ in equation (4–41) we get:

$$h_2 = 6500 \times 10^{-6}$$

$$\lambda_{111} = \frac{2}{3} h_2 = 4300 \times 10^{-6}$$

Clark has predicted $\lambda_{111} = 4800 \times 10^{-6}$ [2]. →→→

4.7 Temperature variation of the magnetization curves of $DyFe_2$:

Figures (4–27) and (4–28) show the variation of magnetization at 18 Tesla with temperature in the direction parallel and perpendicular to the cooling direction. The behaviour is normal and there is no break in the magnetization-temperature curve as reported by Ross and Crangle[45] . It is not possible to estimate the saturation magnetization because of the linearity of the magnetization curves which make the extrapolation procedures useless.

Figure (4–27) is the magnetization measured along the cooling direction of the sample showing higher values of magnetization than measured to the cooling direction, Fig. (4–28). This is due to the crystallite alignment within the sample in the cooling direction.

From these results it is not possible to obtain the angular distribution of the crystallite about the cooling direction. Indeed the first problem is that of unknown texture, since preferential orientation of the [100] or [110] crystallite directions will produce an increase in the measured magnetization in the parallel configuration. Hence to express the degree of alignment numerically it is first necessary to assume an angular distribution which may be, for example, Gaussians, linear or a function of angle away from the cooling direction of any desired complexity. A simple model which assumed a fraction ρ of the crystallites to be randomly distributed and the remaining fraction $(1-\rho)$ to be perfectly aligned was proposed. This, if it is a valid model, should yield a result for ρ such that $0 \leqslant \rho \leqslant 1$. However calculations gave a meaning less result of $\rho = -2.7$. Therefore to attach any numerical value to the degree of alignment one would first need

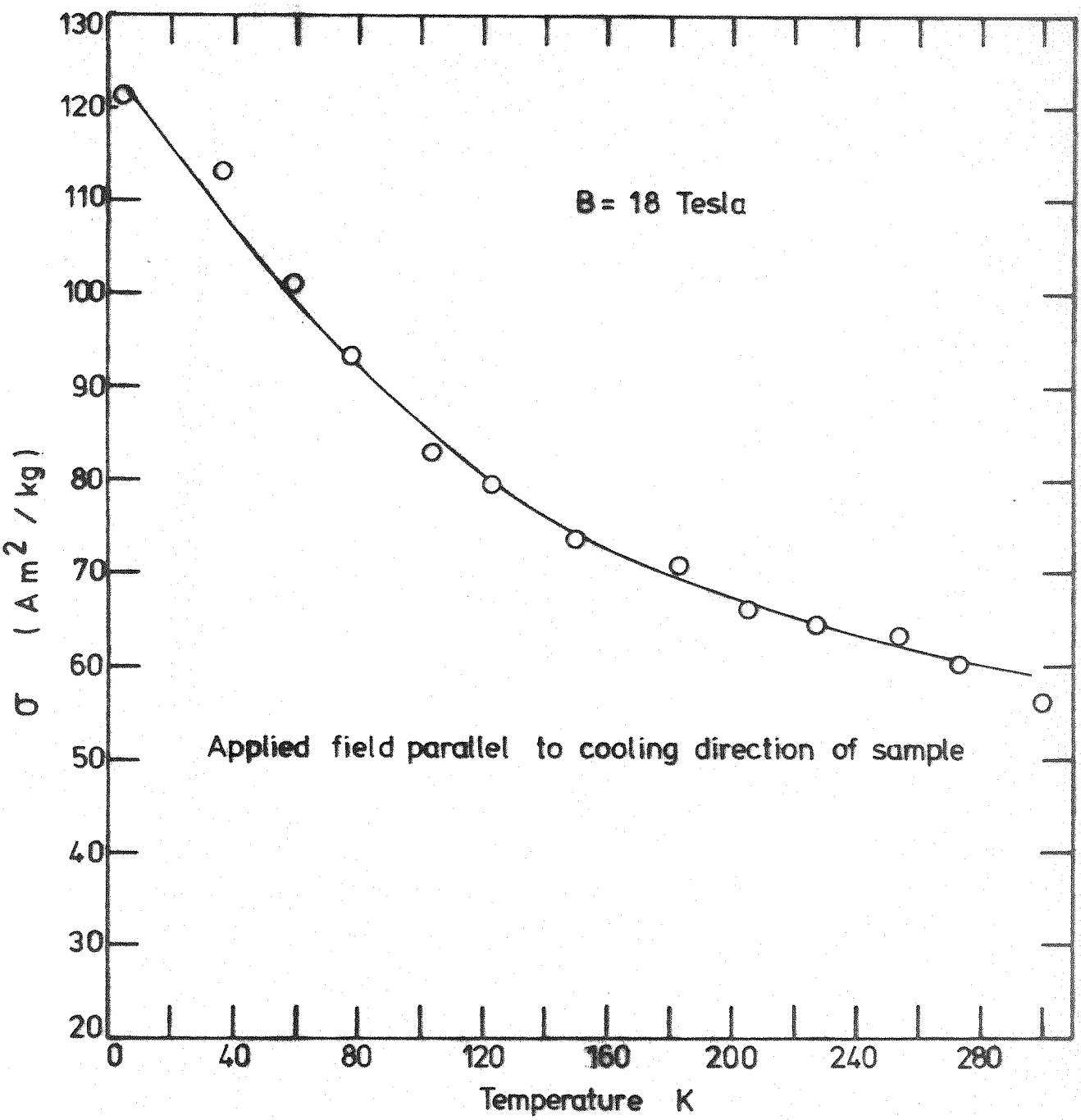

Fig. 4·27 Variation of Magnetization of $DyFe_2$ with temperature

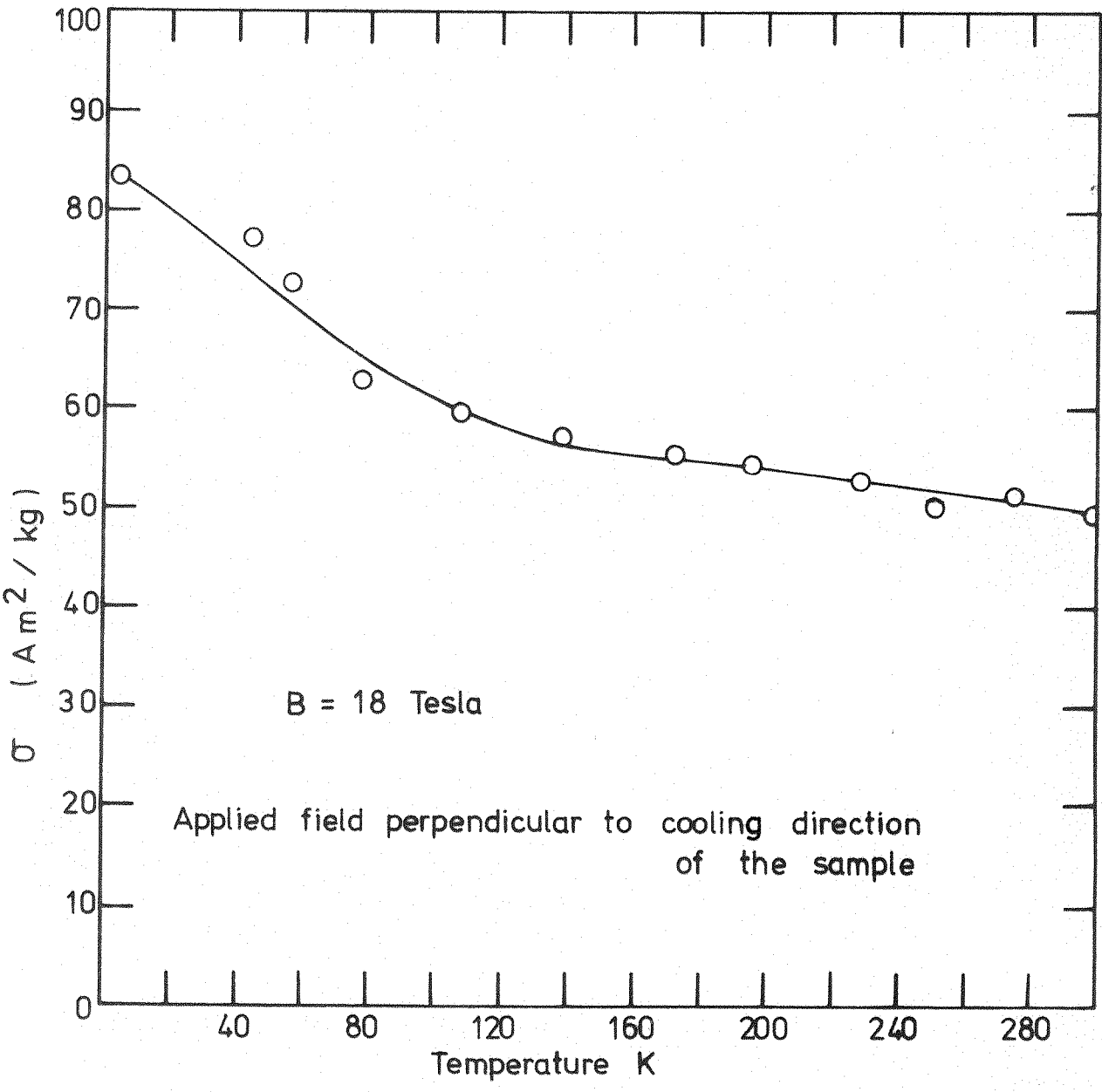

Fig. 4.28 Variation of magnetization of $DyFe_2$ with temperature

to find the type of distribution. This information, for a bulk sample up to approximately 1 cm^3 may be obtained using neutron diffraction techniques. However, the arc furnace method of preparation does not seem to reproduce these effects consistently and consequently detailed analysis of the above magnetization measurements using various proposed models would not be worthwhile.

4.8 The measurement of magnetization in pulsed magnetic fields:

The magnetization of $DyFe_2$ has been measured in this work by using an induction technique. It is determined by measuring the e.m.f. induced in a suitable search coil by the variation of the magnetic moment as the field is applied.

A search coil mounted co-axially in a field produced by a pulsed coil with a specimen at its centre, gives an output voltage:

$$V = -\frac{\partial \Phi}{\partial t}$$

where Φ is the flux due to the applied field and the magnetization signal of the specimen. Usually the applied field term is much larger than the magnetization signal (about 10^4 times larger). Hence the magnetization signal is swamped by the signal due to the magnetic field. Therefore it is necessary to subtract this very large term in order to measure the magnetization.

The first measurement of magnetization using the induction method was carried out by Jacobs and Lawrence[52] . They used a compensating coil inseries opposition to the search coil which contained the sample. Hence the unwanted field signal can be removed. Under ideal conditions the signal remaining is:

$$V = G\,n\,A\frac{\partial M}{\partial t}$$

where G is a coupling constant dependent on the geometry of the coils and the sample.

This induction method of measuring the magnetization has been further developed by several groups of workers. The system used in the present work is described fully by Melville[35] and Mattocks[53].

Under working conditions when the temperature is very low, the coil former contracts and the coils not only change their areas, but may change their positions. Signal balance is then lost. Therefore there will be a residual signal imbalances having a phase angles of 0 or 180° with respect to the applied field, there is also a quadrature phase signal resulting from eddy currents in the metals in and around the specimen chamber. Therefore a compensating circuit has to be used to cancel these signals, it works as follows:

The two pickup coils were connected to a balancing network which was used to compensate for the inphase and out of phase signals. The inphase signal was taken directly from the field pickup coil mounted separately near the sample, and a phase shift circuit associated with a further pickup coil was used to obtain an out of phase compensating signal.

The relevant circuits and apparatus are described in detail by Mattocks [53]. Calibration of the magnetization signal is carried out using a standard sample of nickel, taking the specific magnetization to be 58.6 $A.m^2/Kg$ at 4K.

4.9 Form of the magnetostriction-field curves of $TbFe_2$ Compound:

The magnetostriction of $TbFe_2$ λ_{11} and $\lambda\perp$ have been measured between 16K and 300K and at pulsed magnetic fields up to ~ 18Tesla.

Figures (4–29) and (4–30) show the isotherms of λ_{11} and $\lambda\perp$ against the applied field. The magnetostriction increases with decreasing temperature in agreement with the usual negative $(\partial\lambda/\partial T)$. The magnetostriction of $TbFe_2$ is near saturation at all temperatures.

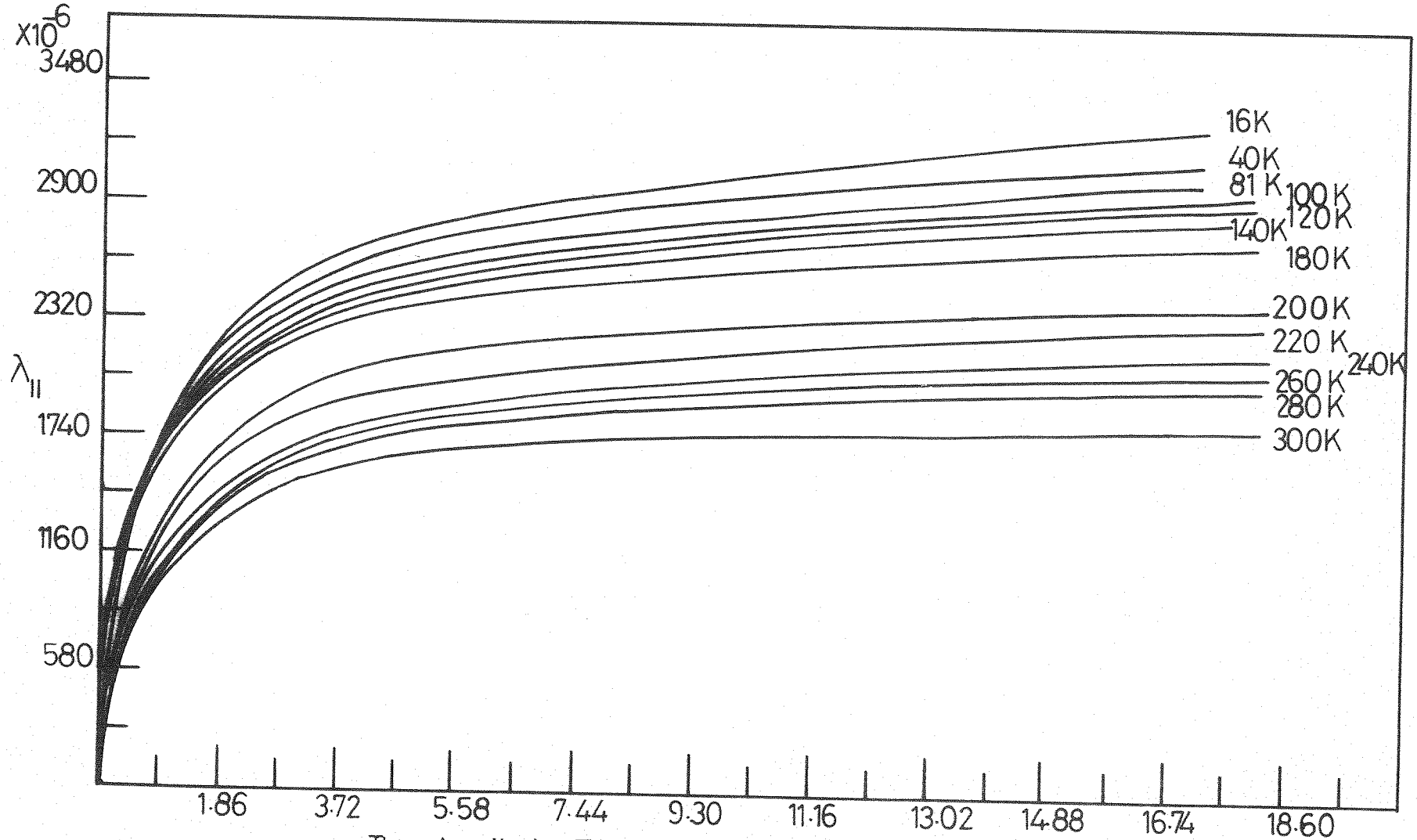

Fig. 4.29 Magnetostriction isotherms of $TbFe_2$ parallel to the applied field.

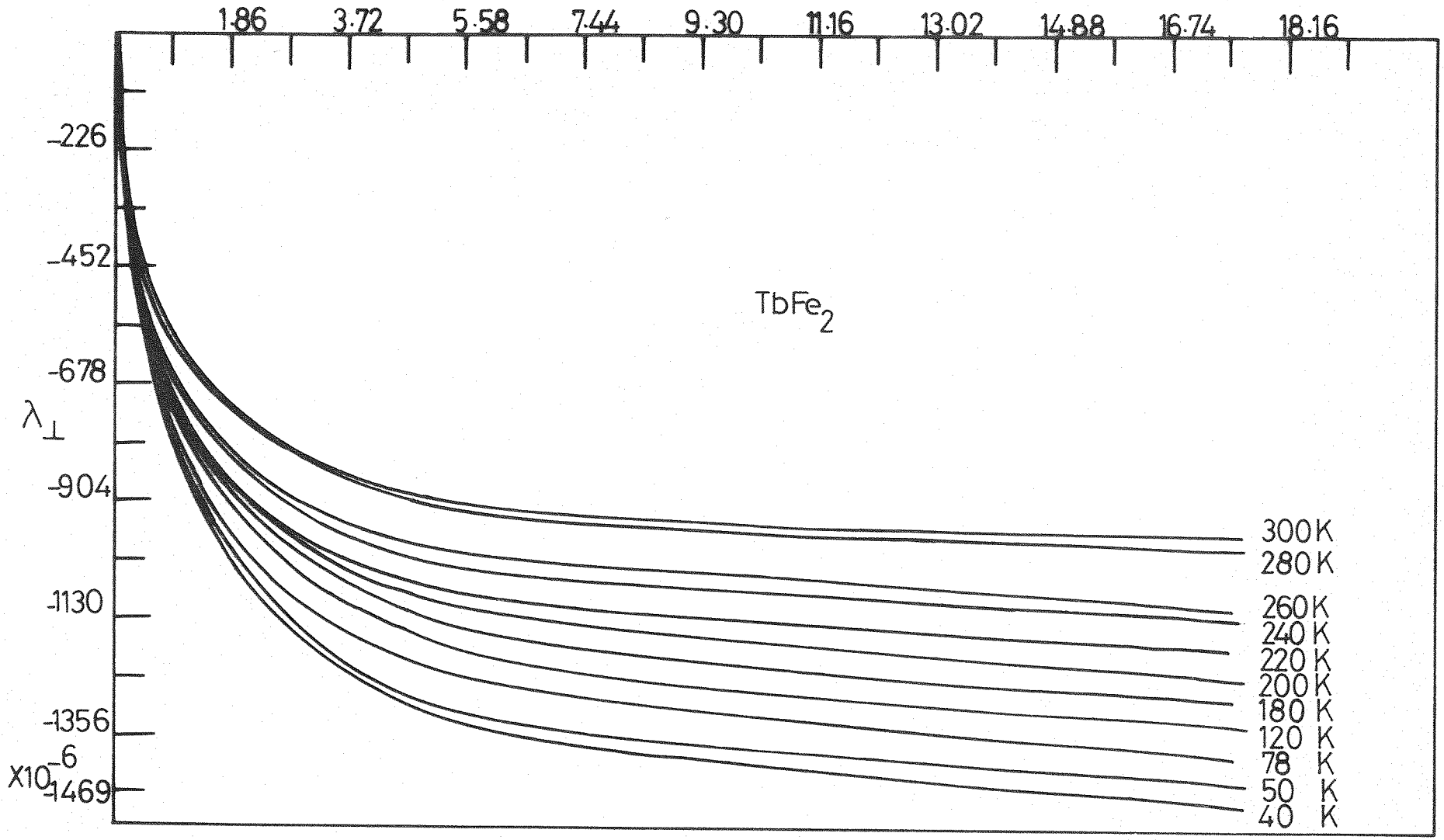

Fig. 4.30 Magnetostriction isotherms of $TbFe_2$ perpendicular to the applied field.

The initial excursion of the magnetostriction curves up to ~ 1 Tesla can be associated with the domain wall displacements, while above this field value it is due to the rotation of the magnetization against anisotropy.

4.10 Temperature variation of the magnetostriction of $TbFe_2$:

Figure (4–31) shows the variation of the λ_{11} and $\lambda\perp$ with the temperature, while Figure 4-32 shows the variation of the magnetostriction $(\lambda_{11} - \lambda\perp)$ with temperature.

The variation of λ_{11}, $\lambda\perp$ and λt with temperature is normal. A plot of $\Delta\ell/\ell = (\lambda_{11} - \lambda\perp)$ Vs. 1/H for $H \to \infty$ at each temperature was shown in Fig. (4–32), then the saturation magnetostriction λs at each temperature was calculated from the following formula: $\lambda s = \frac{2}{3}(\lambda_{11} - \lambda\perp)$. Figure (4–34) is a plot of λs Vs. temperature. By extrapolation of λs-temperature curve in Fig. (4–34) to $T = 0$, λs found to be = 3340 x 10^{-6}, this value is the highest in RFe_2 series.

Assuming that $TbFe_2$ polycrystalline sample is the aggregate of single domain particles without interaction, it can be shown that $\lambda = h_1 (C_1 - \frac{1}{3}) + 2h_2 C_2 + h_3 (C_3 - \frac{1}{3})$ for $K_1 < 0$ [54]. Where h_1's are the single crystal magnetostriction coefficients and the C_1's are the constants obtained from the averaging procedure, while λ is the strain measured parallel to the applied field.

At the end of the domain wall process (B small) it was shown by Lee and Bishop (1966)[54] that $C_1 - \frac{1}{3} = 0$, $C_2 = 0.21$ for $K_1 < 0$. In the case of $TbFe_2$, K_1 is < 0, therefore by extrapolation the magnetostriction field curves to H = 0, we can estimate the remanence at the end of the domain wall displacements.

At 16K, λ_{11} at the end of the domain wall process = 2610 x 10^{-6}.

$$\lambda_{11} = h_1 (C_1 - \frac{1}{3}) + 2h_2 C_2 \qquad (4\text{–}42)$$

$$C_1 - \frac{1}{3} = 0,\ C_2 = 0.2$$

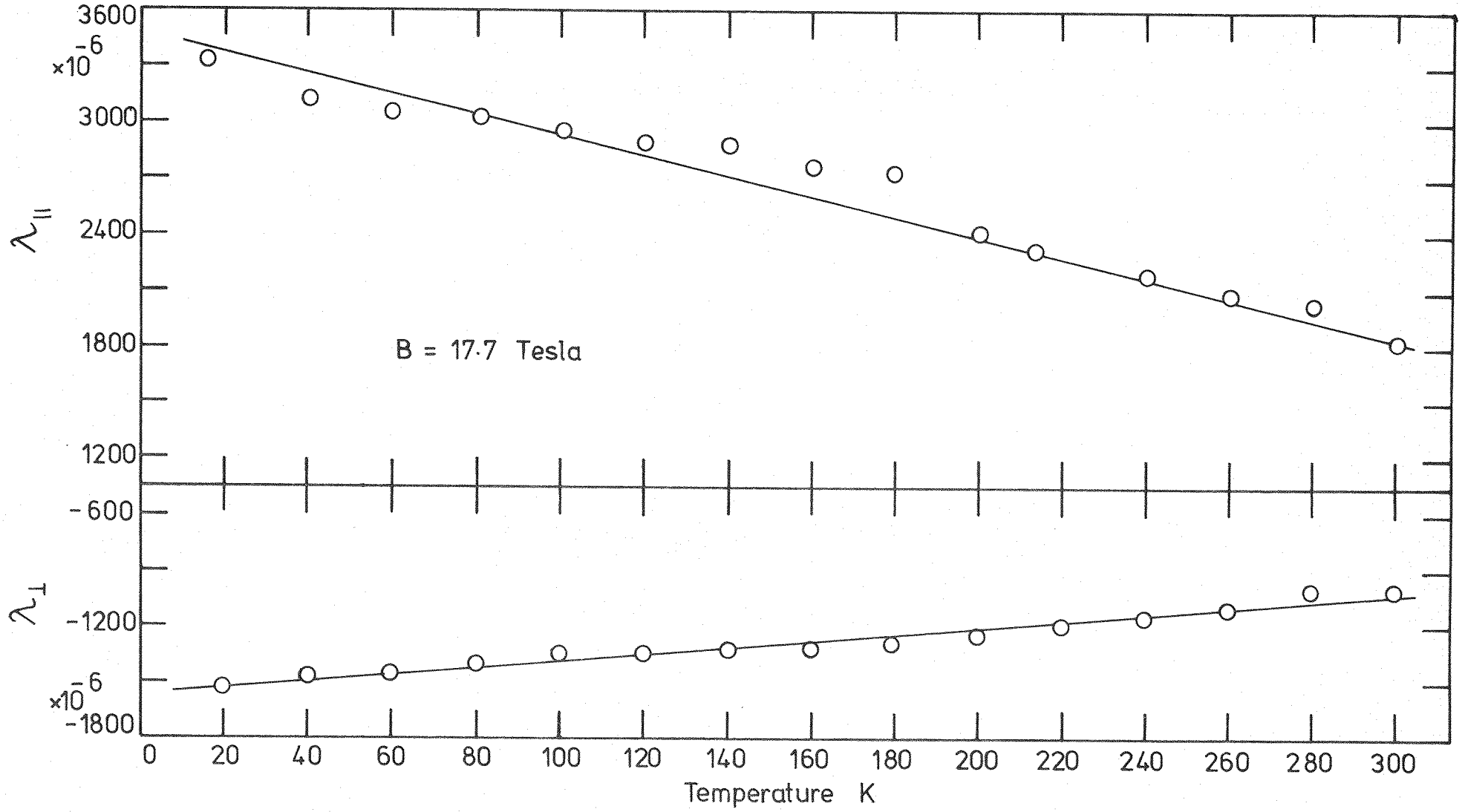

Fig. 4·31 Variation of Magnetostriction of $TbFe_2$ ($\lambda_{\parallel}$ and $\lambda_{\perp}$)

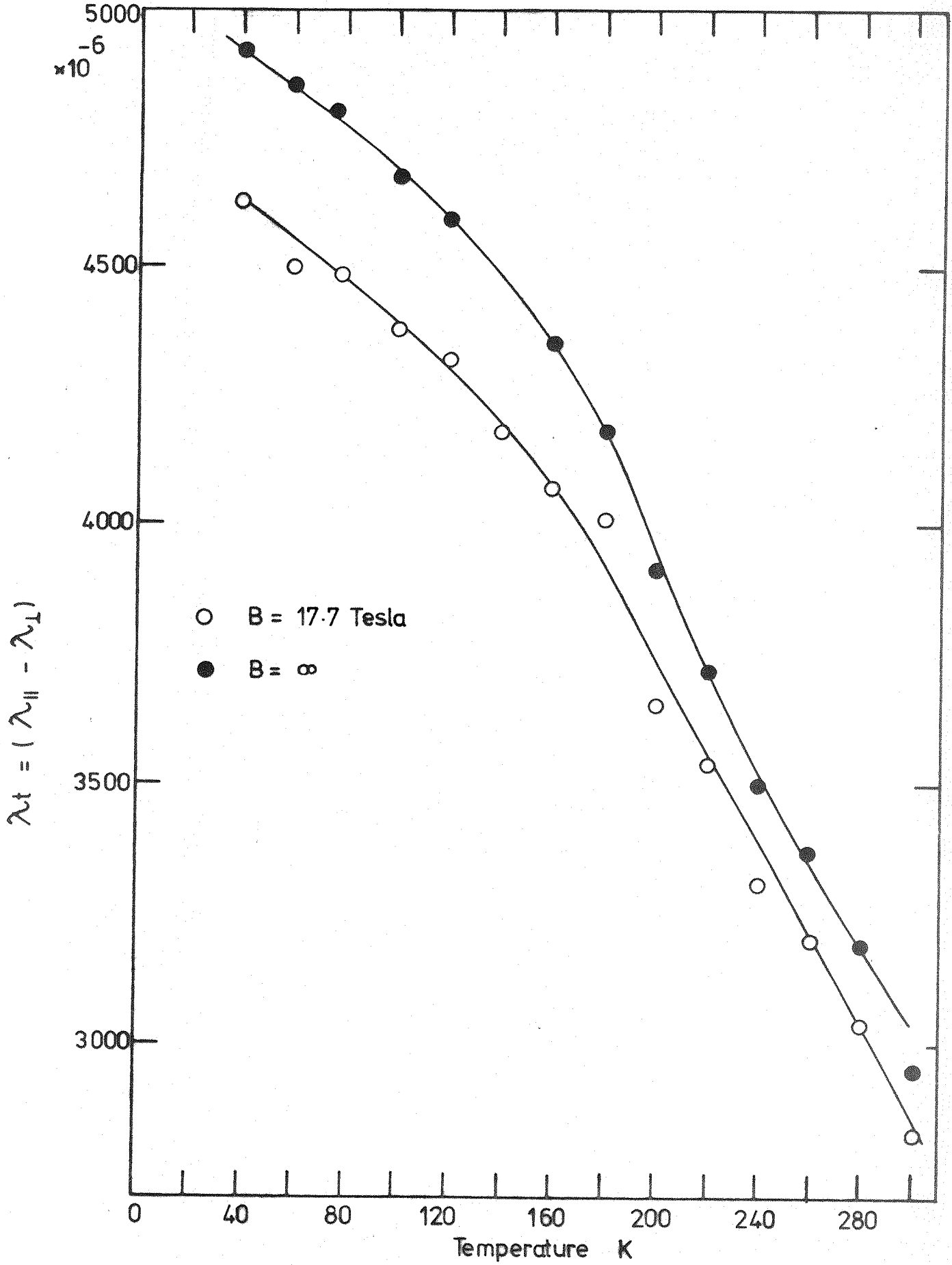

Fig. 4·32 Total Magnetostriction ($\lambda_{\parallel} - \lambda_{\perp}$) of $TbFe_2$ versus temperature

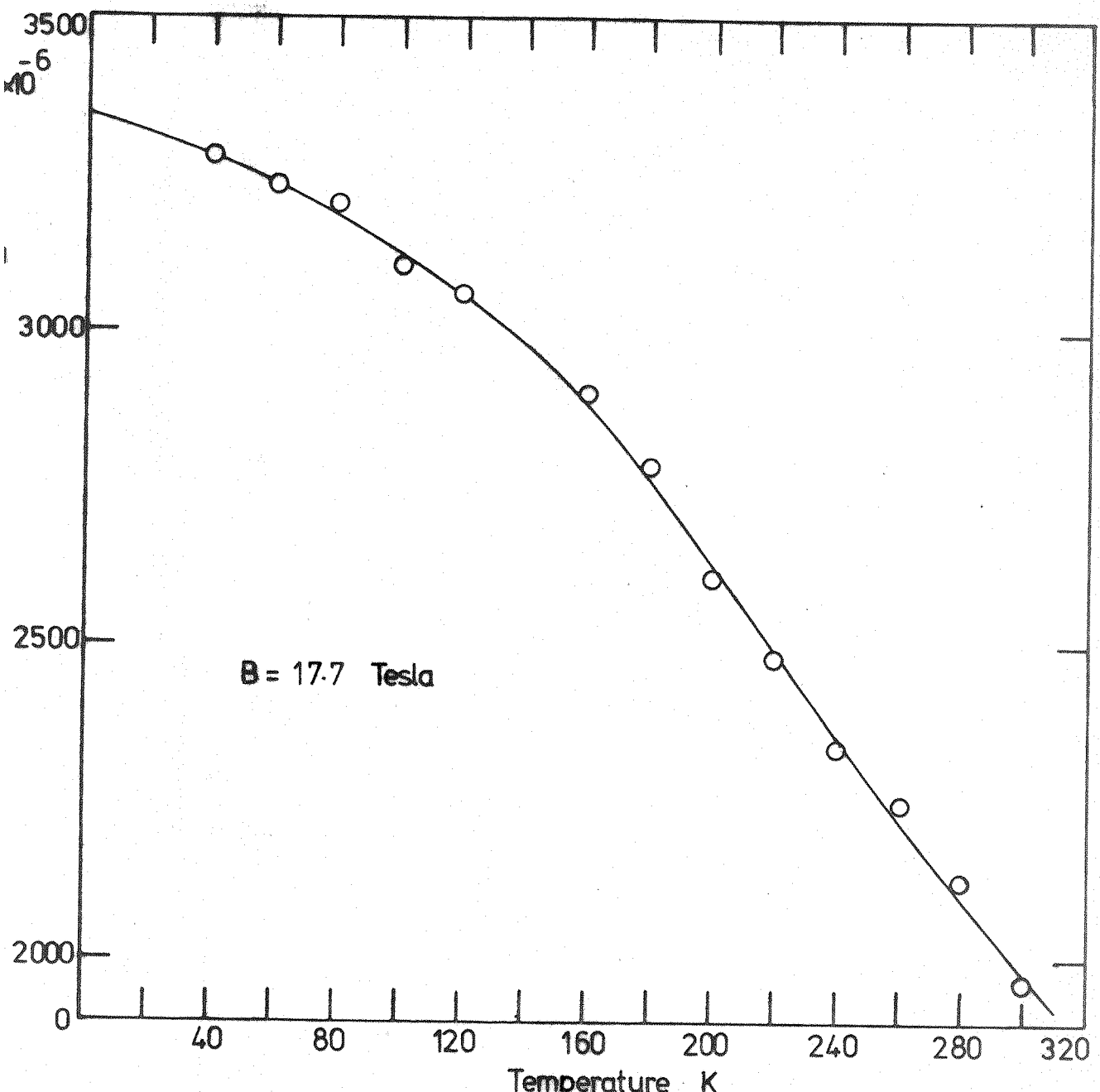

Fig. 4.33 Saturation magnetostriction versus temperature

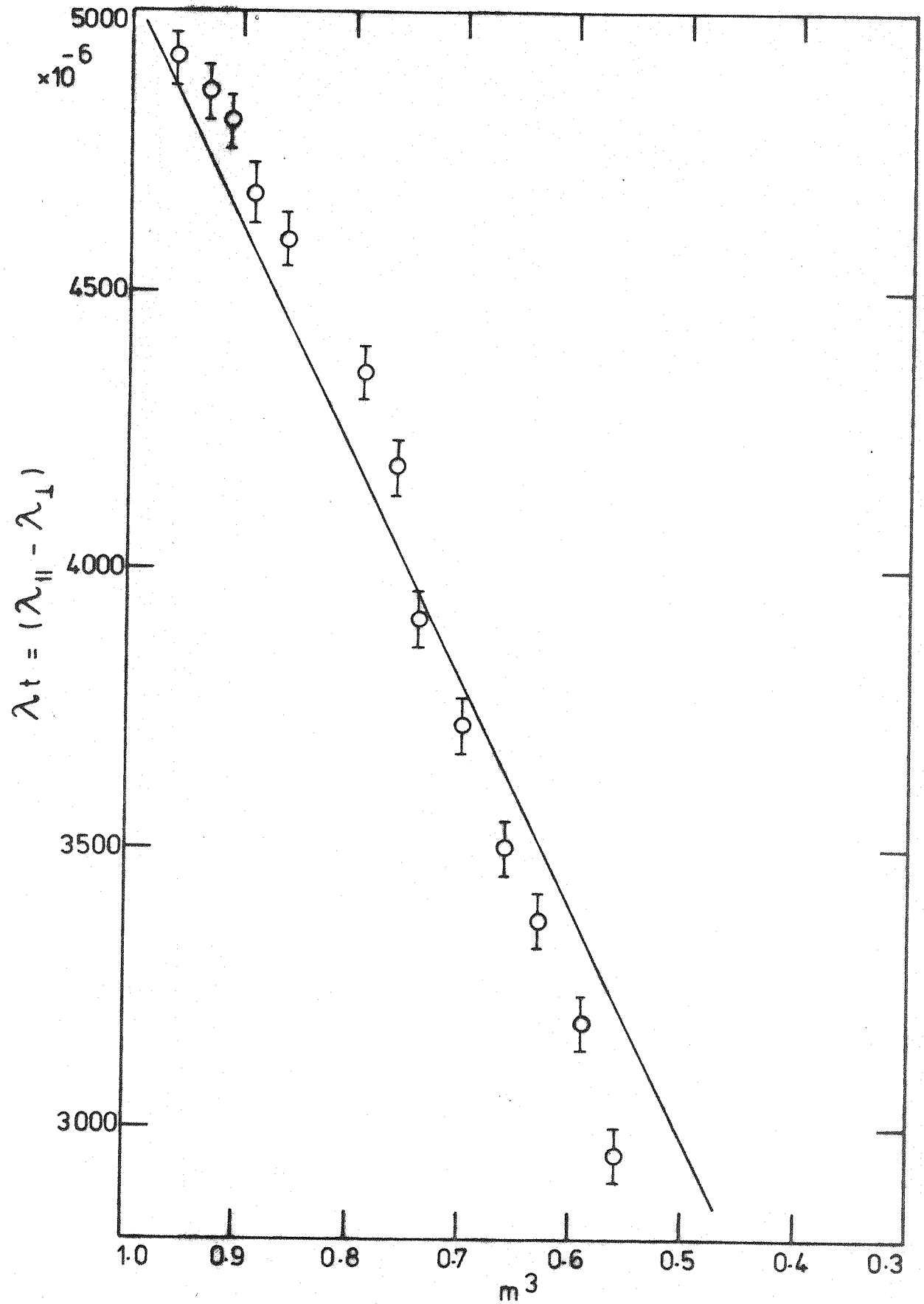

Fig. 4·34 Dependence of magnetostriction of $TbFe_2$ on the reduced magnetization of the Tb sub-lattice

Therefore $h_2 = 6525 \times 10^{-6}$

$$h_2 = \frac{3}{2}\lambda_{111}$$

or $\lambda_{111} = 4350 \times 10^{-6}$

At saturation $\lambda_{11} = \lambda s = \frac{2}{3}(\lambda_{11} - \lambda\perp)$

there equation (3–42) becomes:

$$\lambda_{11} - \lambda\perp = \frac{3}{2}[h_1 (C_1 - \frac{1}{3}) + 2h_2 C_2] \qquad (4–43)$$

At saturation $C_1 = 0.6$ and $C_2 = 0.2$.

$$(\lambda_{11} - \lambda t)_s = 5100 \times 10^{-6} \text{ at 0K.}$$

By substituting these values in equation (4–43) h_1 can be estimated:

$$h_1 = 7850 \times 10^{-6}$$

$$\lambda_{100} = 5200 \times 10^{-6}.$$

These calculations show that λ_{111} and λ_{100} are in the same order and have a same sign.

4.11 The origin of the magnetostriction in RFe_2 compounds:

The origin of the huge magnetostriction in the $TbFe_2$ and $DyFe_2$ compounds is the large strain dependent anisotropy of the rare earth ions. A.E. Clark and H.S. Belson [48] have measured the magnetostriction of YFe_2 and they found λs was only $\sim 2 \times 10^{-6}$. From this result they concluded that the contribution of the Fe ions to the magnetostriction is negligible. The magnetostriction remains large at room temperature because of the large rare-earth iron exchange interaction which keeps the rare earth spins aligned even at high temperatures.

By extrapolation the λs-temperature curve in Fig. (4–33) to T = 0, $\lambda s(0)$ was found to be equal $\sim 3340 \times 10^{-6}$ which is in vary good agreement with the value $\sim 3333 \times 10^{-6}$ predicted by the single ion theory of Tsuya et al. [55] (1964).

Also $\lambda t(0)$ at saturation was found from the extrapolation of Fig. (4–34), it is $\sim 5060 \times 10^{-6}$.

Callen and Callen[56] and Callen and Shtrikman[57] have shown that the temperature dependence of the magnetostriction follows the power law $m^{\ell(\ell+1)/2}$ for magnetic anisotropy at low temperature, and the normalized hyperbolic. Bessel function $I_{\ell+1/2}$ ($\mathcal{L}^{-1}(m)$) in the molecular field approximation at all temperatures, where m is the reduced magnetic moment, $\mathcal{L}^{-1}(m)$ is the inverse of the langevin function, and ℓ is the order of the spin operator in the magnetoelastic Hamiltonian (for lowest order $\ell = 2$). At low temperature the hyperbolic Bessel function reduces to the power law. Therefore $\lambda_t(T)/\lambda t(0)$ must scale as m^3_{RE} at low temperatures if the rare earth ion is the main source of the magnetostriction. A plot of $A\ell/\ell$ for $TbFe_2$ *vs* m_R^3 was shown in Fig. (4–34), where m_R is the reduced magnetization of the Tb sublattice calculated from the magnetization measurement of Burzo [26]. The λt_s values used in Fig. (3–5) are the extrapolated values to $H \to \infty$ at all temperatures. The extrapolated value of Fig. (3–35) to $T = 0$ is ~ 5030 which is in good agreement with that found by Clark[2] ($\sim 5000 \times 10^{-6}$). The points in Fig. (3–35) scale very well at low temperature. Table 4–1 shows the magnetostriction data for $TbFe_2$ and $DyFe_2$ measured by previous workers, while table 4–2 shows the measurement of the present work.

TABLE 4–1

Magnetostriction data for $TbFe_2$ and $DyFe_2$ (previous workers)

1 $TbFe_2$	$(\lambda_{11} - \lambda\perp) \times 10^{+6}$	
T(K)	Measured values	Infinite field extrapolated values
0	–	5100[48]
	–	4700[2]
300	1850[48] at 2.5 Tesla	2630
	2160[7] at 1.75 Tesla	2580
	2640[2] at 2.5 Tesla	2800

2 $DyFe_2$	$(\lambda_{11} - \lambda\perp) \times 10^{+6}$	
T(K)	Measured values	Infinite field extrapolated values
0	–	–
300	330[7] at 1.75 Tesla	–
	600[48] at 2.5 Tesla	–
	650[2] at 2.5 Tesla	–

TABLE 4.2

Magnetostriction results for $TbFe_2$ and $DyFe_2$ (present workers)

1 $TbFe_2$	$(\lambda_{11} - \lambda\perp) \times 10^{+6}$	
T(K)	Measured values	Infinite field extrapolated values
0	–	5080
300	2825 at ~ 18 Tesla	2950

2 $DyFe_2$	$(\lambda_{11} - \lambda\perp) \times 10^{+6}$	
T(K)	Measured values	Infinite field extrapolated values
0	–	–
300	1048 at ~ 18 Tesla	1270

REFERENCES

Chapter 1

1. A.E. Clark and J.R. Cullen, AIP Conference Proceeding No. 24. (20th Annual Conference – 1974).

2. N.C. Koon, A.I. Schindler, C.M. Williams, and F.L. Carter. J. of Applied Physics Vol. 45, No. 12, December, 1974.

3. A.E. Clark and H.S. Belson. Physics Review B. Vol. 5, Nu. 9, May, 1972.

Chapter 2

1. W.P. Mason, Rev. 96 302 (1954).

2. Mahajahi, G.S. Phil. Trans. London (A), 228, 63 (1929).

3. J.H. Van Vleck, Rev. Mod. Phys. 25 220 (1953).

4. Stevens K.W.H. Proc. Soc. A65. 209 (952).

5. Hutchings M.T. Solid state physics. 16 227 (1964).

6. E. Callen and H. Callen, Phys. Rev. 129, 578 (1963).

7. H. Callen and S. Shtrikman, Solid state Commun. 3 5 (1965).

8. C. Kittel and J. Van Vleck, Phys. Rev. 118, 1231 (1960).

Chapter 3

1. Ch. Fabry, Eclairage Electrique 17, 133 (1898).

2. H. Deslandres and A. Perot, Comptes Rendues 158, 226 (1914): Contribution a la realisation de champs magnetiques eleves. Concentration des amperes-tours dans un tres petit volume.

3. H. Deslandres and A. Perot, Comptes Rendues 158, 658 (1914): project d'un electro-aimant susceptible de donner un champ magnetique de 100 000 Gauss.

4. H. Deslandres and A. Perot, Comptes Rendues 159, 438 (1914): Deuxieme serie d'essais pour l'accroissement des champs magnetiques actuels. Emploi de l'eau avec le nouveau mode de refroidissement.

5. N.E. Alekseeviskii, Soviet Phys. Uspekhi (Engl. transl.) 7, 629 (1965) Peter Leonidovich Kapitza (Personalia).

6. P.L. Kapitza, Proc. Roy. Soc. A105, 691 (1924): A method of producing strong magnetic fields.

7. P.L. Kapitza, Proc. Roy. Soc. A115, 658 (1927): Further Development of the method of obtaining strong magnetic fields.

8. Strakhovskii, G.M. and Kravtrov N.V., Soviet physics Uspekh: 3, No. 2 260 (1960) translation of USP. F12 Nank 70, 693 (1960).

9. C.M. Fowler, W.B. Garn and R.S. Caird, J. Appl. Phys. 31, 558 (1960). Production of very high magnetic fields by implosion.

10. McKinnon J.B., Ph.D. Thesis, The University of Sheffield (1966).

11. Melville, D., Ph.D. Thesis. The University of Sheffield (1969).

12. Mattocks, P.G. Ph.D. Thesis, The University of Southampton (1975).

13. Tektronix. Q-unit. Instruction manual.

14. Greenough, R.D. and Lee, E.W., Cryogenics 7, 7 (1967).

15. Asgar, M. Ph.D. Thesis. University of Southampton (1970).

16. A. Del Moral and D. Melville. Anales de Fisica. Vol. 70. pp. 219–222, 1974.

17. J.A. Ricodeau, M.Phil. Thesis. University of Southampton (1971).

18. M.P. Dariel, U. Atzmony and R. Guiser, J. of the less common metals, 34 (1974) 315–319.

19. A.E. Clark, 19th Conf. on Magnetism and Magnetic Materials No. 1973, AIP Conf. Proc. 18, 1015 (1974).

20. Zijlstra, H., Experimental Methods in Magnetism. ed. Wohlfarth, E.P., Vol. 2 (North Holland 1967).

21. Lowell, H.H., NASA Technical Rep. R–32. (Washington D.C., 1959).

22. Timoshenko, S. 1934. Theory of Elasticity (New York, McGraw-Hill).

23. Cosslett, V.E., Introduction to electron optics, (Oxford Clarendon Press, 1946) p. 106.

24. A.E. Clark and J.R. Cullen, AIP Conference Proceedings No. 24. Magnetism and Magnetic Materials 1974 (20th Annual Conference – San Francisco).

25. Rosenberg, H.M. Low Temperature Solid State Physics (Oxford, 1963).

Chapter 4

1. J.W. Ross, Ph.D. Thesis, University of Sheffield (1964).

2. A.E. Clark, 19th Conf. on Magnetism and Magnetic Materials. No. (1973) AIP Conf. Proc. 18, 1015 (1974).

3. A.E. Clark and J.R. Cullen, AIP Conference Proceedings No. 24. (20th Annual Conference 1974).

4. A.E. Clark and H.S. Belson, Physics Review B. Vol. 5, No. 9. May 1972.

5. A.E. Clark and H.S. Belson. Physical Review B. Vol. 5, No. 9. 1 May, 1972.

6. N.C. Koon, A.I. Schindler, and F.L. Carter. Physics Letters. Vol. 37A, No. 5, 20 December, 1971.

7. N.C. Koon, A.I. Schindler, C.M. Williams, and F.L. Carter. Journal of Applied Physics, Vol. 45, No. 12. December 1974.

8. G.K. Wertheim, V. Jaccarino, and J.H. Wernick, Phys. Rev. A 135, 151 (1964).

9. G.H. Bowden, B. Bunburg, A.P. Guimares and R.E. Snyder, J. Phys. C1, 1376 (1968).

10. V. Atzmony, M. Dariel, E. Bauminger, D. Lebenbaun, I. Nowik, and S. Offer, Physics Rev. B7. 4220 (1973).

11. M.P. Dariel and V. Atzmony, Int. J. Magnetism, 4, 213 (1973).

12. Lamaire, R., Paccard, D., Pauthenet, R. : J. Appl. Phys. 39, 1092 (1968).

13. Burzo, E., Rev. Roum. Phys. 15, 573 (1970) and 15, 689 (1970).

14. Givord, D., Givord, F., Lemaire, R. Conf. Ins. on Mag. Grenoble (1970).

15. A.E. Roy. Cobalt 1, 13, (1974).

16. E.A. Skarbeck, and W.E. Wallace. Journal App. Phys. 34, 1356 (1963).

17. J. Farrell and W.E. Wallace, Inorg. Chem. 5, 105, (1966).

18. K.N.R. Taylor, H.D. Ellis, and M.I. Darby. Phys. Cell. 20, 327 (1966).

19. E. Burzo. Solid State Communications Vol. 14, pp. 1295–1298 (1974).

20. J. Crangle and J.W. Ross. Proc. Ins. Conf. on Mag. Nottingham (p. 240) (1964).

21. A.M. Bisliyeu, S.A. Nikitin, Y.E.M. Savitskiy, V.F. Terekhova and V.Y.E. Kollesnichenko, F12. Metal mettalloved 36, No. 5, 965–970 (1973).

22. R. Grossinger and W. Steiner. Phys. Stat. Sol. (a) 28, K135 (1975).

23. K.H.J. Buschow, Phys. Stat, Sol. (A)F, 199 (1971).

24. W .E. Wallace, and A.E. Skrcbek , Rare earth Research II. ed. (K.S. Vores Gordon & Breach) p. 431 (1963).

25. K.H.J. Buschow and R.D. Van staple, J. Appl. Phys. 41 (1970) 4066.

26. E. Burzo, Z. Angew 32 (1971) 127.

27. M.O. Bargouth and G. Will. Journal De physique Colloque C_6 Supplement au no. 2–3 Tome 32, Fevrier–Mars 1971. Page C_1 – 675.

28. P. Hendy, Southampton University – Private Communication.

29. S.A. Nikitin and A.M. Bislieu, Sov. Phys. Solid State, Vol. 15, No. 12, June (1974).

30. M.A. Ruderman and C. Kittel Phys. Rev. 96, 99 (1954).

31. G.K. Wertheim and J.H. Wernick. Phys. Rev. 125, 1937 (1962).

32. W.E. Wallace, J. Chem. Phys. 41, 3857 (1964).

33. R. Lemaire and J. Schewei , Phys. Lett 21. 366, (1966).

34. R.M. Moon, W.C. Koehler and J. Farrell. Journal Appl. Phys. 36, 978 (1965).

35. D. Melville. Ph.D. Thesis. University of Sheffield (1969).

36. J.B. Friauf, J. Am. Chem. Soc. 49, 3107 (1927). Ibid. Phys. Rev. 29, 34 (1927).

37. F. Lanes and K. Lohberg, Nachr. Gottinger Akad. Wiss Math. Phys. K1. IV. Newe Folge 1, 6, 59 (1932).

38. F. Laves and H. Witte. Metallwirt. 14, 645 (1935).

39. V.F. Novy, R.C. Vickery, E.V. Kleber. Transactions of the Metallurgical Society of Aime. 580. Vol. 221, June 1961.

40. K.H.J. Buschow and A.S. Van Der Goot. Phys. Stat. Sol. 35, 515 (1969).

41. R.C. Mansey, G.V. Raynor and I.R.Harris. J. less common metals. 14 (1968).

42. K.H.J. Buschow and A.S. Van Der Goot. PHys. Stat. Sol. 35, 515 (1969).

43. K.H.J. Buschow and J.S. Van Wieringen. Phys. Stat. Sol. 42, 231 (1970).

44. Wallace, W.E., Skrabek , A.E., in Rare Earth Research. Edited by K. Vorres. Vol. 2, p. 431. New York. Gordon and Beach, 1964.

45. Gangle, J ., Ross, J .W. Proceed. of the Ins. Conf. on magnetism. p. 24. Nottingham (1964).

46. Mansey, R.C. Rayner, G.V. Harris, I.R. J. less common metals, 14, 329 (1968).

47. E. Burzo, 32. Bd. Helt 2, 1971.

48. A.E. Clark, and H.S. Belson. Physical Review Volume 5, Number 9. P. 3642 (1971).

49. J.B. Nelson and D.P. Riley, Proc. Phys. Soc. Lond. 57, 160 (1945).

50. Soshin Chikazumi, Physics of magnetism (1964).

51. A. del Moral and D. Melville. J. Phys. F. Metal Physics. Vol. 5, September, 1975

52. Jacobs, I.S. and Lawrence, P.E. Rev. Sci. Inst. 29, 713 (1958).

53. P.G. Mattocks, Ph.D. Thesis. Physics Department, Southampton University (1975).

54. E.W. Lee and J.E.L. Bishop. Proc. Phys. Soc. 1966, Vol. 89.

55. Tsuya, A. Clark, and R. Bozorth, in proceedings of the international conference on magnetism, Nottingham, 1964 (The institute of physics and the physical society, London (1965), p. 250.

56. Callen and H. Callen. Phys. Rev. 129, 578 (1963).

57. H. Callen and S. Shtrikman, Solid State Commun. 3, 5 (1965).

SYMBOLS

A	area of search coil
a	radius of the specimen; lattice parameter
a_1	inner radius of magnet
a_2	outer radius of magnet
B_{ei}	Kelvin function
B_{er}	
C	capacitance of energy storage bank; specific heat
C_H	heat capacity of a system at constant magnetic field
D	density of specimen
d	width of domain
E	electric field; energy; young modules
E_w	wall energy
G	search coil. Coupling constant
H	magnetic field
H_d	demagnetizing field
$H(a, t)$	radius and time function of field
K_0, K_1, K_2	anisotropy constants
α_i	direction cosines of the magnetization
e_{ij}	stress components
$E_{mag.st.}$	magnetostatic energy
$\gamma_1, \gamma_2, \gamma_3$	direction cosines of bond directions
C_{ij}	elastic moduli
E_{magel}	magnetoelastic energy
E_T	total energy
$\lambda 100$	the elongation along (100) direction for a single crystal
$\lambda 111$	the elongation along (111) direction for a single crystal
λ	the longitudinal magnetostriction for a polycrystalline sample
λs	saturation magnetostriction
λt	total magnetostriction $= \lambda 11 - \lambda \perp$
$\partial \nu$	volume magnetostriction
ν	
j	current density
$\lambda 11$	magnetostriction parallel to the applied field
$\lambda \perp$	magnetostriction perpendicular to the applied field
μ_0	permeability of free space
$\mu\beta$	Bohr magneton
ρ	resistivity
σ	specific magnetization; stress
τ	pulse length
τ_{s-L}	spin-lattice relaxation time
τ_{s-s}	spin-spin relaxation time
Φ	magnetic flux
w	angular frequency
L	inductance of magnet
M	magnetization; 3d element

Ms	saturation magnetization
h	height
i	current
i_{max}	maximum current
$\mathcal{H}$	Hamiltonian
B_n^m	numerical coefficients
O_n^m	stevens operators
B	magnetic field
Br	radial component of magnetic field
m	mass
fr	radial force
ϵr	radial strain
$\epsilon\theta$	azimuthal strain
ν	poissons ratio
V	volume; voltage
N	demagnetizing factor; number of atoms/unit volume
n	number of turns
R	resistance; rare earth element
r	radial co-ordinate
T	temperature
t	time; thickness
α	$= \frac{a_2}{a_1}$
β	$= \ell/a_1$
γ	gyromagnetic ratio; surface energy of domain wall
s	spin quantum number; entropy
g	gauge factor